AD-A037 663 POLYTECHNIC INST OF NEW YORK BROOKLYN DEPT OF ELECTR--ETC F/G 20/9
AN EXPERIMENTAL AND THEORETICAL STUDY OF THE PROPAGATION OF HIG--ETC(U)
JUN 76 E E KUNHARDT, B R CHEO AF-AFOSR-2668-74

UNCLASSIFIED POLY-EE/EP-76-011 AFOSR-TR-77-0158 NL

1 OF 2
AD A037663

AFOSR - TR - 77 - 0158

(3)

POLY-EE/EP-76-011

AN EXPERIMENTAL AND THEORETICAL STUDY OF THE PROPAGATION OF HIGH AMPLITUDE PULSES IN A BOUNDED MAGNETO-PLASMA

Erich E. Kunhardt and
Bernard R-S. Cheo

Scientific Report

Grant No. AFOSR-74-2668
Project No. 9751-03

June 1976

Prepared for
Air Force Office of Scientific Research
Arlington, Virginia

Polytechnic

Polytechnic Institute of New York
Department of Electrical Engineering
and Electrophysics
Brooklyn, New York 11201

Unclassified

SECURITY CLASSIFICATION OF THIS PAGE (When Data Entered)

REPORT DOCUMENTATION PAGE		READ INSTRUCTIONS BEFORE COMPLETING FORM
1. REPORT NUMBER AFOSR - TR - 77 - 0158	2. GOVT ACCESSION NO.	3. RECIPIENT'S CATALOG NUMBER
4. TITLE (and Subtitle) AN EXPERIMENTAL AND THEORETICAL STUDY OF THE PROPAGATION OF HIGH AMPLITUDE PULSES IN A BOUNDED MAGNETO-PLASMA.		5. TYPE OF REPORT & PERIOD COVERED Scientific - Interim rept.
		6. PERFORMING ORG. REPORT NUMBER
7. AUTHOR(s) Erich E. Kunhardt, Bernard R-S. Cheo		8. CONTRACT OR GRANT NUMBER(s) AFOSR 74-2668
9. PERFORMING ORGANIZATION NAME AND ADDRESS Polytechnic Institute of New York, Department of Electrical Engineering & Electrophysics, Brooklyn, New York 11201		10. PROGRAM ELEMENT, PROJECT, TASK AREA & WORK UNIT NUMBERS 9751-03 61102F 119p.
11. CONTROLLING OFFICE NAME AND ADDRESS Air Force Office of Scientific Research/NP, Bolling AFB, DC 20332		12. REPORT DATE June 1976
		13. NUMBER OF PAGES 118
14. MONITORING AGENCY NAME & ADDRESS (if different from Controlling Office) POLY-EE/EP-76-011		15. SECURITY CLASS. (of this report) Unclassified
		15a. DECLASSIFICATION/DOWNGRADING SCHEDULE

16. DISTRIBUTION STATEMENT (of this Report)

~~Approved for Public Release; Distribution Unlimited~~

AF-AFOSR-2668-74

17. DISTRIBUTION STATEMENT (of the abstract entered in Block 20, if different from Report)

9751 03

18. SUPPLEMENTARY NOTES

TECH, OTHER

19. KEY WORDS (Continue on reverse side if necessary and identify by block number)

20. ABSTRACT (Continue on reverse side if necessary and identify by block number)

Experiments on the propagation of narrow, high amplitude pulses along a plasma column have been conducted. The evolution of the pulse in space-time has been observed as a function of initial pulse strength. This technique gives insight into the competitive effects due to dispersion and nonlinearities. For a plasma, the positive column of a hot cathode, D. C. discharge in Argon is used. The pressure varied from 1 to 10m Torr Hg, and the averaged electron densities are of the order of 10 to 9 up to 10 to 10 cubic centimeters. The pulses for excitation are generated by a home made device capable of producing (over)

DD FORM 1473, 1 JAN 73 EDITION OF 1 NOV 65 IS OBSOLETE

408 717

Unclassified

SECURITY CLASSIFICATION OF THIS PAGE (When Data Entered)

1B

subnanosecond pulses with 3200 volts peak amplitude, into a 50 ohm line, at a repetitive rate of approximately 100 p.p.s.

POLY-EE/EP-76-011

AN EXPERIMENTAL AND THEORETICAL STUDY OF THE PROPAGATION OF HIGH AMPLITUDE PULSES IN A BOUNDED MAGNETO-PLASMA

Erich E. Kunhardt and Bernard R-S. Cheo

Department of Electrical Engineering and Electrophysics
Polytechnic Institute of New York
Brooklyn, New York 11201

Scientific Report

Grant No. AFOSR-74-2668
Project No. 9751-03

June 1976

Prepared for

Air Force Office of Scientific Research
Arlington, Virginia

10 to the 9th power

10 to the 10th power

to

per

ABSTRACT

Experiments on the propagation of narrow, high amplitude pulses along a plasma column have been conducted. The evolution of the pulse in space-time has been observed as a function of initial pulse strength. This technique gives insight into the competitive effects due to dispersion and nonlinearities.

For a plasma, the positive column of a hot cathode, D.C. discharge in Argon is used. The pressure varied from 1 to 10 m Torr Hg, and the averaged electron densities are of the order of 10^9 - 10^{10} cm^{-3}. The pulses for excitation are generated by a home made device capable of producing subnanosecond pulses with 3200 volts peak amplitude, into a 50 Ω line, at a repetitive rate of approximately 100 p.p.s.

OHM

At each operating point, i.e., for a given pressure and discharge current, recordings were obtained for different values of excitation pulse amplitude and background static magnetic field.

For zero static magnetic field, two types of recordings were taken. For the first type, the position of the receiver was fixed and oscillograms in time were recorded. In the second type, the sampling time is kept fixed and the receiving probe is moved along the column. From the oscillograms, we observe that the dispersion is negative and that the group velocity increases with plasma density. As the amplitude of the input pulse is increased, nonlinear effects start to play a role. Under experimental conditions, these effects did not lead to quantitatively different behavior than linear phenomena. From numerically taken Fourier transforms of the observed propagating wavepackets, the transfer of energy between different frequency components forming the disturbance have been observed. The region of interaction in the frequency domain is seen to be a function of distance along the column and of wave velocity.

For finite static magnetic field, recordings of the first type were obtained as a function of pulse amplitude. Again, the dispersion is negative and the group velocity increases with both ω_p and ω_c. Contrary to the $\underline{B}_o = 0$ case, for large pulse amplitude, qualitatively different wave phenomena were observed: in particular the nonlinear waves show modulational splitting. This phenomenon was observed both in time and in the frequency domain.

TABLE OF CONTENTS

			Page
Abstract			
List of Illustrations			
I.	Introduction		1
II.	Experimental Program		4
	2.1	Description of the Apparatus	4
		2.1.1 The Plasma	4
		2.1.2 The Pulse Generator	9
		2.1.3 Parallel Plate Structure	9
	2.2	The Experiment	11
		2.2.1 Zero Axial Magnetic Field	11
		2.2.2 Finite Axial Magnetic Field	17
III.	Analytical Formulation of the Experiment		19
	3.1	Analytical Model	19
	3.2	Functional Relation Between κ_a and ω	29
	3.3	Final Form of Amplitude Equation	34
	3.4	Analysis of the Amplitude Equation	38
IV.	Results		50
	4.1	Zero Axial Magnetic Field	50
		4.1.1 Linear Regime	50
		4.1.2 Nonlinear Regime	68
	4.2	Finite Axial Magnetic Field	74
		4.2.1 Linear Regime	74
		4.2.2 Nonlinear Regime	78
V.	Concluding Remarks		90
VI.	Appendices		92
	6.1	Formal Derivation of Operators	92
	6.2	Evaluation of the Eigenvectors	93
		6.2.1 Eigenvectors for Zero Magnetic Field	95
		6.2.2 Eigenvectors for Large Magnetic Fields	99
	6.3	Explicit Evaluation of Nonlinear and Collision Operators	102
		6.3.1 Zero Magnetic Field	102
		6.3.2 Infinite Magnetic Field	105
		6.3.3 Weak Magnetic Field	108
VII.	References		110

LIST OF ILLUSTRATIONS

Figure		Page
2.1	Basic experimental set up	5
2.2	D.C. discharge tube, associated vacuum system and D.C. circuitry	7
2.3	BBG output and Fourier spectrum	10
2.4	Parallel plate structure	12
2.5	Block diagram of impulse generation, transmission and reception	14
2.6	Arrangement to record spatial profile of wavepackets	16
2.7	Block diagram of experiment, finite magnetic field	18
3.1	The magneto-plasma column	20
3.2	Computer plot of dispersion equation	31
3.3	Velocity of first peak of wavepacket vs. plasma frequency	45
3.4	α' parameter vs. plasma frequency	47
4.1	Effect of pressure on propagating wavepacket	52
4.2	Effect of polarity of exciting pulse	54
4.3	Evolution in space of initial pulse	55
4.4	Linear oscillograms for different receiver positions (positive pulse) f_p = 1.4GHz. a) z = 27 cm, b) z = 56 cm c) z = 90 cm	57
4.5	Fourier transform of wavepacket for different positions	58
4.6	Linear oscillograms for different plasma frequencies z = 27 cm. a) f_p = .76GHz, b) f_p = .9GHz, c) f_p = 1.4GHz	59
4.7	Velocity of first peak vs. plasma frequency	60
4.8	Normalized time position of zeros of electric field	63
4.9	Amplitude of wavepacket envelope vs. time	65
4.10	Oscillograms for different plasma frequencies. Tube radius = .3 cm	66
4.11	Zero crossing for small tube.	67
4.12	Response as a function of input pulse strength	69
4.13	Amplitude of wavepacket envelope vs. time	70
4.14	Amplitude of wavepacket vs. distance	71
4.15	Linear and nonlinear spectrum for different plasma frequencies	72
4.16	Nonlinear spectrum for different receiver locations	73
4.17	Response to high negative pulse	75

LIST OF ILLUSTRATIONS (Con't.)

Figure		Page
4.18	Linear oscillograms for different plasma frequencies. Cyclotron frequency = .6 GHz. a) f_p = 1.4 GHz, b) f_p = 1.6 GHz c) f_p = 1.7 GHz	76
4.19	Linear oscillograms for different cyclotron frequencies. Cyclotron frequency a) f_c = .6 GHz, b) f_c = .84 GHz, c) f_c = 1 GHz	77
4.20	Normalized time position of zeros of electric field	79
4.21	Velocity of first peak vs. plasma frequency	80
4.22	Oscillogram taken at z = 56 cm. Cyclotron frequency = .6 GHz	81
4.22	a) Oscillogram taken at z = 34 cm. Cyclotron frequency = .6 GHz	82
4.23	Linear Fourier transform	83
4.24	Fourier transform of Fig. 4.22 b)	84
4.25	Fourier transform of Fig. 4.22 c)	85
4.26	Fourier transform of Fig. 4.22 d)	86
4.27	Time separation of wavepackets	88

I. Introduction

The general problem we are concerned with is that of the interaction of a plasma medium with an electromagnetic field. At linear level of excitation, the various problems of wave propagation have been explored at length and a fair amount of understanding has been reached. At nonlinear levels of excitation, due to the lack of a general method of attack, the analysis made to date are mostly ad hoc and under various forms of idealization and approximation. The purpose of this investigation is to study some of these interactions both theoretically and experimentally. The results have yielded new data and insight into the problem of the competition between dispersion and non-linearity in a number of plasma configurations. The comparison between theoretical result and experimental data is generally favorable.

Theoretical studies in the linear and weakly nonlinear regimes may be grouped into two categories, namely, analysis in unbounded and bounded plasmas. Experimental investigations on the other hand must be performed with plasmas of bounded geometry. There are experiments, however, where the pertinent dimensions are such that to a good approximation, the waves under consideration may be thought as propagating in an infinite medium and the results behave as predicted by unbounded plasma theory.[1] Studies in unbounded plasmas have been many, and several text books have been written on this subject. Comprehensive expositions have been done by Ginzburg[2] and Stix[3] for the linear regime; and for the weakly nonlinear regime by Tsytovich,[4] Davidson[5] and F. Einaudi et. al.[6].

The bounded geometry considered in this investigation are: a circular plasma column imbeded in an infinite dielectric (free space) and a circular magneto plasma column surrounded by a conducting waveguide of the same dimension as the plasma column. These structures are known to support numerous types of waves. The work in this study is concerned with the propagation of the slow mode whose characteristics do not depend on ion motion. These waves are sometimes called "space charge" or "electron plasma" waves. They differ from the "true" electron plasma waves in an infinite plasma since the boundary conditions posed by the system have altered the wave

structure. Practical interest in these modes are the possibilities of applications in laboratory plasma diagnostics[7,8,9], high gain microwave devices[10,11], and plasma heating[12].

The basic experimental results of linear slow wave propagation have been well documented [13,14] and good agreements with theoretical analysis have been obtained[15,16]. However, the situation is different for the weakly nonlinear regime. Very few theoretical analysis of the boundary value problem have been done[17,18,19,20]. The emphasis in most of these studies has been on the nonlinear coupling of waves, in particular three wave interaction[21]. This problem takes a variety of forms. Perulli, et.al. [22] studied the decay of a slow wave into two other slow waves with different azimuthal variation. Larsen[23] used the method of the averaged Lagrangian to analyze the interaction of three slow waves. Kuhn[24] formulated the same problem from a coupled mode formalism. Aside from experiments on surface wave echo (spatial)[25], experimental work has been confined to the mixing of two pump waves of different frequencies to produce a third at the beat frequency[26].

All of the theoretical and experimental efforts mentioned thus far have one feature in common: they are all concerned with steady state situations. Recently, transient techniques have been employed in the experimental investigation of wave propagation in plasmas. Voltage steps and pulses (base band and RF) have been used to excite transient waves. Schmitt[27] was one of the first experimentalists to use pulse excitation to study plasmas. He observed the dispersion of base band pulses propagating through a plasma filled coaxial line. Proni, et.al. [28] and Tregruis, et.al. [29] used microwave pulses to excite transient electron plasma waves in systems where the boundary had no effect. The only reported applications of base band pulses to study the propagation of space charge waves were by Anicin, et.al. [30] for the symetric mode, and by Demokan, et.al. [31] for the dipole mode. Recently Landt et.al. used various types of transient inputs to study the linear properties of these modes[32]. These experiments were limited to the linear regime.

In the nonlinear regime, pulse excitations and time domain

observations have been reported by Sindoris, Cheo and Grody[33] in a Tonks-Dattner type structure using a home developed device called a Bouncing Ball Generator (BBG), which produced baseband pulses 120 picosecond wide at 1.1 KV into 50 ohm. Other nonlinear transient work includes the observation by Ikezi et. al.[34] of the propagation of electron plasma waves excited by voltage steps, and the observation by K. Saeki et. al.[48] of electron plasma wave shocks. Manheimer[49] has studied the development of finite amplitude electron plasma waves in a bounded plasma with infinite magnetic field using the method of expansion in terms of a complete set of linear solutions. He did not include the effect of dispersion, but predicted the steepening observed in (48).

The work in this effort consists of a comprehensive investigation of linear and nonlinear phenomena affecting the propagation of very short base band pulses along a glow discharge magneto plasma column. The advantages of this approach over nonlinear steady state studies are: 1) by keeping the duty cycle low, heating of the background electrons (a major problem in CW experiments) need not be considered; 2) if the transient response is short compared to ionization times, background electron density changes will not occur; 3) the ability to observe short-lived phenomenon is greatly enhanced because of the expanded time resolution. The major advantage of transient studies both large and small amplitude excitations is that we can observe the development in time or in space of an initial disturbance produced at some point. Tremendous insight is gained into the competitive effects of dispersion and nonlinearity.

The source that was used to excite the transient waves is an improved version of the BBG mentioned in the experiment of Sindoris et. al.[33]. The new BBG produces a pulse 0.50 nanosecond wide at 3.2 KV into 50 ohm. This generator and the techniques developed presented us with the unique tools for such comprehensive studies.

In chapter II of this report the experimental program is presented. To analyze the experimental observations a nonlinear theory for wave propagation along plasma column was developed. This theoretical analysis is presented in chapter III. In Chapter IV the experimental results are then analyzed.

II. Experimental Program

The basic experimental set up is shown schematically in figure 2.1, where the plasma is the positive column of a glow discharge confined in a glasss tube 175 cm long, with A and K the anode and cathode respectively. M-M' represents a set of coils providing an axial D.C. magnetic field up to 1.2K Gauss. WG is a removable conducting wall surrounding the plasma tube. L is a pair of parallel plates connected to the pulse generator (BBG) which establishes an impulse like electric field in the plasma. The wave evolution in space-time as a function of initial pulse strength is monitored by the receiving structure R on a sampling scope. The work was done in two stages. The first consisted of a comprehensive investigation of linear and nonlinear phenomena affecting the propagation of pulses along the positive column of a glow discharge. The second stage involved the addition of a uniform longitudinal magnetic field variable up to 1.2K Gauss and the surrounding of the plasma column by a conducting wall. Subsequently, a description of the experimental apparatus and procedure is given.

2.1 Description of the Apparatus

2.1.1 the plasma

For a plasma, the positive column of a hot cathode, glow discharge in argon is used. Fig. 2.2 shows a layout of the discharge tube and its associated vacuum and electrical systems. The discharge tube comprises two Western Electric mercury vapor cathodes contained in a round flask and connected by means of a quick glass to glass joints to a 175 cm long glass tube, the end of which is terminated with a hallow anode. Because of the quick coupler, glass tube sections of different diameter may be used.

It was necessary, due to the type (sampling technique) and amount of measurements that had to be performed, to provide a clean and stable discharge. By allowing Argon gas to flow through the discharge tube at a slow rate; contamination, due mainly to ion bombardment of the cathode, is reduced since such impurities are constantly

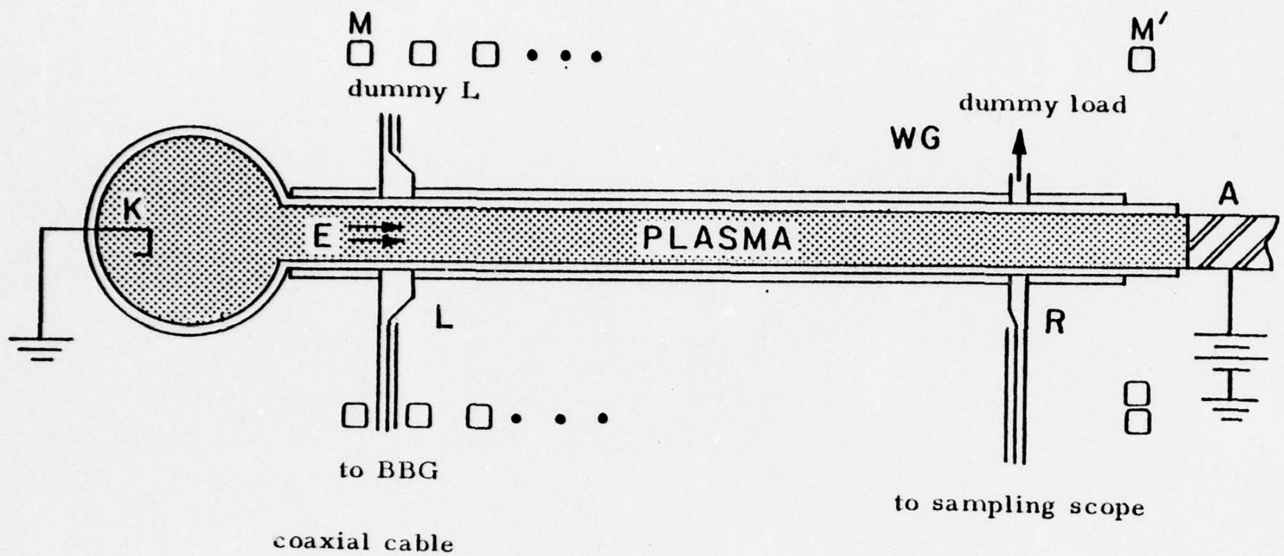

Fig. 2.1 Basic experimental set up

removed from the tube. To provide effective regulation of the gas pressure, the argon inflow is regulated by a flow meter valve and needle valve and the evacuation rate by a high vacuum valve. Adjustment of these valves provide the desired pressure.

Once the discharge is operating, the desired range of electron densities is obtained by varying the current through the pentode regulator circuit. Stability of the system, over all range considered, was excellent.

Basic parameters of the positive column, i. e. electron temperature, density, and collision frequency, were measured. Electron temperature is obtained using the well known method of Langmuir probe[35]. To measure average electron number density, the cavity perturbation method is used[9]. The cavity is mounted in a carriage which can move along the plasma column. The electron density variation along the column is found to be less than 0.5%. During the experiments, the density is constantly monitored to prevent drifts from the operating point, due primarily to pressure variations.

The cavity is also used to measure the total collision frequency of the electrons. By measuring the change in Q of the microwave cavity due to the plasma, this parameter may be calculated[36]. The collision frequency of electrons with ions and with neutrals is also calculated using the equation[37]

$$\nu_{e\beta} = n_\beta \, Q_{e\beta} \, v \tag{2-1}$$

where

$\beta \equiv$ implies ions or neutrals

$Q_{e\beta} \equiv$ collision corssection for collision of electrons with β-type particles

$v \equiv$ average velocity given by $\left(\frac{8KT}{\Pi m}\right)^{1/2}$

$n_\beta \equiv$ density of β particles

For neutrals, at 20° C:

$$n_\beta = \frac{A}{22400} \; \frac{P}{760} \; \frac{273}{293}$$

where $A = 6.02 \times 10^{23}$ particles/mole

P = pressure in mm.

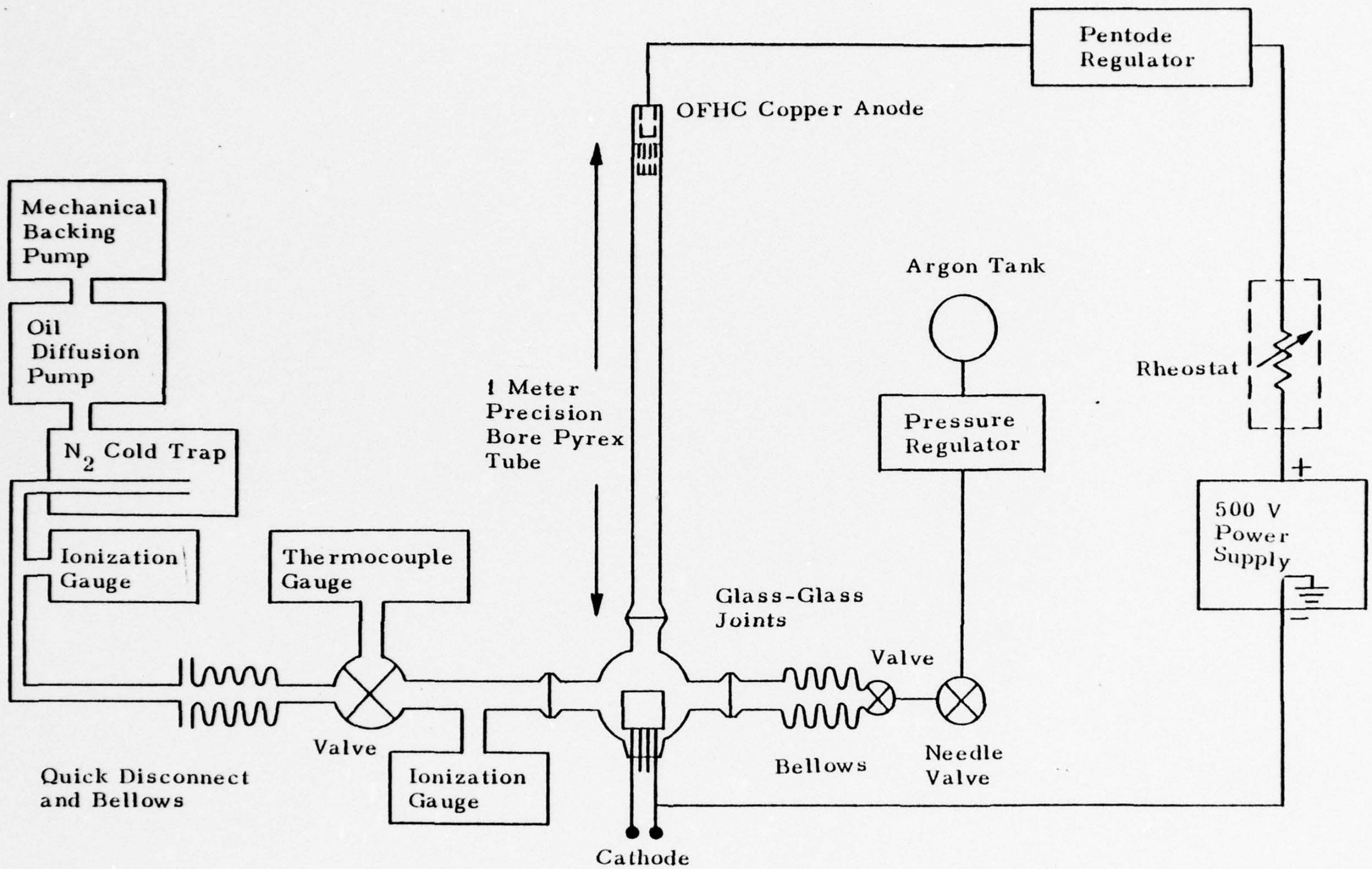

Fig. 2.2 D.C. discharge tube, associated vacuum system and D.C. circuitry

Table 2.1

Typical Discharge Characteristics

Radius of column	.66 cm
Neutral density (at 1μ)	3.3×10^{13} cm^{-3}
Percent ionization	.01%
Electron neutral collision frequency	17.2 MHz
Electron neutral collision time	100 n sec.
Debye length λ_D	1 mm
Electron thermal speed	1.5×10^{8} cm/sec.
Electron density	2×10^{10} cm^{-3}
Electron cyclotron frequency	.632 GHz
Electron plasma frequency	1.3 GHz

Typical parameters obtained using the experimental techniques mentioned above are shown in table 2. 1.

2. 1. 2 The pulse generator

A Bouncing Ball Generator (BBG) is the source for the pulses used in the experiment. This generator has previously been used in time domain studies of EM precursors and in impulse stimulated emission from plasmas[33]. The generator, at the time of those experiments, produced base band pulses with peak voltage of 1. 1 kilovolts and a risetime faster than 120 picoseconds. For this experiment, the BBG was modified and is now capable of producing pulses with peak voltage of 3. 2 kilovolts with approximately 200 picoseconds rise time. The peak power into a 50 ohm line is 259 kilowatts. The average power, however, is 4 milliwatts because of the short pulse duration. The display of the BBG output pulse shown in Fig. 2. 3 is an X-Y recorder plot of the oscillogram from the sampling scope. To obtain such an oscillogram, the pulse, after being attenuated 63 dB is applied to the scope through a 60 nanosecond delay cable (RG-9B/u) of 4. 4 dB insertion loss. The output of the scope is then used to drive the X-Y recorder. Also shown in fig. 2. 3 is the voltage spectrum of the pulse. This is obtained from Fourier analysis using a computer of the time domain signal. The spectrum is extremely wide, extending from D. C. and almost flat to 1 GHz.

To control the amplitude of the pulse, wide band attenuators (GR type 874-GL) are used at the output of the BBG. Also at the output, a pre-trigger pick off has been installed to obtain a trigger signal for the scope.

2. 1. 3 Parallel plate structure

To couple the BBG pulse to the plasma, a section of parallel plate transmission line is used. The parallel plate coupling structure consists of a wide band coaxial to parallel plate transition which opens up to a length of uniform transmission line, then tapers down again to a coaxial line. The line is then attenuated by 20 dB and terminated with a 50 Ω load. The dimensions of the structure are such as to keep a constant 50 ohms characteristic impedance along the structure over a

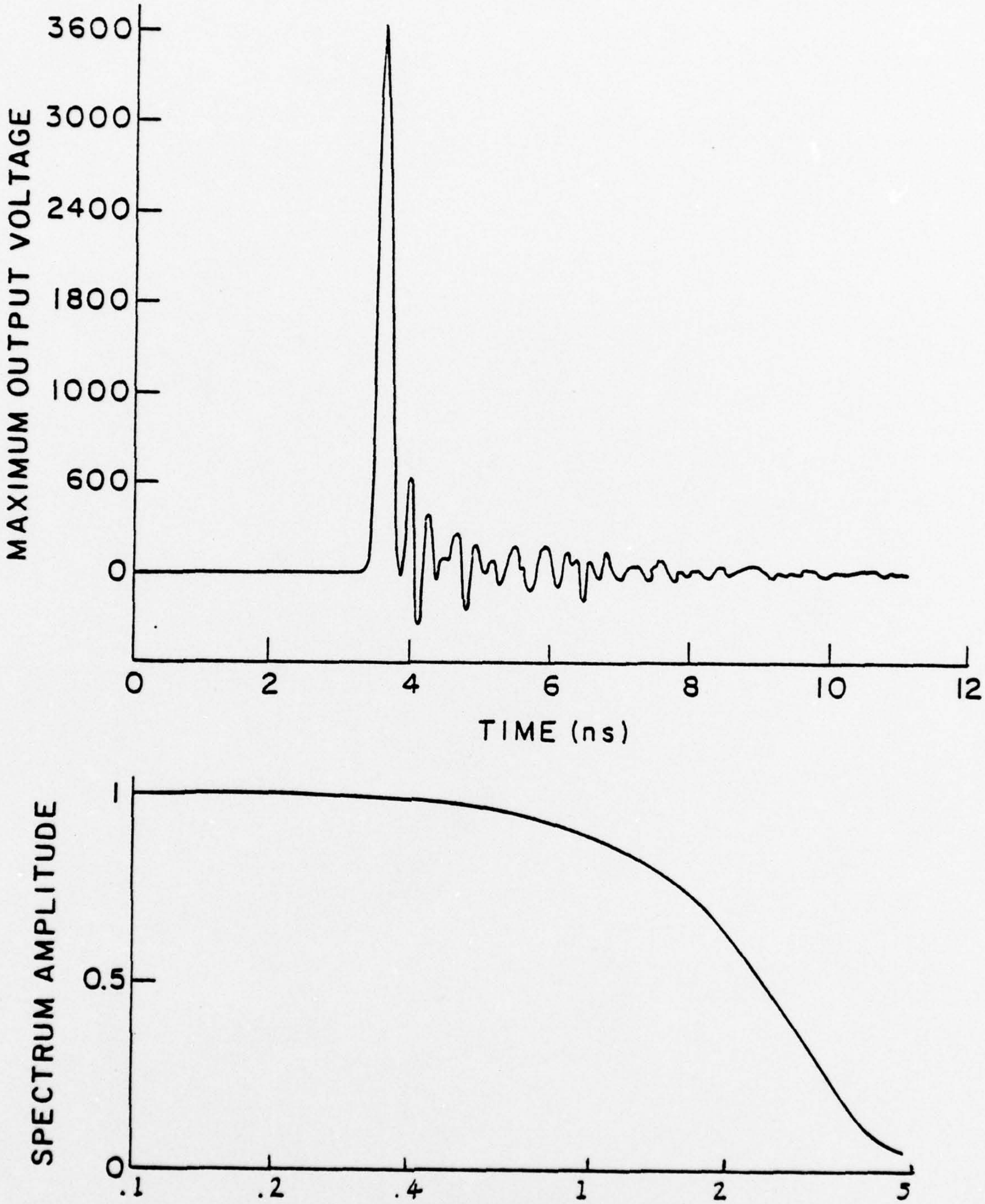

Fig. 2.3 BBG output and Fourier spectrum

wide range of frequencies. The plasma tube is inserted perpendicular to the plane of the plates through holes made at the center of the plates, as shown in fig. 2.4. The holes are made to fit tightly around the column.

The plate structure is a very good wide band coupler with an almost flat passband extending from 50 MHz to approximately 2 GHz. This feature of the structure made it a suitable coupler in the pulse experiments because of the wide bandwidth of the exciting pulse. A similar structure is also used to couple the propagating wavepacket to the sampling scope. The receiving plates are mounted on a carriage to allow for movement along the column.

2.1.4 Sampling scope and recorder

To observe the input pulse and the propagating wavepackets, a Tektronix 564 storage scope with sampling plug-ins is used. To facilitate further analysis, the observed oscillograms are also recorded using a Hewlet-Packard X-Y recorder connected to the output of the storage scope.

It must be remarked that the sampling technique for observing fast transient time phenomena requires that each experiment be identical. This in turn demands that the input pulse be identical for each experiment and that the plasma relaxes to its initial state before the following pulse arrives at the launcher. The last condition may be ascertained by comparing the width of the packet with respect to the pulse separation. However, considering that the BBG is an electromechanical device, it is remarkable that the pulses it produces are identical within a few percent of each other, to the extent that the technique was succesful.

2.2 The Experiment

2.2.1 Zero axial magnetic field

For the investigation, the apparatus described in section 2.1 was arranged as shown in fig. 2.5. The output pulse of the BBG, after attenuation to the desired voltage, is coupled to the plasma through the wide band parallel plate structure. A 60 nanosecond delay cable is used between the generator and the plates. For high amplitude pulses,

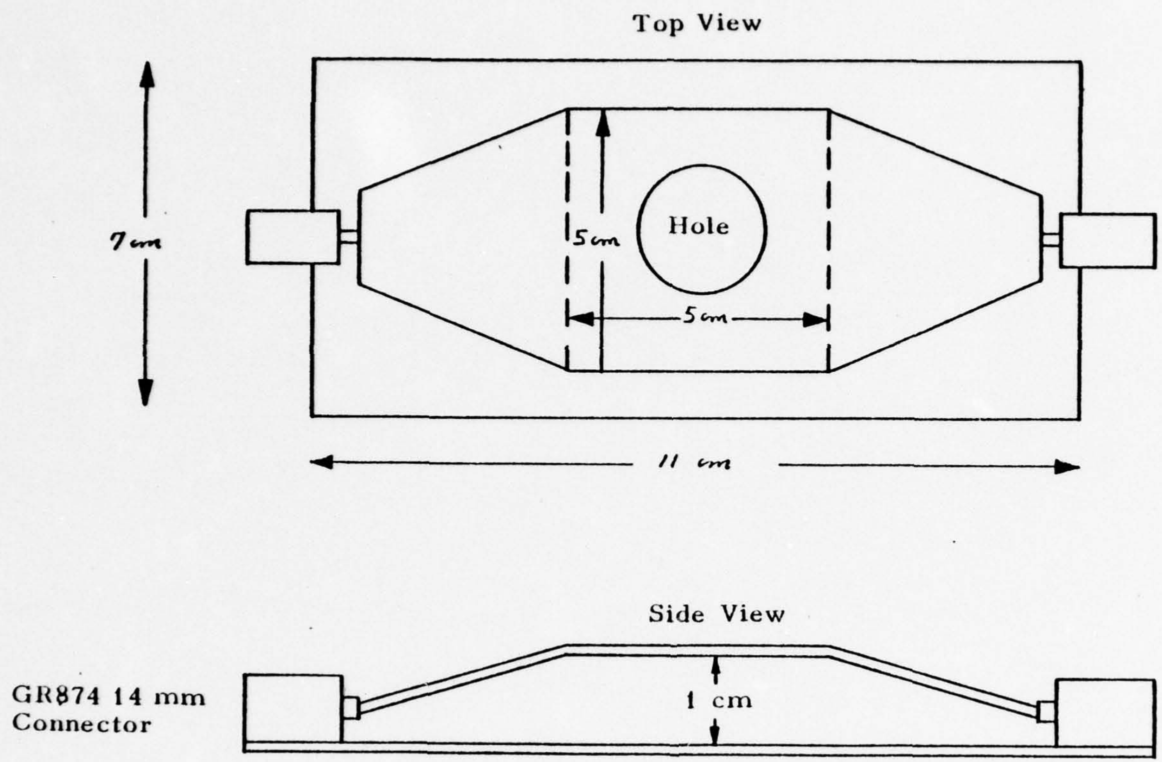

Fig. 2.4 Parallel plate structure

difficulty is encountered with reflections from the plates (due to a small mismatch), that travel back to the BBG. At the BBG, these are once again reflected (the BBG is an open transmission line) and return to the plates generating unwanted signals. By introducing the delay line, the reflection arrives at the plates 120 ns after the original pulse, long after the observations are made.

The plasma column is inserted perpendicular to the plane of the plates through the holes at the center. The holes are made to fit tightly around the column. As the pulse propagates along the parallel plates, the region of plasma within the plates (1 cm separation) feels uniformly around the column the effect of the electric field of the pulse. The field is directed parallel to the axis of the column, such that electrons are accelerated towards the anode.

With this mode of coupling, circularly symmetric waves are excited in the plasma and they propagate along the column towards the anode. To prevent waves from propagating towards the cathode, the section of plasma between cathode and launcher is surrounded with a copper sheet and no wave can propagate under those conditions. More will be said on this in chapter III. Since the tube is of finite length, wide band microwave absorbers are used at the end of the column to prevent possible reflections from the anode and into the receiver.

The receiver is mounted on a carriage and can be moved along the whole length of the column. These plates pick up the longitudinal electric field associated with the propagating wave. The field strength is displayed on the sampling scope and also plotted on paper using the X-Y recorder. A trigger pulse from the BBG is used to properly synchronize the time of sampling.

Two types of oscillograms were recorded. First, for a fixed position of the receiving plate, oscillograms in time were taken. The analog output of the scope drives the Y axis of the plotter, while the scope's time base is used to drive the X axis. In this manner, a replica of the trace that appears on the scope's screen is plotted. Secondly, the spatial distribution of the waves, for fixed sampling time, were obtained. The Y axis of the plotter is driven as in the time measure-

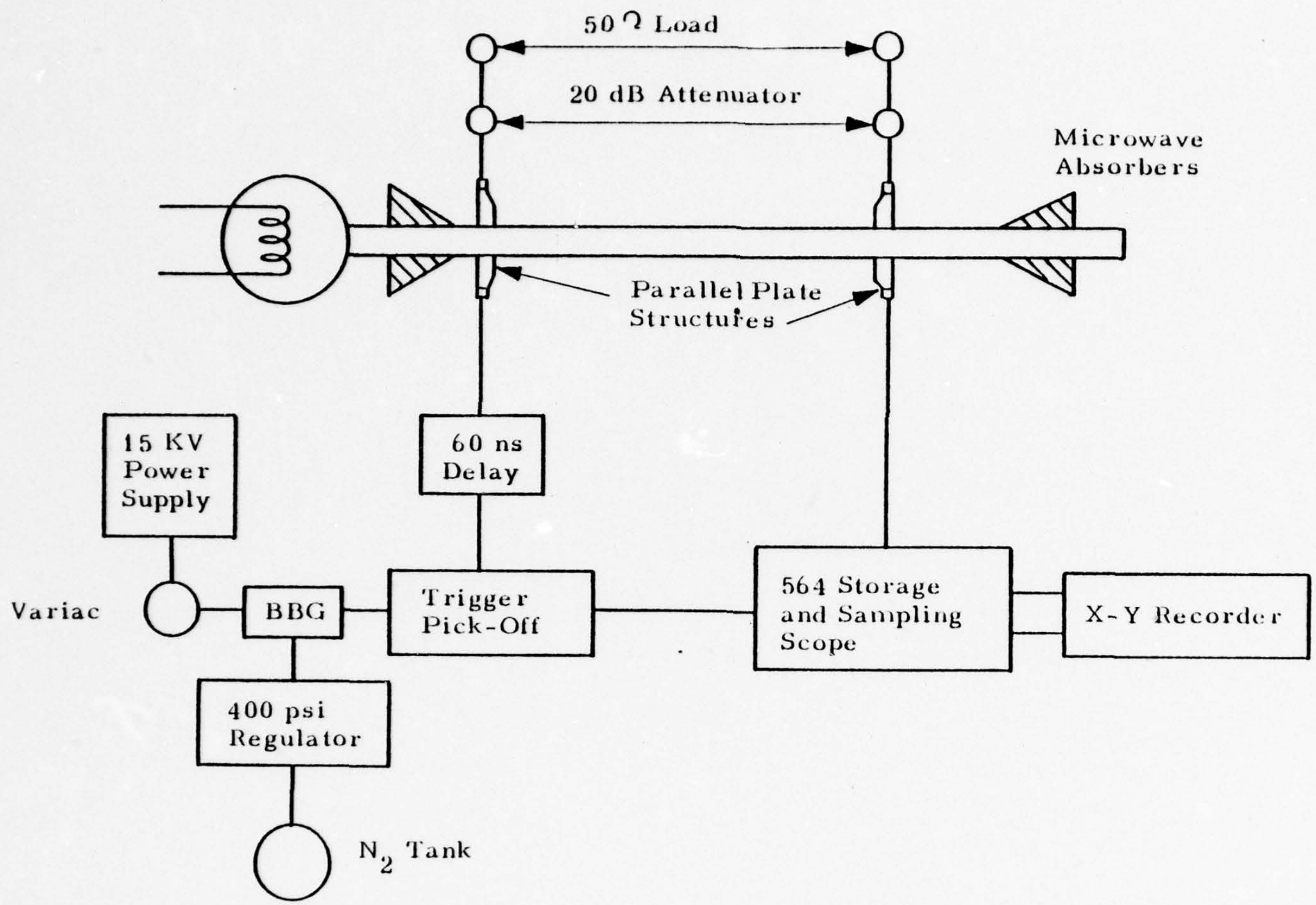

Fig. 2.5 Block diagram of impulse generation, transmission and reception

ments; the X axis however is driven by a voltage proportional to the position of the receiver with respect to the launcher. The arrangement is shown in fig. 2. 6. A constant voltage is applied across the potentiometer. As the crank is turned to move the probe, the arm of the potentiometer rotates a distance proportional to the probe's motion along the axis of the column. Thus the voltage of the arm is equivalent to the distance of the probe with respect to the structure. This voltage increases continuously as the receiving structure moves away from the launcher.

Both types of oscillograms were taken under different operating conditions. The argon discharge was operated over a range of neutral gas pressure and D. C. discharge current. The pressure was varied from 1 to 10 μ Hg and the current between 20 and 300 mA. In this domain, the electron temperature ranged between 2. 5 and 5 eV. (the high temperature corresponding to the lowest pressure), while the average electron densities were of the order of 10^9-10^{10} cm^{-3} (the low densities corresponding to the lowest pressures and discharge currents). The range of electron collision frequencies has been tabulated in sec. 2. 1. 1. To investigate the effect of column radius on the propagation of the waves, column section of diameters; . 6 cm, . 952 cm and 1. 32 cm, were used.

Finally, the characteristic of the waves as a function of exciting pulse polarity and amplitude were investigated. A BBG was also constructed to produce negative pulses. For a negative pulse, ions are accelerated towards the anode. Since the amplitude of the BBG pulse (both positive and negative) is constant, attenuators are used to obtain the lowest desired level of excitation (this corresponded to approximately 100 volts). Then, the peak voltage of the exiting pulse (numerically equal to the longitudinal electric field the charged particles between the plates feel) is progressively increased (by reducing the attenuation) to its maximum value. In taking the oscillograms, each time the exciting pulse is increased, the received waves are attenuated by a corresponding value to keep the gain of the system fixed, allowing direct comparison of the profiles of the received signals.

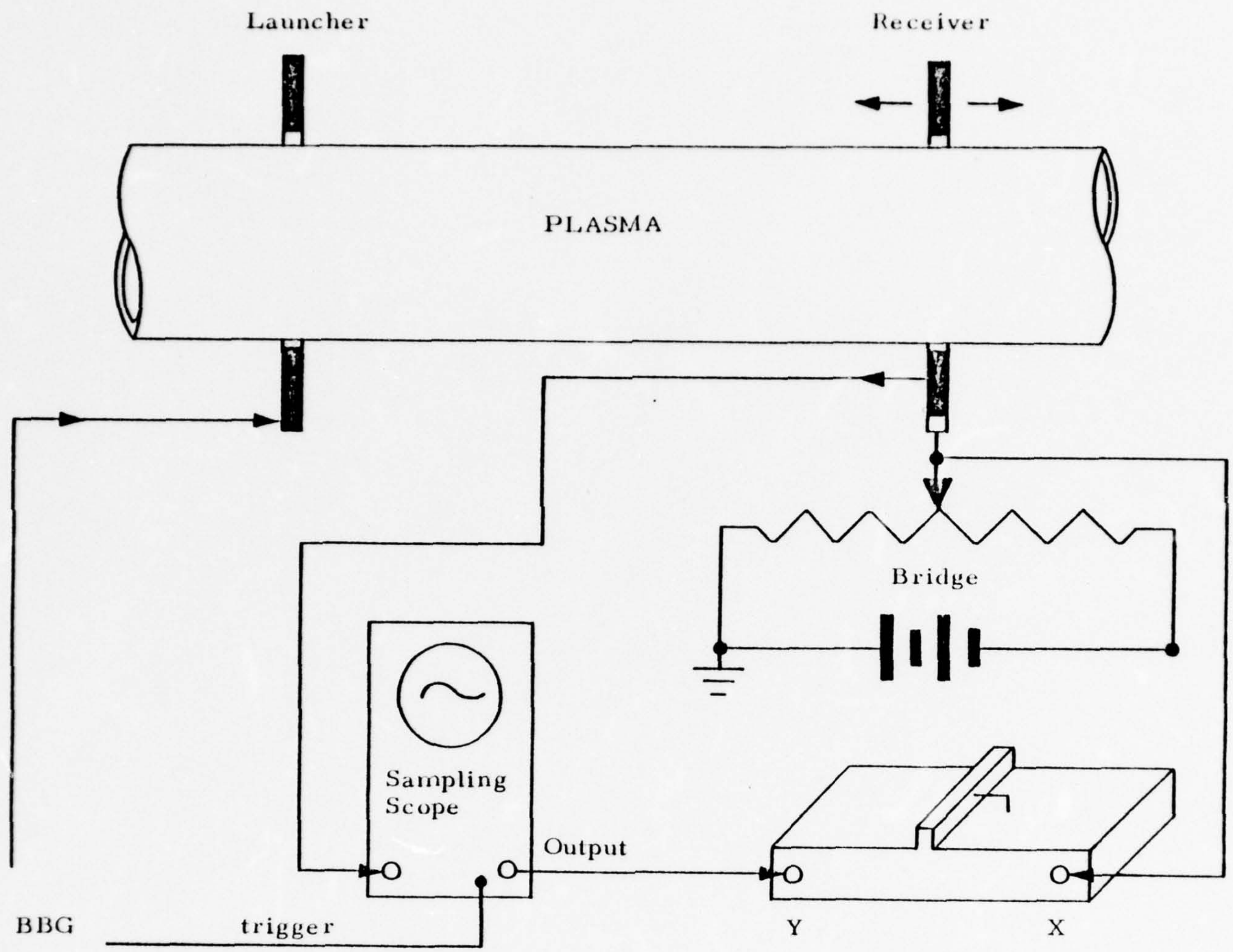

Fig. 2.6 Arrangement to record spatial profile of wavepackets

2.2.2 Finite axial magnetic field

To study the propagation of large amplitude pulses along magneto plasma columns, a uniform magnetic field of strength up to 1.2 K Gauss was added to the set-up of fig. 2.5. The field was produced by seven ESI 49 coils arranged in such a fashion that the magnetic field variation over the test region was only $\pm$ 1% . Moreover, the test section in fig. 2.5 was surrounded with a conductor, except at the launcher, and receiver locations.

Initially, the same method (i.e. tube inserted perpendicular to the plates through holes made in them) was used to couple the pulse to the magneto plasma column. It proved to be very inefficient in exciting propagating bulk waves due to great coupling losses. The tube section was then redesigned and copper rings were inserted such that the parallel plates were in direct contact with the plasma. This improved the coupling greatly and proved to be necessary to launch the waves. The modified set up is shown in fig. 2.7. Similar recordings as for the case of no magnetic field were obtained under different conditions of: plasma frequency, magnetic field strength and background neutral pressure.

Before presenting the results of the experiments (both with and without magnetic field), an analytical formulation and analysis of the experimental conditions will be given in the next chapter. In the light of knowledge acquired from such analysis experimental data will then be presented and analyzed.

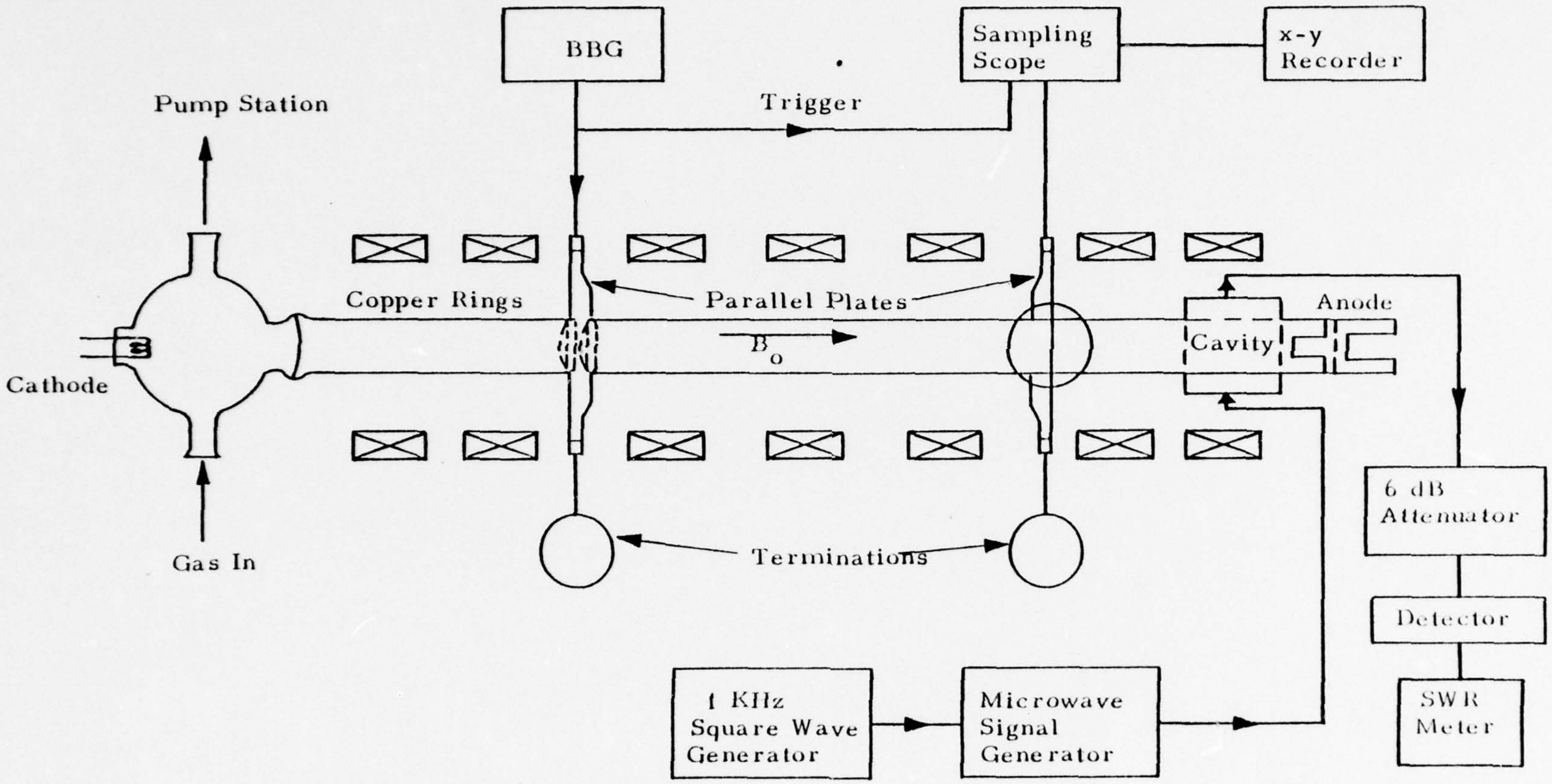

Fig. 2.7 Block diagram of experiment, finite magnetic field

III. Analytical Formulation of the Experiment

The problem posed by the experiment is as follows: a plasma column of circular cross-section of radius b, and infinite length, either in free space or surrounded by a conductor, is excited at z = 0 by a finite amplitude source of electromagnetic radiation. In general, a finite axial D. C. Magnetic field is present as shown in Figure 3.1. The spatial and temporal evolution of the excited bounded modes is investigated. This analysis involves the adoption of an appropriate idealized model which is mathematically tractable.

3.1 Analytical Model

Consider a homogeneous plasma column imbedded in the gas from which it is formed by partial ionization. The plasma is considered to be a cold electron gas moving through a stationary neutralizing background of ions. The dynamical interaction between electrons and the background is described by a constant collision frequency ν_c. The interaction is assumed to be such that there is no loss of electrons due to ionization, recombination or attachment. Since the percentage ionization of the discharge is low (.01%), it may be assumed that ν_c is basically the electron neutral collision frequency. The fact that the background density of the discharge is dependent on radius, undermines the assumption of a uniform plasma column, but a compromise is necessary if the finite amplitude analysis is to be mathematically tractable. The effects introduced by the inhomogeneity will be discussed at the proper place.

Quantitatively, Euler's equations will be used to describe the dynamics of the electrons[37]:

$$d_t n + \nabla \cdot n\underset{\sim}{v} = 0 \qquad (3\text{-}1)$$

$$mnd_t\underset{\sim}{v} + mn\underset{\sim}{v} \cdot \nabla \underset{\sim}{v} + mn\nu_c\underset{\sim}{v} + en\underset{\sim}{E} + n\underset{\sim}{v} \times \mu_o \underset{\sim}{H}_o = 0 \qquad (3\text{-}2)$$

where

$n(\underset{\sim}{r}, t)$	$\equiv$	electron number density
$\underset{\sim}{v}(\underset{\sim}{r}, t)$	$\equiv$	average electron velocity
ν_c	$\equiv$	collision frequency for momentum transfer between electrons and neutrals
$\underset{\sim}{E}(\underset{\sim}{r}, t)$	$\equiv$	electric field intensity
$\underset{\sim}{H}_o$	$\equiv$	background magnetic field intensity

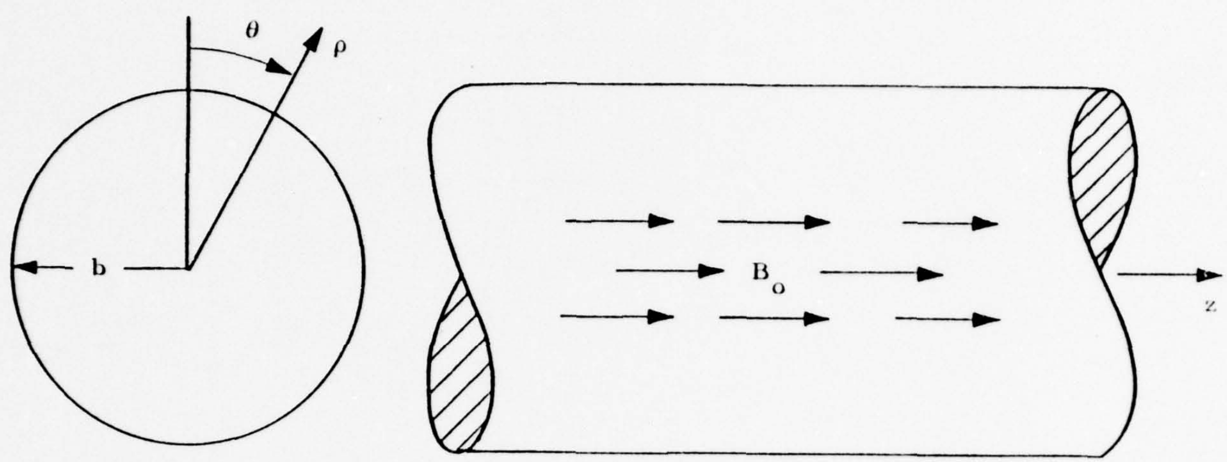

Fig. 3.1 The Magneto-Plasma Column

When stated in the form of (3-1)-(3-2), a series of assumptions must be appended to the exact Euler system. These assumptions may be found in a standard text on plasma dynamics[38].

Since it is our interest to study the interaction of the above plasma model with an electromagnetic field, Maxwell's equations must be added to (3-1) and (3-2):

$$\nabla \times \underset{\sim}{E} = -\mu_o \, d_t \, \underset{\sim}{H} \tag{3-3}$$

$$\nabla \times \underset{\sim}{H} = \epsilon_o \, d_t \, \underset{\sim}{E} + \underset{\sim}{J}_e \tag{3-4}$$

where

$\underset{\sim}{J}_e$ $\equiv$ electric current source.

$\underset{\sim}{J}_e$ involves all electric current densities present, applied or induced. The interaction of plasma and EM field occurs through the quantities $\underset{\sim}{J}_e$ and ne $\underset{\sim}{E}$ in a self-consistent manner. Explicitly

$$\underset{\sim}{J}_e = \underset{\sim}{J}_{app} + \underset{\sim}{J}_c \tag{3-5}$$

where

$\underset{\sim}{J}_{app}$ $\equiv$ externally applied electric current

$\underset{\sim}{J}_c$ $\equiv$ electron convection current in plasma and is given by

$$\underset{\sim}{J}_c = -\, en\underset{\sim}{v} \quad . \tag{3-6}$$

Other contributions to $\underset{\sim}{J}_e$ (such as polarization, currents, drift currents due to plasma inhomogeneities, $\underset{\sim}{E} \times \underset{\sim}{H}$ drifts, etc; and conduction currents) will be neglected. Equations (3-1)-(3-6) form a determinate system of equations through which any interaction problem may be studied, once $\underset{\sim}{J}_{app}$ is specified.

Redefining the product $n\underset{\sim}{v}$ as a new variable:

$$\underset{\sim}{u} = n\underset{\sim}{v} \tag{3-7}$$

and considering n which is a function of space and time as composed of two parts: a time independent part or background and a time dependent part or fluctuating term:

$$n(\underset{\sim}{r}, t) = n_o + \tilde{n}(\underset{\sim}{r}, t) \tag{3-8}$$

where

n_o ≡ background electron density

$\tilde{n}$ ≡ time varying electron density

and $n_o \gg \tilde{n}$.

The system (3-1)-(3-6) simplifies to[39]:

$$d_t\tilde{n} + \nabla \cdot \underset{\sim}{u} = 0 \tag{3-9}$$

$$md_t\underset{\sim}{u} + \frac{m}{n_o} \nabla \cdot \underset{\sim}{u}\,\underset{\sim}{u} = -\,ne\,\underset{\sim}{E} - e\mu_o\underset{\sim}{u} \times \underset{\sim}{H}_o - m\nu_c\,\underset{\sim}{u} \tag{3-10}$$

$$\nabla \times \underset{\sim}{H} = \epsilon_o d_t \underset{\sim}{E} - e\underset{\sim}{u} + J_{app} \tag{3-11}$$

$$\nabla \times \underset{\sim}{E} = -\,\mu_o d_t \underset{\sim}{H} \tag{3-12}$$

To this set of equations, we also add

$$\epsilon_o \nabla \cdot \underset{\sim}{E} = -\,e(n - n_o) = -\,e\,\tilde{n} \tag{3-13}$$

and

$$\nabla \cdot \underset{\sim}{H} = 0 \tag{3-14}$$

Formally solving equations (3-10) to second order in $\tilde{\underset{\sim}{u}}$ (see Appendix 1) and using the results in eqs. 11; the system is reduced to:

$$\nabla \times \underset{\sim}{H} = \underset{\approx}{\epsilon} \cdot \underset{\sim}{E} + N(\underset{\sim}{E}) + J_{app} \tag{3-15a}$$

$$\nabla \times \underset{\sim}{E} = -\,\mu_o d_t \underset{\sim}{H} \tag{3-15b}$$

where $\underset{\approx}{\epsilon}$ is a linear operator given by:

$$\underset{\approx}{\epsilon} \rightarrow (\epsilon_o d_t \underset{\approx}{1} + e\,\underset{\approx}{\Pi})$$

and $N(\underset{\sim}{E})$ is a nonlinear term in $\underset{\sim}{E}$ given by:

$$N(\underset{\sim}{E}) \rightarrow \underset{\approx}{\Pi}\left(\frac{m}{n_o^2} \nabla \cdot \underset{\approx}{\Pi}\,\underset{\sim}{E}\,\underset{\approx}{\Pi}\,\underset{\sim}{E} - \frac{\epsilon_o}{n_o}\,\underset{\sim}{E}\,\nabla \cdot \underset{\sim}{E}\right)$$

with

$\underset{\approx}{1}$ ≡ unit dyad

and

$$\underline{\underline{\Pi}}\,(d_t, \mathbf{H}, \nu_c) \equiv \left(m\, d_t \underline{\underline{1}} - e\mu_o \mathbf{H}_o \times \underline{\underline{1}} + m\nu_c \underline{\underline{1}}\right)^{-1} e\, n_o$$

Decomposing the gradient operator as $\nabla = \nabla_t + d_z\, \mathbf{z}_o$, Eq 3-15 may be cast into a form appropriate for guided wave analysis[40]. Written in operator form:

$$(L + i\, d_z \Gamma)\psi = N(\psi) + i\, J_{a\,pp} \tag{3-16}$$

where, for $\rho < b$ (where b is the radius of the column)

$$L \rightarrow i \begin{pmatrix} -\epsilon_o d_t \underline{\underline{1}} - e\underline{\underline{\Pi}} & \nabla_t \times \underline{\underline{1}} \\ -\nabla_t \times \underline{\underline{1}} & -\mu_o d_t \underline{\underline{1}} \end{pmatrix} \qquad \boldsymbol{\psi}(\mathbf{r}, t) \begin{pmatrix} \mathbf{E} \\ \mathbf{H} \end{pmatrix} \tag{3-16a}$$

$$\Gamma \rightarrow \begin{pmatrix} 0 & -\mathbf{z}_o \times \underline{\underline{1}} \\ \mathbf{z}_o \times 1 & 0 \end{pmatrix} \qquad N(\psi) \rightarrow i \begin{pmatrix} N(\mathbf{E}) \\ 0 \end{pmatrix} \tag{3-16b}$$

for $\rho > b$, $n_o \rightarrow 0$ and the equations reduce to Maxwell's equation in free space.

Along with these defining equations, boundary conditions must be specified. These are:

For a column in free space

a) plasma boundary is assumed sharp

b) at $\rho = b$, tangential $\mathbf{E}$ and $\mathbf{H}$ fields are continuous

c) solutions must be finite everywhere

d) conditions at the source will be deferred until later

When the column is surrounded by conductor, the above conditions apply except that b) must be restated as: Tangential $\mathbf{E}$ and $\mathbf{H}$ fields are zero @ $\rho = b$.

Now we proceed to obtain a solution to the above posed problem. As a matter of convenience, the source term in Eq. 3-16 will be dropped until the time it needs to be considered to interpret the experimental results.

Taking Fourier transform in time of 3-16, one obtains:

$$L(-i\omega, \nabla_t)\, \psi(\mathbf{r}, \omega) + i\,\Gamma d_z\, \psi(\mathbf{r}, \omega) = N[\psi(\mathbf{r}, \omega)] \tag{3-17}$$

where the transformed operators are obtained from Equations 3-17 by recognizing that $\partial_t \rightarrow -i\omega$ in the transform domain and that the transform of a product is the convolution of the individual transform (see Appendix 1).

We shall seek solutions of the problem in the form of an expansion in terms of the eigenfunctions of the transverse, lossless operator L_0, where $L_0 = L\big|_{\nu_c = 0}$. Assume that $\psi(r, \omega)$ lies in the space spanned by the transverse, lossless eigenvectors; moreover, that the operators in Eq.(3-17) act on this space. Then $\psi(r, \omega)$ may be represented as:

$$\psi(r, \omega) = \sum_{\alpha} \mathcal{a}_{\alpha}(z, \omega)\, \psi_{\alpha}(r, \omega) \tag{3-18}$$

where the eigenvalue problem for the ψ_α is defined:

$$L_o(-i\omega, \nabla_t)\, \psi_\alpha = \kappa_\alpha(\omega)\, \Gamma \psi_\alpha \tag{3-19}$$

the eigenvectors ψ_α possess the orthogonality property

$$(\psi_\alpha, \Gamma \psi_\beta) = \delta_{\alpha\beta} \tag{3-19a}$$

Using this property of the ψ_α's, the amplitudes in Eq. (3-18) are found to be given by:

$$\mathcal{a}_\alpha = (\psi, \Gamma \psi_\alpha) \tag{3-20}$$

where ψ is the actual nonlinear, lossy field. The equation for determining the co-efficients $\mathcal{a}_\alpha$ may then be obtained as follows: Scalar multiply Eq (3-17) by ψ_α and (3-19) by ψ and subtract:

$$(\psi_\alpha, L\psi) - (\psi, L_o\psi_\alpha) + i\,\partial_z(\Gamma\psi, \psi_\alpha) + \kappa_\alpha(\omega)(\Gamma\psi_\alpha, \psi)\,[N(\psi), \psi_\alpha]$$

or

$$[\psi_\alpha\,(L-L_o)\psi] + i\,\partial_z(\psi, \Gamma\psi_\alpha) + \kappa_\alpha(\omega)\,(\psi, \Gamma\psi_\alpha) = [N(\psi), \psi_\alpha]$$

identifying $(L-L_o)$ as the loss operator ν, using Eq. (3-20) and then replacing $\psi(\rho, \omega)$ by the expansion Eq. (3-18), we obtain for the amplitudes:

$$i\partial_z \mathcal{Q}_\alpha(z,\omega) + \kappa_\alpha(\omega)\mathcal{Q}_\alpha(z,\omega) + i\gamma(\omega)\mathcal{Q}_\alpha(z,\omega) = i[\underset{\approx}{\Xi}_\alpha, N(\mathcal{Q}_\alpha \underset{\sim}{\Xi})] \tag{3-21}$$

where $\gamma(\omega) \equiv (\psi_\alpha, \underset{=}{\nu}\, \psi_\alpha)$

Thus, the solution of the field problem is cast into a study of the evolution in z of the modal amplitudes. To arrive at an explicit form, we must evaluate the two inner products involved. To do this, an explicit form for the eigenvectors, ψ_α, must be obtained. Keeping in mind that the goal is in the analysis of the experimental results, we are interested in obtaining a set of eigenvectors to represent the guided field produced by an electric current source directed along $\underset{\sim}{z}_o$ and independent of θ. These are obtained in Appendix 2, for both $\underset{\sim}{H}_o \neq 0$, and $H_o = 0$. The results are summarized below:

For zero magnetic field, the discrete spectrum contains a single eigenvector and the corresponding eigenvalue, i.e., $\alpha = 1$. The properly normalized eigenvector, i.e., normalized as in Eq. (3-19a), is given in component form:

$$E_{\alpha\rho} = \begin{cases} (\kappa_\alpha(\omega)/\omega\epsilon_o)^{1/2}(1/2\beta)^{1/2} \dfrac{I_1(\kappa_{\perp 1}\rho)}{\kappa_{\perp 1}} & \rho < b \\[2ex] (\kappa_\alpha(\omega)/\omega\epsilon_o)^{1/2}(1/2\beta)^{1/2} \dfrac{I_0(\kappa_{\perp 1}b)}{K_0(\kappa_{\perp 2}b)} \dfrac{K_1(\kappa_{\perp 2}\rho)}{\kappa_{\perp 2}} & \rho > b \end{cases} \tag{3-22a}$$

$$H_{\alpha\theta} = \begin{cases} (\omega\epsilon_o/\kappa_\alpha(\omega))^{1/2}(1/2\beta)^{1/2}(1-\omega_p^2/\omega^2) \dfrac{I_1(\kappa_{\perp 1}\rho)}{\kappa_{\perp 1}} & \rho < b \\[2ex] (\omega\epsilon_o/\kappa_\alpha(\omega))^{1/2}(1/2\beta)^{1/2} \dfrac{I_0(\kappa_{\perp 1}b)}{K_0(\kappa_{\perp 2}b)} \dfrac{K_1(\kappa_{\perp 1}\rho)}{\kappa_{\perp 2}} & \rho > b \end{cases} \tag{3-22b}$$

$$E_{\alpha z} = \begin{cases} i(1/\omega\epsilon_o\kappa_\alpha(\omega))^{1/2}(1/2\beta)^{1/\alpha} I_0(\kappa_{\perp 1}\rho) & \rho < b \\[2ex] i(1/\omega\epsilon_o\kappa_\alpha(\omega))^{1/2}(1/2\beta)^{1/2} \dfrac{I_0(\kappa_{\perp 1}b)}{K_0(\kappa_{\perp 2}b)} K_0(\kappa_{\perp 2}\rho) & \rho > b \end{cases} \tag{3-22c}$$

I_1, I_0, K_0, K_1, are the modified Bessel functions of the given order, $\kappa_{\perp 1}$, $\kappa_{\perp 2}$ and the eigenvalue $\kappa(\omega)$ (the α may be dropped from the eigenvalue; however, it will be retained on the eigenvector so as to differentiate it from the total field) are related as follows:

$$\kappa_{\perp 1}^2 = \kappa^2 - (1 - \omega_p^2/\omega^2)\,\kappa_0^2 \tag{3-23a}$$

$$\kappa_{\perp 1}^2 = \kappa^2 - \kappa_0^2 \qquad \kappa_0^2 = \omega^2 \mu_o \epsilon_o \tag{3-23b}$$

$$(1 - \omega_p^2/\omega^2)\,\frac{I_1(\kappa_{\perp 1} b)}{\kappa_{\perp 1}^2 I_o(\kappa_{\perp 1} b)} + \frac{K_1(\kappa_{\perp 2} b)}{\kappa_{\perp 2} K_o(\kappa_{\perp 2} b)} = 0 \tag{3-23c}$$

For low Magnetic fields ($\omega_c < \omega_p$), column surrounded by conductor, we make the assumption that the waves are slow and therefore are primarily of a TM type.[8] The exact eigenvectors are then approximated by the quasi-static eigenvectors:

$$E_{\alpha_z} = iAJ_o(\kappa_{\perp 1} \rho) \tag{3-24a}$$

$$E_{\alpha_\rho} = A\kappa_\alpha \frac{\epsilon_3}{\epsilon_1}\,\frac{J_1(\kappa_{\perp 1} \rho)}{\kappa_{\perp 1}} \tag{3-24b}$$

$$H_{\alpha_\theta} = A\omega \epsilon_o \epsilon_3 \,\frac{J_1(\kappa_{\perp 1} \rho)}{\kappa_{\perp 1}} \tag{3-24c}$$

Where J_o, J_1 are the Bessel function of the first kind,

$$\epsilon_3 = \epsilon_o \left[1 - \frac{\omega_p^2}{\omega^2 - \omega_c^2}\right], \quad \epsilon_1 = 1 - \frac{\omega_p^2}{\omega^2}, \quad \kappa_{\perp 1}^2 = -\kappa_2^2 \frac{\epsilon_3}{\epsilon_1} \text{ and } \kappa_{\perp 1} b = p_n \tag{3-24d}$$

p_n is the nth zero of J_o. The normalization constant is given (from Eq. 3-19a) by:

$$A = \frac{\kappa_{\perp 1}}{(\omega\kappa_\alpha\epsilon_o/\epsilon_1)^{1/2}\,\epsilon_3 b J_1(\kappa_{\perp 1} b)} \tag{3-25}$$

In the limit of large magnetic fields; i. e. $\omega_c/\omega >> 1$, $\omega_c/\omega_p >> 1$; the eigenvectors are obtained from the exact equations and are given by:

$$E_{\alpha_z} = iA' J_o(\kappa_{\perp 1}\rho) \tag{3-26a}$$

$$E_{\alpha_\rho} = A' \frac{\kappa_\alpha \epsilon}{\kappa_{\perp 1}} J_1(\kappa_{\perp 1}\rho) \tag{3-26b}$$

$$H_{\alpha_\theta} = A' \frac{\omega\epsilon_o\epsilon}{\kappa_{\perp 1}} J_1(\kappa_{\perp 1}\rho) \tag{3-26c}$$

where

$$\kappa_{\perp 1}^{\ 2} = \epsilon(\omega^2\mu_o\epsilon_o - \kappa_\alpha^2) \qquad \epsilon = 1 - \omega_p^2/\omega^2$$

$$\kappa_{\perp 1} b = p_n$$

and the normalization constant given by:

$$A' = \frac{\kappa_{\perp 1}}{(\omega\kappa_\alpha\epsilon_o)^{1/2}\,\epsilon b J_1(\kappa_{\perp 1} b)} \tag{3-27}$$

For completeness, the properly normalized eigenvectors for the case of a column in free space with an infinite magnetic field present are also derived in Appendix 2, but not reproduced here.

Using these eigenvectors, the various terms in equation 3-21 can be evaluated explicitly. Expanding the various inner product, the amplitude equation may be rewritten as:

$$i d_z \mathcal{a}_\alpha(z,\omega) + \kappa_\alpha(\omega)\mathcal{a}_\alpha(z,\omega) + i\gamma(\omega)\mathcal{a}_\alpha(z,\omega)$$

$$= \int_{-\infty}^{\infty} \mathcal{L}(\omega,\omega_1,\omega_2)\,\mathcal{a}_\alpha(z,\omega_1)\ \mathcal{a}_\alpha(z,\omega_2)\,\delta(\omega-\omega_1-\omega_2)\,d\omega_1 d\omega_2 \tag{3-28}$$

where $\mathcal{L}(\omega,\omega_1,\omega_2)$ is the Kernel of the integral operator. The effects of collisions have been neglected in R.H.S. $\gamma(\omega)$ and $\mathcal{L}(\omega,\omega_1,\omega_2)$ are given by (see Appendix 3):

For zero magnetic field, column in free space,

$$\mathcal{L} \rightarrow \frac{e\epsilon_o}{m}\frac{\omega_p^2}{\omega_1\omega_2}\int_o^b [P(\omega,\omega_1,\omega_2,\rho) - W(\omega,\omega_1,\omega_2,\rho)]\,\rho d\rho \tag{3-29}$$

where

$$P(\omega,\omega_1,\omega_2,\rho) = \left(\frac{\kappa(\omega_1)\kappa(\omega_2)\kappa(\omega)}{\omega_1\omega_2\omega\,\epsilon_0^3 2^3\beta^1\beta^2\beta^o}\right)^{1/2} \frac{I_1'^{(2)}}{\kappa_{\perp 1}^{(2)}}\ \frac{I_1'^{(0)}}{\kappa_{\perp 1}^{(2)}}\ \frac{I_1'^{(2)}}{\kappa_{\perp 1}^{(1)}} \tag{3-29a}$$

$$W(\omega,\omega_1,\omega_2,\rho) = \kappa(\omega_1)\left(\frac{\kappa(\omega_1)\kappa(\omega)}{\kappa(\omega_2)\omega_1\omega_2\omega\,\epsilon_o^3 2^3\beta\ \beta^1\beta^2}\right)^{1/2} I_0^{(2)}\frac{I_1^{(0)}}{\kappa_{\perp 1}^{(0)}}\frac{I_1^{(1)}}{\kappa_{\perp 1}^{(0)}}$$

$$+\left(\frac{\kappa(\omega_2)}{\kappa(\omega_1)\kappa(\omega)\omega_1\omega_2\omega\,\epsilon_o^3 2^3\beta\ \beta^1\beta^2}\right)^{1/2}\left[I_0^{(1)}\,I_0^{(2)}\,I_0^{(0)} - \frac{I_1^{(2)}}{\kappa_{\perp 1}^{(2)}}\,I_0^{(0)}\right] \tag{3-29b}$$

$f^{(i)} \rightarrow f(\omega_i)$ $i = 0, 1, 2;$ $\omega_o \equiv \omega$, and the prime denotes $\frac{d}{d\rho}$ and

$$\gamma(\omega) = \frac{\omega_p^2\nu}{\omega^2+\nu^2}\ \frac{\kappa\ (\omega)}{\omega\, 2\,\beta}\left\{\int_o^b \frac{I_1^2(\kappa_{\perp 1}\rho)}{\kappa_{\perp 1}^2}\rho d\rho + \int_o^b \frac{I_o^2(\kappa_{\perp 1}\rho)}{\kappa_\alpha^2}\rho d\rho\right\}$$

For small axial magnetic fields, column surrounded by a conductor:

$$\mathcal{L} \to \frac{-e\epsilon_o}{m}\left[\left(2 - \frac{\omega_p^2}{\omega_p^2+\omega_c^2}\right)\frac{\omega_p^2}{\omega\,\omega_1\,\omega_2} + \frac{\omega_p^2\,\omega_c^2}{\omega\,\omega_1^2\quad(\omega_p^2+\omega_c^2)}\right]$$

$$\kappa_\alpha(\omega_1)A(\omega_1)\,A(\omega_2)\,A(\omega)\int_o^b J_o^3(\kappa_{\perp 1}\,\rho)\;\rho\;d\;\rho \tag{3-30}$$

this form of $\mathcal{L}$ is obtained by using the assumption that the maximum contribution to the nonlinear term is due to the coupling of the longitudinal component of the total field. This is consistent with the quasi-static assumption (see Appendix 3). When the axial field goes to infinity,

$$\mathcal{L} \to \frac{-e\epsilon_o}{m}\left[\frac{2\,\omega_p^2}{\omega\,\omega_1\,\omega_2} + \frac{\omega_p^2}{\omega\,\omega_1^2}\right]\kappa_\alpha(\omega_1)\,A'(\omega_1)\,A'(\omega)\,A'(\omega_\alpha)$$

$$\int_o^b J_o^3(\kappa_{\perp 1}\,\rho)\rho\;d\;\rho \tag{3-31}$$

Note that equation 3-30 reduces to the above equation in the limit $\omega_c \to \infty$.

The collision term is given by:

$$\gamma(\omega) \to \int_o^b\left[A^2(\omega)\,J_o^2(\kappa_{\perp 1}\,\rho)\;\rho\;d\;\rho\right]\frac{\omega_p^2\,\nu\,\epsilon_o}{\omega^2+\nu^2} \tag{3-32}$$

The above forms of $\mathcal{L}$ and γ apply for the column in free space, with an infinite axial magnetic field present. However the proper normalization $A(\omega)$ must be used (see Appendix 2).

To continue the analysis, the functional dependence of κ_α on ω must be obtained.

3.2 Functional relation between κ_α and ω

a) No axial magnetic field:

Since there is only one mode present, the functional relationship may be obtained from equations (2-23). This set of equations is

transcendental and an explicit solution for κ_α in terms of ω is impossible. Computer solution of these equations is shown in figure 3.2. In order to carry analytical methods further so as to gain insight into the phenomena, an approximate analytical function of ω will be used for κ_α. The approximation is derived from the behavior of κ_α in equations 2.23 for large and small ω.

For $\omega \to 0$, equation (2-23c) reduces to:[16]

$$- (\kappa_\alpha^2 b^2 - \kappa_o^2 b^2) \ln (\kappa_\alpha^2 b^2 - \kappa_o^2 b^2)^{1/2} = Kp \frac{I_o(Kp)}{I_1(Kp)} \frac{\omega^2}{\omega_p^2}$$

where $Kp = \dfrac{\omega_p b}{c}$ $\kappa_o = \dfrac{\omega}{c}$ $c \equiv$ speed of light.

Equation (2-23c) may be further reduced to

$$\kappa_\alpha = \left(Kp \frac{I_o(Kp)}{I_1(Kp)} + \frac{\omega_p^2 b^2}{2c^2} \right)^{1/2} \frac{\omega}{\omega_p} \tag{3-33}$$

thus for $\omega \to 0$, κ_α and ω are linearly related. Moreover, for $\omega \to \omega_p/\sqrt{2}$, a resonance is observed. The appropriate choice of approximate equation must take cognizance of these facts. Such a choice is given by:

$$\kappa_\alpha^2 = \frac{\omega^2}{v_o^2} \left(\frac{1}{1-2\ \omega^2/\omega_p^2} \right) \tag{3-34}$$

where

$$v_o^2 = \omega_p^2 b^2 \left(Kp \frac{I_o(Kp)}{I_1(Kp)} + \frac{\omega_p^2 b^2}{2c^2} \right)^{-1} .$$

the values of κ_α obtained from (3-34) were compared with those obtained by computer solution of equations (3-23) and (3-34). The values of v_o obtained for a best fit were:

$$v_o = \begin{cases} (.5163422)\ \omega_p b & \text{for 14 point fit} \\ (.67165)\ \omega_p b & \text{for 21 point fit} \end{cases} \tag{3-34a}$$

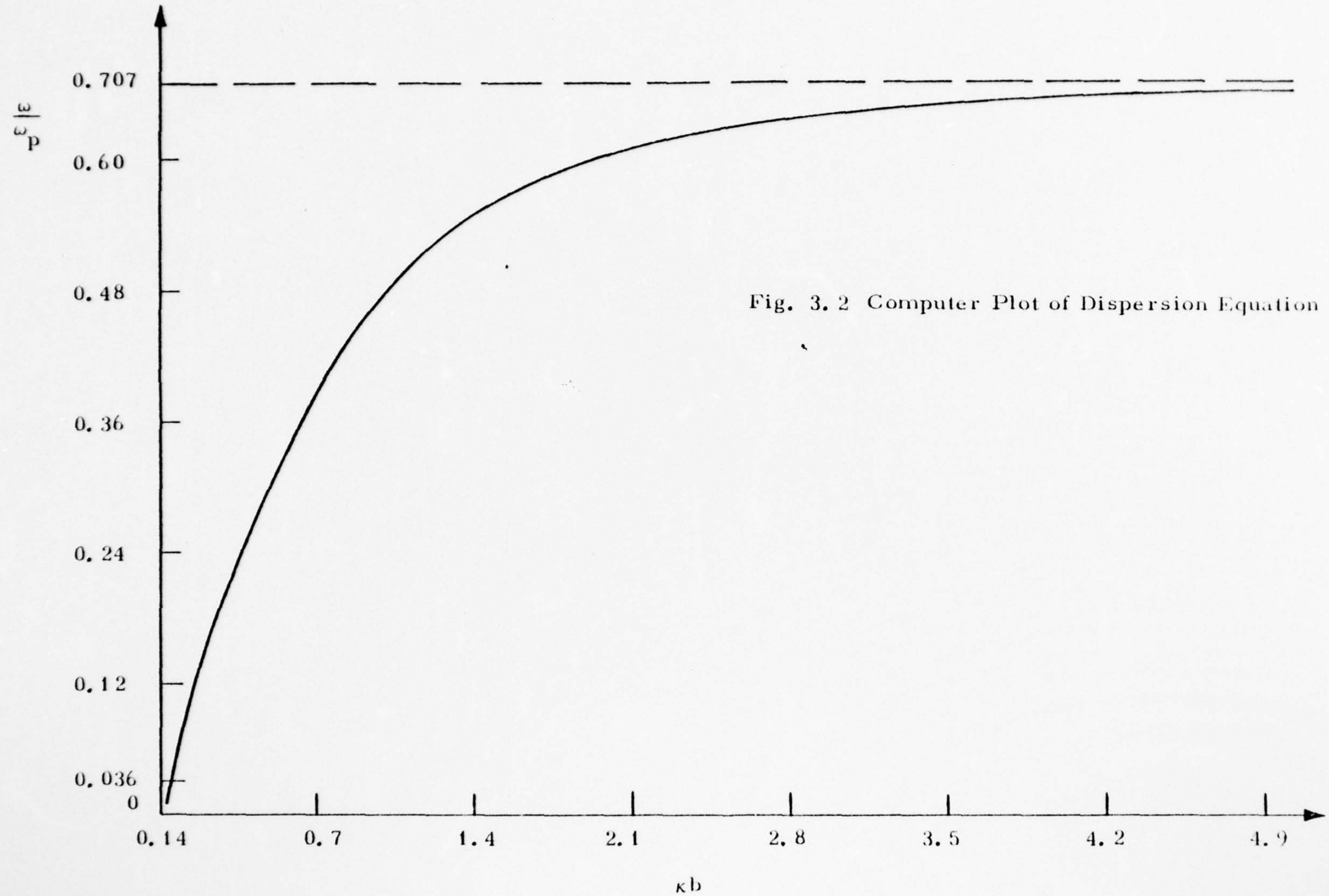

Fig. 3.2 Computer Plot of Dispersion Equation

Since for the range of interest $\omega < \omega_p$; equation (3-34) may be expanded as:

$$\kappa_\alpha = \frac{\omega}{v_o}\left(1 + \omega^2/\omega_p^2\right) \tag{3-35}$$

where only the positive mode will be considered. Equation (3-35) is the desired relationship for the no static magnetic field case.

b) Weak magnetic fields; column surrounded by conductor

From equation (2-24d); solving for the propagation constant[8]

$$\kappa_\alpha^2 = \left(\frac{p_n}{b}\right)^2 \left[\frac{-\omega^2(\omega^2 - \omega_p^2 - \omega_c^2)}{(\omega^2 - \omega_p^2)(\omega^2 - \omega_c^2)}\right] \tag{3-36}$$

For $\omega_c < \omega_p$, the low frequency passband of equation (3-36) is similar to equation (3-34), except that resonance now occurs at ω_c. For $\omega < \omega_c < \omega_p$ and fixing on modes moving in direction $z > 0$; equation (3-36) may be approximated by an equation similar to (3-35) as:

$$\kappa_\alpha(\omega) = \kappa_n(\omega) = \frac{\omega}{v_s}\left(1 + 1/2\,\omega^2/\omega_c^2\right) \tag{3-37}$$

where $$v_s = \frac{b}{p_n}\frac{\omega_p \omega_c}{(\omega_p^2 + \omega_c^2)^{1/2}}$$

When the magnetic field goes to infinity, κ_α is given by:

$$\kappa_\alpha^2 = \kappa_o^2 - \frac{\kappa_\perp^2}{[1 - \omega_p^2/\omega^2]}$$

again, in the region of interest, i.e. slow waves, the above becomes:

$$\kappa_\alpha^2 = \frac{\kappa_\perp^2 \omega^2/\omega_p^2}{(1 - \omega^2/\omega_p^2)}$$

or

$$\kappa_\alpha = \kappa_n(\omega) = \frac{\omega}{v_\infty}(1 + 1/2\, \omega^2/\omega_p^2) \tag{3-38}$$

Where $v_\infty = \omega_p/\kappa_\perp$ and $\kappa_\perp = p_n/b$. (3-38a)

By equations (3-35), (3-37) and (3-38), the coefficients that appear in the amplitude equation (3-28) have been explicitly defined. In the next section the final form of the amplitude equation is obtained.

3.3 Final Form of Amplitude Equation

Using the approximate relations, derived in 3.2, between κ_α and ω; Eq. (3-28) may be written in its final form.

A. No Magnetic Field:

Using Eq. (3-35), Eq. (3-3a), and the results of Appendix 3 in Equation (3-28), we finally obtain for the modal amplitude:

$$i\, d_z \mathcal{a}_\alpha(z,\omega) + \left(-\frac{\omega}{v_o} + \frac{\omega^3}{v_o \omega_p^2}\right) \mathcal{a}_\alpha(z,\omega) + i\, \frac{\nu_c}{v_o}\, \mathcal{a}_\alpha(z,\omega)$$

$$= C_1 \int_o^\Omega \omega_1 \omega_2 \omega\, \mathcal{a}_\alpha(z,\omega_2)\, \mathcal{a}_\alpha(z,\omega_1)\, d\lambda + C_2 \int_o^\Omega \omega_1^2 \omega\, \mathcal{a}_\alpha(z,\omega_1)\, \mathcal{a}_\alpha(z,\omega_2)\, d\lambda$$

$$+ C_3 \int_o^\Omega \omega_2 \omega_1^2\, \mathcal{a}_\alpha(z,\omega_1)\, \mathcal{a}_\alpha(z,\omega_2)\, d\lambda + C_4 \int_o^\Omega \omega_2\, \mathcal{a}_\alpha(z,\omega_2)\, \mathcal{a}_\alpha(z,\omega_1)\, d\lambda \tag{3-39}$$

where: $d\lambda \rightarrow \delta(\omega - \omega_1 - \omega_2)\, d\omega_1\, d\omega_2$

$$C_1 = \frac{e}{m}\, \frac{b}{2^5} \left\{ \frac{1}{\omega_p^2 v_d^6 v_o^3 \epsilon_o} \right\}^{1/2} \tag{3-39a}$$

$$C_2 = -\frac{e}{m}\, \frac{b}{2^4} \left\{ \frac{1}{\omega_p^6 v_d^6 v_o \epsilon_o} \right\}^{1/2} \tag{3-39b}$$

$$C_3 = +\frac{e}{m}\, \frac{b}{2^4} \left\{ \frac{\omega_p^2}{\omega_p v_d^6 v_o^3 \epsilon_o} \right\}^{1/2} \tag{3-39c}$$

$$C_4 = -\frac{e}{m}\, \frac{1}{2b} \left\{ \frac{v_o}{\omega_p^2 v_d^6 \epsilon_o} \right\}^{1/2} \tag{3-39d}$$

and v_d is given in appendix 3.

Multiplying by -i, and recognizing that $-i\omega \rightarrow \partial_t$, the above equation transforms to the time domain as,

$$d_z \mathcal{a}_\alpha(z,t) + \frac{1}{v_o} d_t \mathcal{a}_\alpha(z,t) - \frac{1}{v_o \omega_p^2} d_t^3 \mathcal{a}_\alpha(z,t) + \frac{\nu_c}{v_o} \mathcal{a}_\alpha(z,t) = C_1 \partial_t \left(d_t \mathcal{a}_\alpha(z,t)\right)^2$$

$$+ C_2 d_t (\mathcal{a}_\alpha d_t^2 \mathcal{a}_\alpha) + C_3 d_t^2 \mathcal{a}_\alpha(z,t) d_t \mathcal{a}_\alpha(z,t) + C_4 \mathcal{a}_\alpha(z,t) d_t \mathcal{a}_\alpha(z,t).$$

Expanding the R.H.S. of the above and collecting terms:

$$d_z \mathcal{a}_\alpha(z,t) + \frac{1}{v_o} d_t \mathcal{a}_\alpha(z,t) - \frac{1}{v_o \omega_p^2} d_t^3 \mathcal{a}_\alpha(z,t) + \frac{\nu_c}{v_o} \mathcal{a}_\alpha(z,t)$$

$$= C_1' d_t \mathcal{a}_\alpha(z,t) d_t^2 \mathcal{a}_\alpha(z,t) + C_2 \mathcal{a}_\alpha d_t^3 \mathcal{a}_\alpha + C_4 \mathcal{a}_\alpha d_t \mathcal{a}_\alpha \qquad (3\text{-}40)$$

where $C_1' = 2C_1 + C_2 + C_3$

this equation is the final form of the amplitude equation. It holds for times such that $\mathcal{a}_\alpha(z,\omega) = 0$ for $\omega > \Omega$. Moreover, the linear damping term must be modified for cases where $\mathcal{a}_\alpha(z,\omega) \neq 0$ for $\omega \leq \nu_c$ These implications will be discussed in section 3.4.

B. Infinite Magnetic Field.

The final form of the modal amplitude equation for this case is obtained using equations (3-31), (3-38) and the results of appendix 3 in equation (3.28). Note that from Appendix 3, it has been assumed that only a single mode (the lowest order) is propagating i.e., the α's reduce to only one. For the case of a metal conductor surrounding the plasma column,

$$i d_z \mathcal{a}_\alpha(z,\omega) + \left(\frac{\omega}{v_\infty} + \frac{\omega^3}{2 v_\infty \omega_p^2}\right) \mathcal{a}_\alpha(z,\omega) + i C_c \mathcal{a}_\alpha(z,\omega)$$

$$= C_4' \int_0^\Omega \omega_1 \mathcal{a}_\alpha(z,\omega_1) \mathcal{a}_\alpha(z,\omega_2)\, d\lambda \qquad (3\text{-}41)$$

where $$C_4' = \frac{3e}{m}\left(\frac{k_\perp}{b}\right)^3 \frac{1}{\omega_p^4} \sqrt{\frac{v_\infty}{\epsilon_o}} \; \frac{\int_0^b J_0^3(k_\perp \rho)\rho\, d\rho}{J_1^3(k_\perp b)}$$

and C_c given in Appendix 3.

since $\int_0^b J_0^3(k_\perp \rho)\, d\rho = .72\, b^2/2\, J_1^2(kb)$

$$C_4' = 1.08\ \frac{e}{m}\ \frac{k_\perp^3}{b}\ \frac{1}{\omega_p^4}\ \sqrt{\frac{v_\infty}{\epsilon_o}}\ \frac{1}{J_1(k_\perp b)}$$

multiplying by -i and transforming into time domain:

$$d_z \mathcal{A}_\alpha(z,t) + \frac{1}{v_\infty}\ d_t \mathcal{A}_\alpha(z,t) - \frac{1}{2v_\infty \omega_p^2}\ d_t^3 \mathcal{A}_\alpha(z,t) + C_c \mathcal{A}_\alpha(z,t)$$

$$= C_4^f\ \mathcal{A}_\alpha(z,t)\, d_t \mathcal{A}_\alpha(z,t) \qquad (3\text{-}42)$$

when there is no conducting wall present, the constant C_4^f above is given by:

$$C_4^f = \frac{3}{2}\ \frac{e}{m}\ \frac{}{\omega_p v_\infty^3 b}\ \sqrt{\frac{v_\infty}{\epsilon_o}} \qquad (3\text{-}43)$$

where v_∞ is given by: (3-38a)

Equation (3-28) is a Kortweg-de Vries equation with a damping term for the modal amplitude. It is valid only up to times when the frequency spectrum of $\mathcal{A}_\alpha(z,t)$ contain frequencies close to ω_p.

C. Weak Magnetic Field, column surrounded by a perfect waveguide.

The derivation follows the same fashion as that leading to equation (3-41) (see Appendix 3), with the exception that the constant coefficients are different. From eqs. (3-30), for the nonlinear term; equation (3-37) for the dispersion relation and (3-25) for the normalization constant, we have from appendix 3:

$$d_z \mathcal{A}_\alpha(z,t) + \frac{1}{v_s}\ d_t \mathcal{A}_\alpha(z,t) - \frac{1}{2v_s \omega_c^2}\ d_t^3 \mathcal{A}_\alpha(z,t)$$

$$= C_4'' \mathcal{A}_\alpha(z,t)\, d_t \mathcal{A}_\alpha(z,t) \qquad (3\text{-}44)$$

where C_c = collision coefficient and is approximately given by (3-39)

$$C_4'' = \frac{e}{m}\left(\frac{k_\perp}{b}\right)^3 \frac{\sqrt{(\omega_p^2+\omega_c^2)^3}}{\omega_p^4\omega_c^3} \sqrt{\frac{v_s}{\epsilon_o}} \frac{\int_0^b J_o^3(k_\perp\rho)\,d\rho}{J_1^3(k_\perp b)}$$

$$C_4'' = .36\,\frac{e}{m}\,\frac{k_\perp^3}{b}\,\frac{\omega_c}{\omega_p^4}\sqrt{\frac{v_s}{\epsilon_o}}\,\frac{1}{J_1(k_\perp b)}\,\frac{\sqrt{(\omega_p^2+\omega_c^2)^3}}{\omega_c^3}$$

Equation (3-44a) is also a Kortweg-de Vries equation for the model amplitude. For this case, it is valid up to times when the frequency spectrum of $\mathcal{a}_\alpha(z,t)$ contain frequencies close to the Cyclotron frequency, ω_c.

3.4 Analysis of the Amplitude Equation

Comparing the magnitude of the terms on the right hand side of equation (3-39), we find that the last term [the term whose coefficient is C_4] is the dominant one. From equation 6-37of Appendix 3, observe that this term arises from the nonlinear coupling of the longitudinal electric field of waves of different frequencies. Since, from equations (2-21), the magnitude of the longitudinal field is greater than the transverse field, it is expected that the strongest nonlinearity would result from interactions involving only the longitudinal components of the field. Neglecting the other two terms in the R. H. S. of (3-39), the resulting equation has the same form as equation (3-42), i. e., Eq. (3-39) reduces to the K-de V equation.

Thus the evolution in z of the modal amplitudes is described by an equation of the K-de V type. This results in the recognition that propagation of large amplitude slow waves and surface waves along a plasma column belong to a very general class of nonlinear wave phenomena, i. e., nonlinear dispersive waves. It is important to note that the sign of the nonlinear term in (3-42) is opposite to the corresponding one in (3-39). This difference results in qualitatively different behavior of the solution which will be discussed in the next section.

Noting from Equation (3-18) that, since for each case we are only considering a single mode, the field solution is:

$$\psi(\underset{\sim}{\rho}, t; z) = \int_{-\infty}^{\infty} \mathcal{A}_\alpha(z, \omega)\, \psi_\alpha(\rho, \omega) e^{-i\omega t}\, \frac{d\omega}{2\pi}$$

where $\mathcal{A}_\alpha(z, \omega)$ and $\psi_\alpha(\rho, \omega)$ are given by Eqs. (3-39) and (3-22) respectively, for surface waves and by Eqs. (3-24) and (3-42) respectively for body waves. In particular, for the longitudinal electric field of the waves:

$$E_z(\rho, \omega; z) = \mathcal{A}_\alpha(z, \omega)\, E_\alpha(\rho, \omega)$$

Putting in the value for $E_\alpha(\rho, \omega)$ for either case, we find in the regime $\kappa_\perp b < 1$

$$E_z(\rho, \omega; z) \sim \text{const} \cdot i\omega\, \mathcal{A}_\alpha(z, \omega) \tag{3-45a}$$

or from inversion:

$$E_z(\rho, t; z) \sim -\text{const}\ \partial_t \mathcal{A}_\alpha(z, t). \tag{3-45b}$$

This result is very convenient since it allows the solution of Eqs. (3-42) or (3-39) to be immediately associated with the longitudinal electric field of the wave. Thus the Modal Amplitude acts as a potential whose time derivative is proportional to the longitudinal E field.

Rewriting equations (3-42) and (3-39) as

$$\partial_z \mathcal{A}_\alpha(z, t) + \frac{1}{v_i} \partial_t \mathcal{A}_\alpha(z, t) - C_d \partial_t^3 \mathcal{A}_\alpha(z, t) + C_c' \mathcal{A}_\alpha(z, t) - C_4''' \mathcal{A}_\alpha(z, t)\, \partial_t \mathcal{A}_\alpha(z, t) = 0 \tag{3-46}$$

where

$$v_i = \begin{cases} v_o & \underset{\sim}{B}_o = 0 \\ v_\infty & \underset{\sim}{B}_o = \infty \\ v_s & \text{Weak } B_o \end{cases}$$

$$C_d = \begin{cases} 1/\omega_p^2 v_o & \text{No magnetic field} \\ 1/2\omega_p^2 v_\infty & \text{Infinite magnetic field} \\ 1/2 v_s \omega_c^2 & \text{Weak magnetic field} \end{cases}$$

$$C_c' = \begin{cases} \nu_c/v_o & \text{No magnetic field} \\ \left.\begin{matrix} C_{c_1} \\ \\ C_{c_2} \end{matrix}\right\} & \text{Infinite Magnetic field} \begin{cases} \text{column surrounded by perfect conductor} \\ \text{column in free space} \end{cases} \\ C_{c_3} & \text{Weak magnetic field} \end{cases}$$

$$
C_4^{\prime\prime} = \begin{cases} -\dfrac{1}{2}\dfrac{e}{m}\sqrt{\dfrac{v_o}{\epsilon_o}}\dfrac{1}{v_d^3} & \text{No magnetic field} \\[2ex] \dfrac{3}{2}\dfrac{e}{m}\dfrac{1}{v_d^3}\sqrt{\dfrac{v_\infty}{\epsilon_o}} & \text{Infinite magnetic field; column in free space} \\[2ex] 1.08\,\dfrac{e}{m}\dfrac{k_\perp^3}{b}\dfrac{1}{\omega_p^4}\sqrt{\dfrac{v_\infty}{\epsilon_o}}\dfrac{1}{J_1(k_\perp b)} & \text{Infinite magnetic field; column surrounded by perfect conductor} \\[2ex] \dfrac{.36}{\omega_c^3}\dfrac{e}{m}\dfrac{k_\perp^3}{b}\dfrac{(\omega_p^2+\omega_c^2)^{3/2}}{\omega_p^3}\sqrt{\dfrac{v_s}{\epsilon_o}}\dfrac{1}{J_1(k_\perp b)} & \text{Weak magnetic field} \end{cases}
$$

With the observation made in (3-45), Equation (3-46) may be used as the starting point for the study of pulse propagation, of limited band-width and finite amplitude, along a plasma column with infinite axial magnetic field, or with a weak magnetic field, respectively. Ikezey et al[34], using quasi-static approximation derived a K-de-V Equation for the evolution in time of the potential of an electron acoustic wave propagating in a cylindrical plasma column in an infinite magnetic field and surrounded by a perfect conductor.

The K-de-V equation can be obtained for other kinds of plasma waves, for example ion waves in a cold plasma for the case $\omega_{ce} >> \omega_{pe}$ [41] hydromagnetic waves[42], and for other wave phenomena[43]. For a comprehensive survey of K-de-V literature see [44].

As previously pointed out we could not operate the experiment in the regime $\omega_{ce} >> \omega_{pe}$. Results were obtained only for $\omega_{ce} = 0$ and $\omega_{ce} < \omega_{pe}$. Even though the dispersion relation for symmetric body waves in the regime $f_{ce} < f_{pe}$ can be approximated by an equation of the form (3-37), the structure of the properly normalized and exact eigenvectors is rather complex and is not amenable to analytical manipulation. The coupling coefficients in the equations for the modal amplitudes (more than one mode has to be considered[16]) would not be simple functions of frequency, and numerical solution would have been

inevitable. By properly approximating the exact eigenvectors, the coupling coefficients in the modal amplitude equations could be simplified, and the analytical result in the form of Equation (3-46) was then possible.

Since no attempt is made here to solve the K-de-V equation either analytically or numerically the equation for the modal amplitude will be subsequently normalized so that the results obtained by others[42] may be used to enable us to rephrase the results obtained in Chapter III.

Introducing new variables, and restricting ourselves to experimental conditions:

$$\widehat{\mathcal{A}}_\alpha(z,t) = \begin{cases} +\,\omega_p b\,|C_4'''|\,\mathcal{A}_\alpha(z,t) & \text{No magnetic field} \\ -\,\omega_c b\,|C_4'''|\,\mathcal{A}_\alpha(z,t) & \text{Weak magnetic field} \end{cases} \tag{3-47a}$$

$$z' = \begin{cases} \dfrac{z}{b} & \text{No magnetic field} \\ \dfrac{z}{b} & \text{Weak magnetic field} \end{cases} \tag{3-47b}$$

$$t' = \begin{cases} \omega_p(t - z/v_o) & \text{No magnetic field} \\ \omega_c(t - z/v_s) & \text{Weak magnetic field} \end{cases} \tag{3-47c}$$

We obtain from (3-46) and (3-47):

$$\partial_{z'}\widehat{\mathcal{A}}_\alpha(z',t') + b\,C_c'\,\widehat{\mathcal{A}}_\alpha(z',t')\,\partial_{t'}\widehat{\mathcal{A}}_\alpha(z',t') - \alpha'\partial^3_{t'}\,\widehat{\mathcal{A}}_\alpha(z',t') = 0 \tag{3-48}$$

$$\text{where } \alpha' = \begin{cases} \omega_p b/v_o & \text{No magnetic field} \\ \omega_c b/2v_s & \text{Weak magnetic field} \end{cases}$$

Equation (3-48) is in the "standard form" (neglecting the collision term) discussed by Berezin and Karpman[42]. They investigated the evolution, for different values of α', of a disturbance at $z = 0$, radiated for a bounded time interval Δ, i.e., given $\hat{\mathcal{Q}}_\alpha(0, t') \sim \phi(t'/\Delta)$. How does $\hat{\mathcal{Q}}_\alpha(z', t')$ depend on Δ and α, if $\hat{\mathcal{Q}}_\alpha(z', t')$ evolves as in (3-48).

The boundary condition for (3-48) may be obtained from the experiment as follows: from figure 2-7, as the BBG pulse propagates in the parallel plate structure, part of its energy is coupled to a radiation field, part to a plasma guided field and the rest is dissipated by the termination. The amount of energy that goes into each type depends on how well the parallel plate couples to that mode. Even though we measured the coupling of energy by the parallel plate structure to the guided field as a function of frequency, an absolute measurement on the percentage of energy of the initial pulse that goes into the guided field could not be done. The unnormalized modal amplitude at $z = 0$, i.e., $\mathcal{Q}_\alpha(0, t)$ is related to the longitudinal electric field component of guided field, excited by the pulse, by equation (3-45a), and therefore from equation (3-45b):

a) No magnetic field:

$$\partial_{t'} \hat{\mathcal{Q}}_\alpha(0, t') = -\frac{1}{2}\left(\frac{e}{m}\,\frac{b}{v_o^2}\right) E_z(b, 0, t') \qquad (3\text{-}49)$$

Note that the factor in parenthesis has the dimensions of (coul-sec^2)/(kg-cm) or of (electric field)$^{-1}$ as it should. Since

$v_o = \omega_p b(.67165)$:

$$\partial_{t'} \hat{\mathcal{Q}}_\alpha(0, t') = -1.9503 \times 10^{n} \; \frac{1}{\omega_p^2 b}\, E_z(b, 0, t') \qquad (3\text{-}50)$$

with

ω_p in sec^{-1}

b in cm

E_z in $\frac{\text{kg-cm}}{\text{Coul-sec}^2}$

$E_z(b, 0, t')$ is the longitudinal field, evaluated at the boundary of the column of the "already set up" guided field at $z = 0$. It is not the actual BBG pulse. However, since the field is applied for a finite amount of time, we expect that the guided field at $z = 0$ also possess this characteristic in time, but as mentioned before, its absolute strength is unknown.

b) Weak magnetic field

From (3-24), $E_z(\rho, 0, \omega) \sim \widehat{E}_z(0, \omega)\, J_o(k_\perp \rho)$

$$\partial_{t'} \widehat{\mathcal{A}}_\alpha(0, t') = +(3.664 \times 10^{n})\, \frac{\omega_p^2 + \omega_c^2}{\omega_p^2\, \omega_c^2\, b}\, \widehat{E}_z(0, t') \tag{3-51}$$

Looking into the physical consequences of the above theory, let us first consider the linearized equation obtained from (3-48) when the nonlinear term, $\widehat{\mathcal{A}}_\alpha \partial_{t'} \widehat{\mathcal{A}}_\alpha$, is neglected. The resulting equation is the Airy equation with a damping term

$$\partial_{z'} \widehat{\mathcal{A}}_\alpha(z', t') + b\, C_c' \widehat{\mathcal{A}}_\alpha(z', t') - \alpha' \partial_{t'}^3 \widehat{\mathcal{A}}_\alpha(z', t') = 0$$

whose solution is:

$$\widehat{\mathcal{A}}_\alpha(z', t') = \int_{-\infty}^{\infty} \widehat{\mathcal{A}}_\alpha(\omega)\, e^{i(\kappa(\omega) z' - \omega t')}\, \frac{d\omega}{2\pi} \tag{3-52}$$

with

$$\kappa(\omega) = \alpha' \omega^3 - ib\, C_c'$$

and the normalized amplitude $\widehat{A}_\alpha(\omega)$ is given in terms of the boundary condition (3-50) or (3-51):

$$\widehat{A}_\alpha(\omega) = \frac{1}{(-i\omega)} \int_{-\infty}^{\infty} (\text{const})\, E_z(0, t)\, e^{i\omega t}\, dt$$

and from (3-45), we get for the actual guided field:

$$E_z(z', t') = \int_{-\infty}^{\infty} (\text{const})\, E_z(0, \omega)\, e^{i[\kappa(\omega) z' - \omega t')}\, \frac{d\omega}{2\pi}$$

or

$$E_z(z', t') = (\text{const})\, e^{-bC_c'z'} \int_{-\infty}^{\infty} G(z', t'-t'')\, E_z(0, t')\, dt'' \tag{3-53}$$

with

$$G(z', t') = \frac{1}{(3\alpha' z')^{1/3}}\, \mathrm{Ai}\left(-\frac{-t'}{(3\alpha' z')^{1/3}}\right)$$

where

$$\mathrm{Ai}(x) = \frac{1}{2\pi} \int_{-\infty}^{\infty} e^{i(\tau^3/3 + x\tau)}\, d\tau$$

Since the initial width of the applied signal is sufficiently small, then for large z', $G(z', t')$ is a slow varying function, and the solution (3-53) of the linearized equation can be written in the following form[42]:

$$E_z(z', t') \sim (\text{const})\, \frac{e^{-bC_c'z'}}{(3\alpha' z')^{1/3}}\, \mathrm{Ai}\left(-\frac{t'}{(3\alpha' z')^{1/3}}\right) \quad \text{for large } z' \tag{3-54}$$

E_z does not depend on the character of the initial radiation as long as its width is small. However, for small z', the solution depends strongly on the boundary condition. The solution (3-54) represents a wavepacket moving away from the launcher with the first peak moving with velocity v_o for $\underset{\sim}{B}_o = 0$, and v_s for $\underset{\sim}{B}_o \neq 0$. The packet spreads and its amplitude is reduced as it moves. Figure 3-3 shows a plot of the velocity of the first peak as a function of plasma parameters, i.e., ω_p and ω_c. The solution (3-54) is discussed further in Chapter III in relation to the experimental results.

Next, for the full nonlinear equation, the nonlinear parameter σ[42] provides a measure for the nonlinear effects. To compute σ for typical experimental conditions, assume the boundary conditions for Eq. (3-48) to be given at $z = 0 + \Delta z$, i.e., a few centimeters to the right of the launching plates. Placing the receiving plates close to the launcher, we observe a wave packet of four oscillations extended over an interval of time τ. Thus, take as the boundary condition for $\hat{a}_\alpha(z', t')$ a function of the type:

$$\hat{a}_\alpha(\Delta z', t') = +a_o\, \phi(t'/\tau\omega_i) \tag{3-55}$$

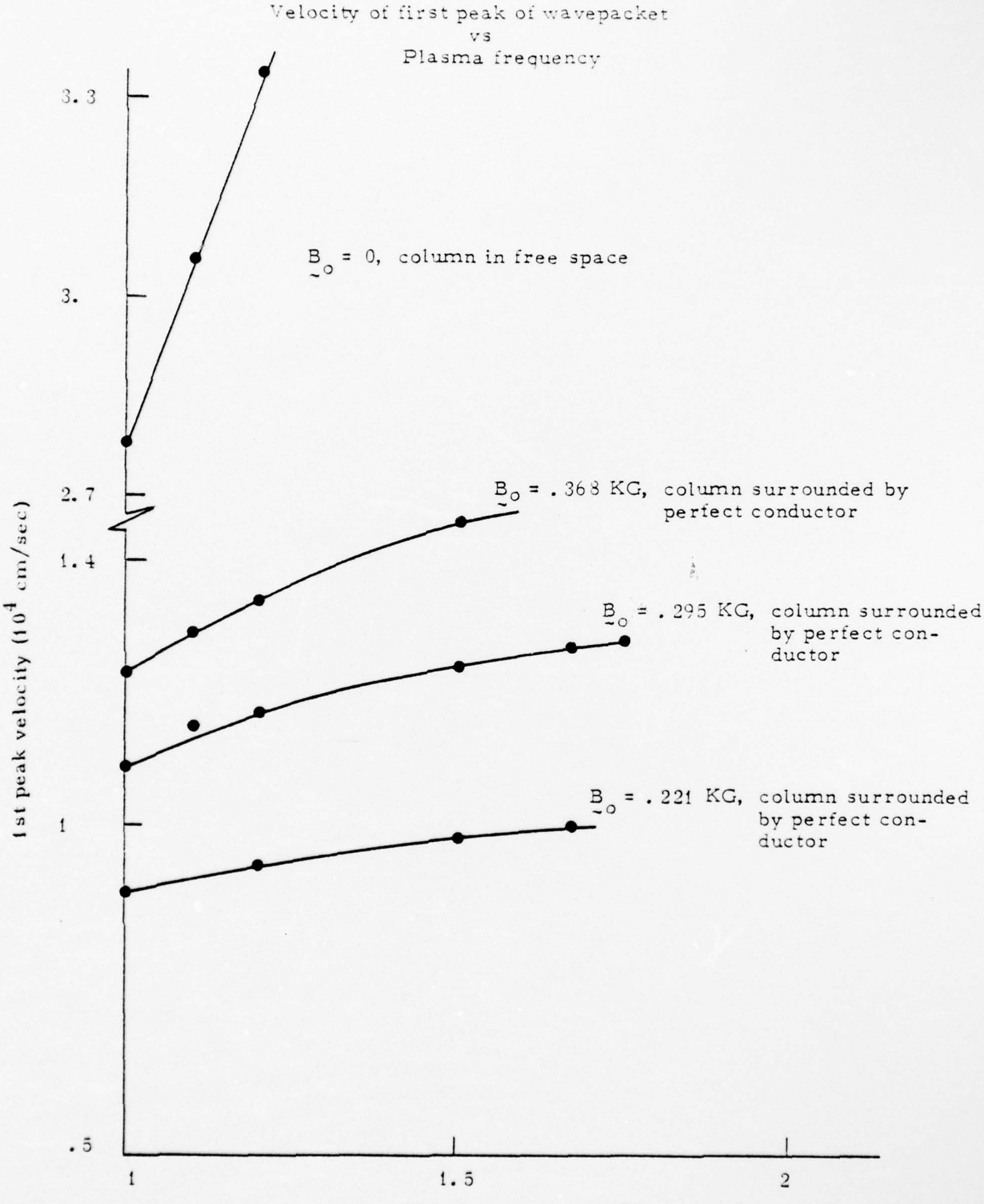
Velocity of first peak of wavepacket
vs
Plasma frequency
3.3
3.
2.7
1.4
1
.5
1
1.5
2
B_o = 0, column in free space
B_o = .368 KG, column surrounded by perfect conductor
B_o = .295 KG, column surrounded by perfect conductor
B_o = .221 KG, column surrounded by perfect conductor
1st peak velocity (10^4 cm/sec)
Plasma frequency (GHz)

Fig. 3.3

where

$$\mathcal{a}_o = \begin{cases} A' \; (1.9503 \times 10^{15}) \; (1/\omega_p^2 b) & B_o = 0 \\ B' \; (3.66 \times 10^{15}) \; \dfrac{\omega_p^2 + \omega_c^2}{\omega_c^2} \; (1/\omega_p^2 b) & B_o \neq 0 \end{cases} \qquad (3\text{-}56a)$$

and

$$\omega_i = \begin{cases} \omega_p & B_o = 0 \\ \omega_c & B_o \neq 0 \end{cases}$$

A' and B' are unknown constant amplitudes in volts/cm which depend on how well the BBG pulse couples to the mode field. From [42],

$$\sigma = \frac{\omega_i \, \tau \sqrt{\mathcal{a}_o}}{\sqrt{\alpha}}$$

Putting in for $\mathcal{a}_o$ and α':

For $\underset{\sim}{B}_o = 0$:

$$\sigma = 4.455 \times 10^7 \; \tau \sqrt{A'} \qquad (3\text{-}57)$$

For $\underset{\sim}{B}_o \neq 0$:

$$\sigma = 7.4467 \times 10^7 \; \tau \left(\frac{\omega_p^2 + \omega_c^2}{\alpha' \omega_p^2} \right)^{1/2} \sqrt{B'}$$

Taking widths of the order of 5 nonsec., $\omega_p \sim 10.49 \times 10^9$ rad/sec., $\omega_c \sim 5.18 \times 10^9$ rad/sec and $\alpha \sim 1.4$ (see figure 3-4 for the behavior of α):

$$\sigma = \begin{cases} .222 \sqrt{A'} & \underset{\sim}{B}_o = 0 \\ .365 \sqrt{B'} & \underset{\sim}{B}_o \neq 0 \end{cases} \qquad (3\text{-}59)$$

From numerical solutions of the K-de-V equation, it is known[42] that a critical $\sigma = \sigma_c = \sqrt{12}$ exists in the sense that qualitatively different solutions are obtained for $\sigma >> \sigma_c$ and $\sigma << \sigma_c$ [42]. For $\sigma > \sigma_c$,

α Parameter
vs
Plasma frequency

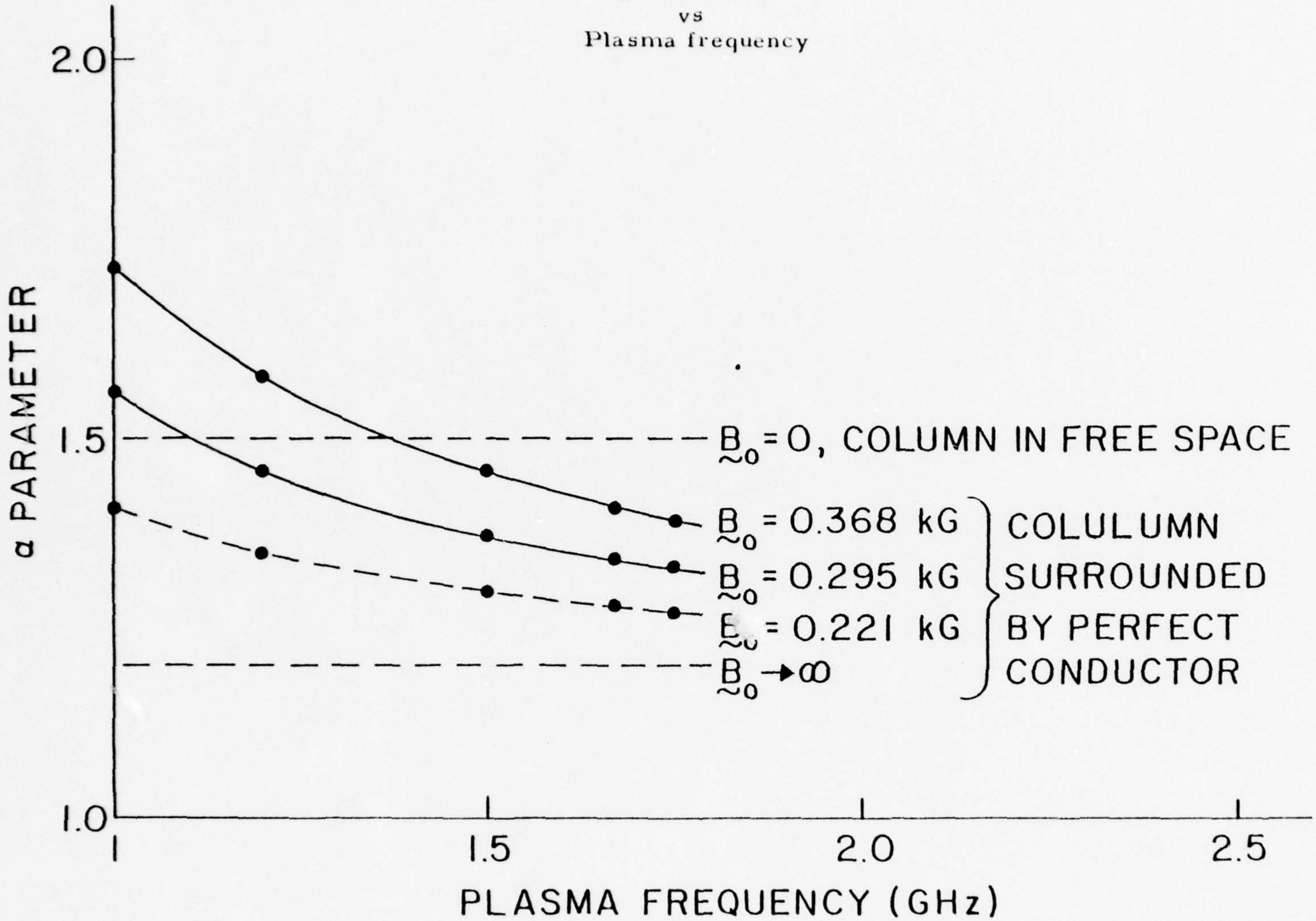

Figure 3.4

nonlinear stationary solutions of the "solitary type" are permissible, whereas for $\sigma < \sigma_c$ "nonsolitary" solutions corresponding to rapidly-oscillating wave packets are obtained.

Experimentally, the maximum field amplitude available at the plates (due to the 4.4 dB attenuation of the 60 nansec. delay line) is 1.92 kilovolts/cm. Even though absolute field amplitude of the excited wave is unknown, i.e., A' or B', the first nonlinear effects which begin to be observed is in the region $\sigma < \sigma_c$. Therefore in the first assessment of nonlinear effects, we proceed as in [45] by expanding the solution of the K-de-V and the wave number as:

$$\widehat{\mathcal{A}}_\alpha(z, t) = \epsilon\, \widehat{\mathcal{A}}_1(\theta) + \epsilon^2\, \widehat{\mathcal{A}}_2(\theta) + \ldots$$

$$\kappa_\alpha(\omega) = \kappa_o(\omega) + \epsilon\, \kappa_1(\omega) + \epsilon^2\, \kappa_2(\omega) + \ldots \qquad (3\text{-}60)$$

where

$$\theta = \kappa_\alpha\, z - \omega t \quad \text{and } \epsilon = \epsilon\,(\widehat{\mathcal{A}}_\alpha).$$

and $\kappa_1(\omega)$ is chosen to be zero to avoid a secular expression of $\widehat{\mathcal{A}}_\alpha$.

In a straightforward fashion, we obtain for the coefficients of the expansion:

$$\widehat{\mathcal{A}}_1 = \cos\theta \qquad \widehat{\mathcal{A}}_2 = -\frac{1}{12\, Cd\, \omega_p\, b\, \omega^2} \cos 2\theta$$

$$\kappa_o(\omega) = \frac{1}{v_i}\,\omega + Cd\,\omega^3 \qquad (3\text{-}61)$$

$$\kappa_2(\omega) = \frac{1}{24\, Cd\, \omega_p^2\, b^2\, \omega}$$

The critical difference between these results and the linear results in equation (3-52) is the dependence of the dispersion equation on the amplitude. The specific consequence of this observation is that the characteristics of the modulation equations[45] become doubly degenerate, i.e., it predicts the eventual splitting of a wave packet into two separate ones propagating with characteristic velocities given by:

$$C_+ = \frac{1}{\kappa_o'(\omega) + \dfrac{a_o}{2\omega_p b}} \quad \text{for the slow wavepacket} \tag{3-62}$$

$$C_- = \frac{1}{\kappa_o'(\omega) - \dfrac{a_o}{2\omega_p b}} \quad \text{for the fast wavepacket.}$$

where a_o is the normalized amplitude of the nonuniform wavetrain, and $\kappa_o'(\omega) = \frac{\omega}{d\omega}\kappa_o$. Using these velocities, we can get an upper estimate as to the distance away from the source at which this separation can be observed:[45]

$$z = \frac{C_+ \; C_-}{C_+ - C_-} \; \tau$$

or using (3-62):

$$z = \frac{\omega_c \, b \, \tau}{-2 a_o}$$

For weakly magnetic field, from equations (3-47) and (3-56a): Note that for surface waves we obtain a negative value for z. The consequence of this result is discussed in the next chapter.)

$$z = \frac{\omega_c^3 \, b^2}{3.66 \times 10^{15}} \; \frac{\omega_p^2}{\omega_p^2 + \omega_c^2} \; \frac{\tau}{2B'}$$

For the typical experimental parameter previously considered:

$$z = \frac{2.06 \times 10^3}{2B'} \; \tau \tag{3-63}$$

thus for a wavepacket of actual field strength of 50 volts/cm, separation of approximately 3 nansec. will result at 61 cm away from the boundary.

These results are used in the analysis of the experimental observations which are discussed next.

IV. Results

In light of the analytical results derived in chapter III, the data obtained using the apparatus described in chapter II will be subsequently presented and analyzed. The results for the no anial magnetic field case are presented in section 4.1; and in section 4.2, the results for the weak axial magnetic field case are presented. As previously mentioned, there are two fundemental differences between these two cases:

1. Even though a Kortweg-de Vries type equation describes the evolution in space-time of a given disturbance, different qualitative results will be obtained in both cases for the same excitation. This is due to the fact that the signs of the nonlinear terms (or of the normalized initial distribution in Eq. 3-46) are opposite. In interpreting the results of this chapter, it is important to note that the Electric field at the launching plate points in the - $\underset{\sim}{z}$ direction for what has been referred to as the positive pulse in the preciding chapters.

2. The coupling structures used for either case were different. The set up shown in Fig. 2-5 was used for the no magnetic field case, where as for the weak magnetic field, the set up is shown in Fig. 2-7. In the latter case, the addition of the brass rings allowed for the pulsed field to be directly coupled to the plasma, improving the launching efficiency for the body waves. For $\underset{\sim}{B}o = O$, surface waves were strongly excited without the need of the brass rings. For these waves, the fields are concentrated at the plasma boundary.

Each of the above sections, i.e., 4.1 and 4.2, are divided into two subsections. The low amplitude or linear results are presented in the first subsection; while in the second subsection, we present the finite amplitude or nonlinear results.

4.1 Zero Axial Magnetic Field

4.1.1 Linear Regime

For experiments in this regime, the peak pulse electric field at the launching plates was kept below 192 Volts/cm. At these field levels, the integral solution, equation (3-53), obtained in section 3.4 is valid. From this equation, the mechanism that affects the propagation of the pulse is dispersion.

The vital experimentally controlled parameters which appear in the solution (3-53) are: the background neutral pressure (i.e. collision fre-

quency), initial pulse polarity, plasma frequency and plasma column radius. As a matter of organization, the effect of each of the above parameters on the propagation of the pulse will be sequentially presented and quantitatively compared to the solution (3-53).

Pressure effects had no particular quantitative interest to us except from the point of view of being able to launch the waves. Due to the increase with pressure of electron-neutral collision, it was difficult to launch the waves as illustrated in the sequence of Fig. 4.1. High attenuation, column striations, and loss of statistical sampling coherence are the factors responsible for this behavior. For the rest of the experiments, the pressure was kept at a point where collision related effects had the least influence on the wavepacket characteristics.

The effect, in this regime, of pulse polarity is trivial: it merely changes the sign of the solution (3-53). In Fig. (4.2a), we display oscillogram in time obtained at $z = 56$ cm for the "positive" pulse and in Fig. (4.2b) for the "negative" pulse. Figure 4.2b is just the negative of Fig. 4.2a. The polarity of the first oscillation is as predicted from the solution (3-54). Quantitative differences in the freguency of oscillation and amplitude are due to slight differences in plasma frequency and initial pulse characteristics. In Fig. a, the "positive" pulse generator produces, at the launching plates, an Electric field pulse in the negative z direction, its strength is approximately 192 volts/cm and its duration is approximately 1 nanosecond. The "negative" generator, in the other hand, produces a field in the positive z direction and its duration is approximately .5 nanosecond. The seemingly reverse naming comes from the fact that the labeling is appropriate for the voltage of the front plate with respect to the ground plate. The evolution in space of the initial disturbance is shown in Fig. 4.3. The a) sequence corresponds to the positive pulse whereas the b) sequence correspond to the negative pulse. This sequence is explained, in terms of equation (3-53) as follows: at $z = o$, the launcher position, a wave is radiated for a bounded time interval. As the pulse travels to the right, i.e., $z > 0$, it rapidly breaks into oscillations due to strong dispersive effects. Since the dispersion is negative, the long wavelength are observed to propagate at a higher speed.

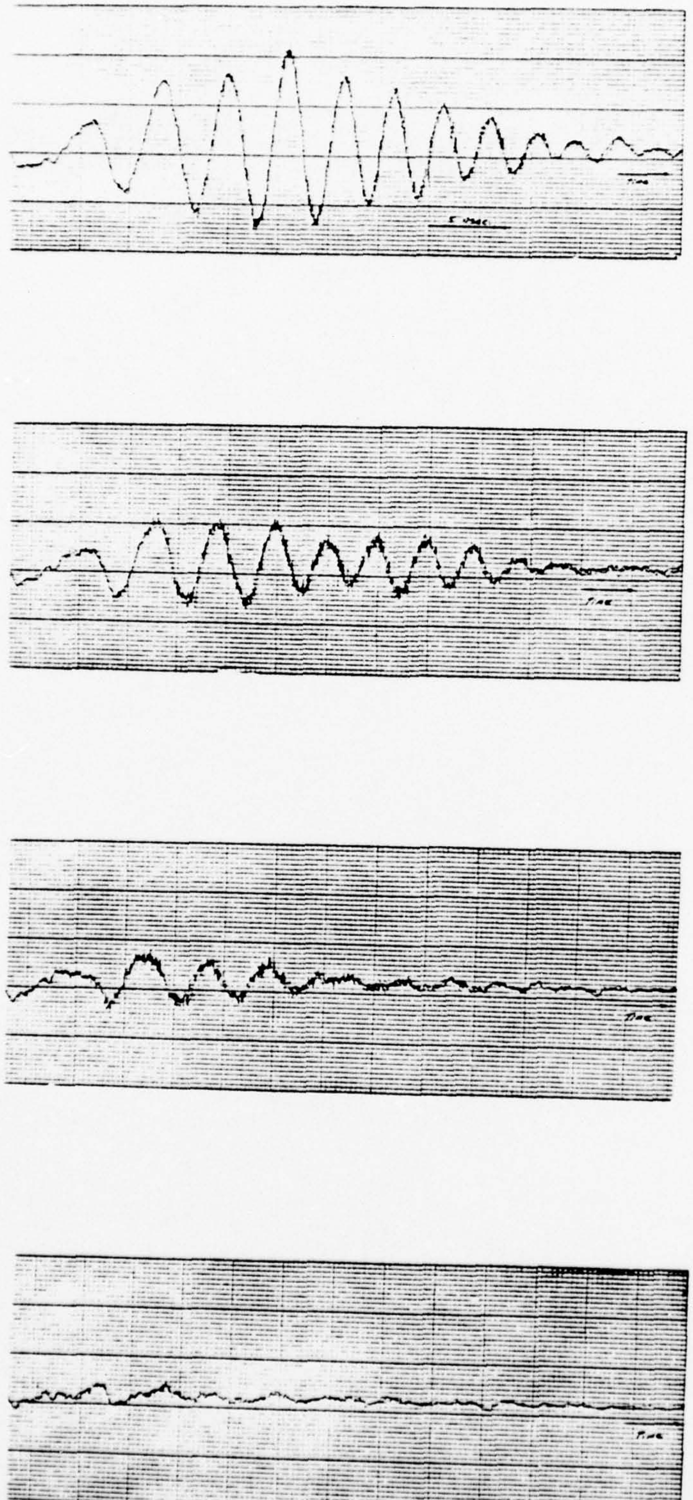

Pressure = 1 μ

Pressure = 5 μ

Pressure = 10 μ

Pressure = 20 μ

Fig. 4.1 Effect of pressure

Figures 4.4 a, b, and c show oscillograms in time for different positions of the receiver. The part of the oscillogram marked with an A corresponds to free space electromagnetic radiation propagating at the speed of light. This radiation is observed even if the plasma were not present (see Fig. 4.2). From these curves, we again observe the negative dispessive properties of the system. This property is further displayed by fourier analyzing the wave forms of Fig. 4.4. From the relation

$$\Delta t \, \Delta\omega \sim 1$$

where Δt = spread of the wavepacket in time

$\Delta\omega$ = spread in frequency

Thus, as the packet propagates and spreads in time due to dispersion, its fourier transform becomes narrower. This is displayed in Fig. (4.5).

As the averaged plasma frequency is changed, the packet characteristics, are also observed to change. The speed of propagation, frequency of oscillation, width of the packet and the normalized amplitude increase as a function of f_p. Time oscillograms for various averaged plasma frequencies are shown in Figure (4.6). Figure (4.7) shows a plot of the velocity of the first peak of the wavepacket as a function of plasma frequency. Two different methods were used to calculate this velocity. The first uses the fact that the first observed disturbance corresponds to the free space electromagnetic radiation travelling at the speed of light. By comparing the time of arrival at the point of observation, of the first peak of the wavepacket with respect to the EM signal, the speed of propagation is obtained. The second method uses the time of flight of the first peak between two points. Also plotted in Figure (4.7) is equation (3-34a). As was pointed out in section 3.4, the speed of propagation of the first peak is given by v_o. The experimental values differ from the theoretical by 20%. This difference lies in the manner that v_o was obtained, i.e. by numerically fitting the solution of the dispersion relation to equation (3-34a). In Equation (3-34a), 14 points were used to determine the low frequency or linear slope of equation (3-34a), i.e., v_o. If fewer points are used, a large v_o is obtained (see equation (3-34b) for example) and a better approximation to the propagation speed.

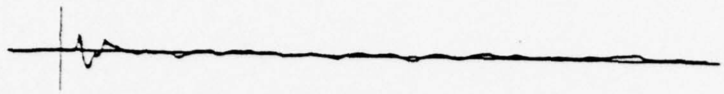

NO PLASMA

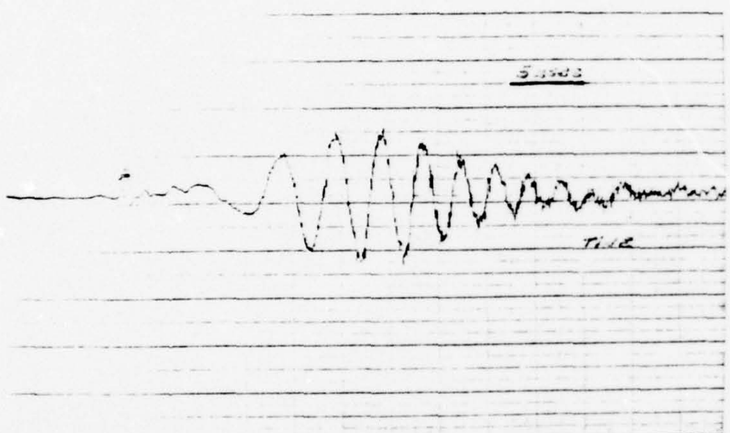

a) "positive" pulse

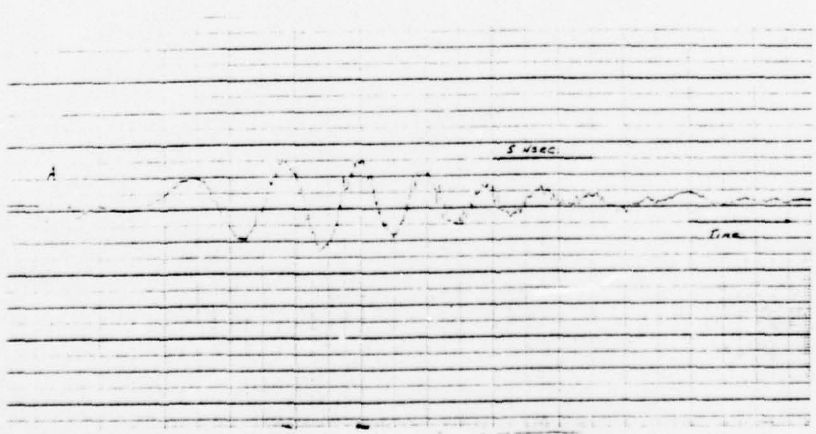

b) "negative" pulse

Fig. 4.2 Effect of polarity of input pulse

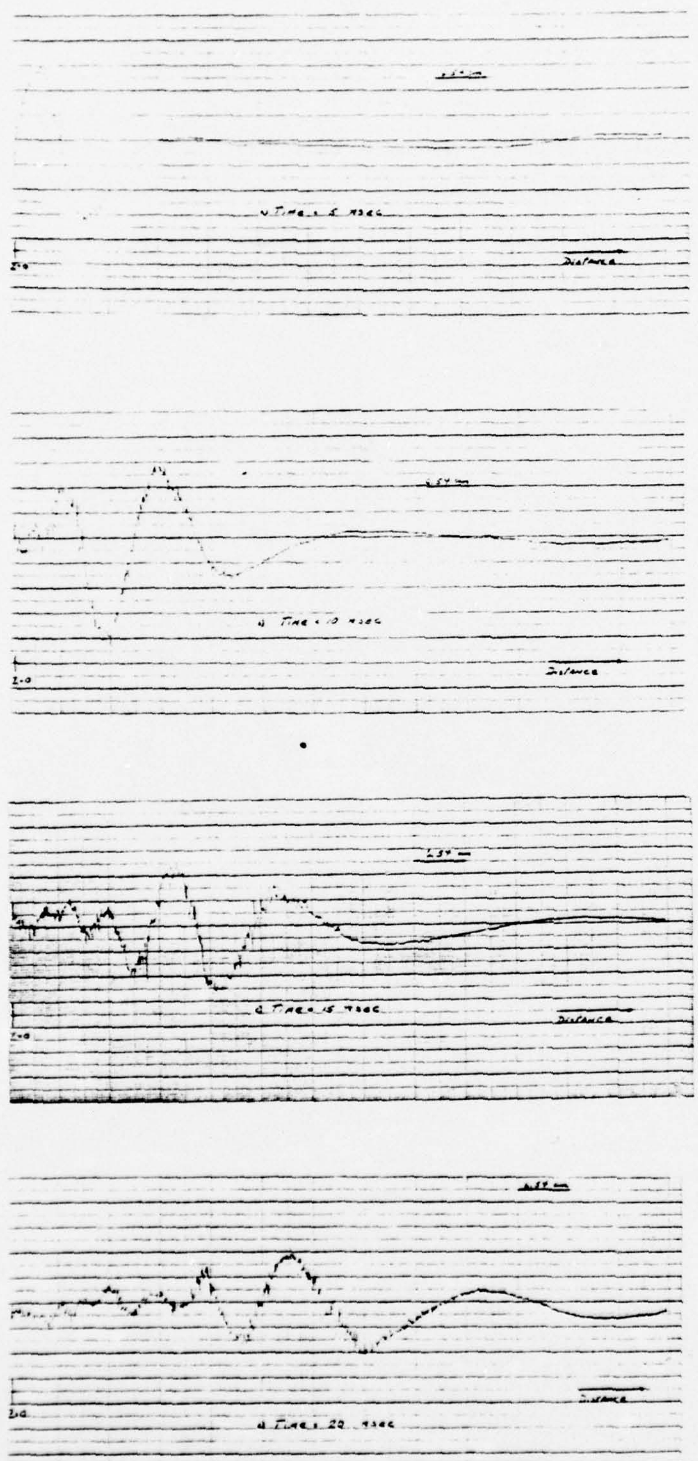

time = 5 nsec.

time = 10 nsec.

time = 15 nsec.

time = 20 nsec.

Fig. 4.3 Evolution in space of initial disturbance
a) "positive" pulse

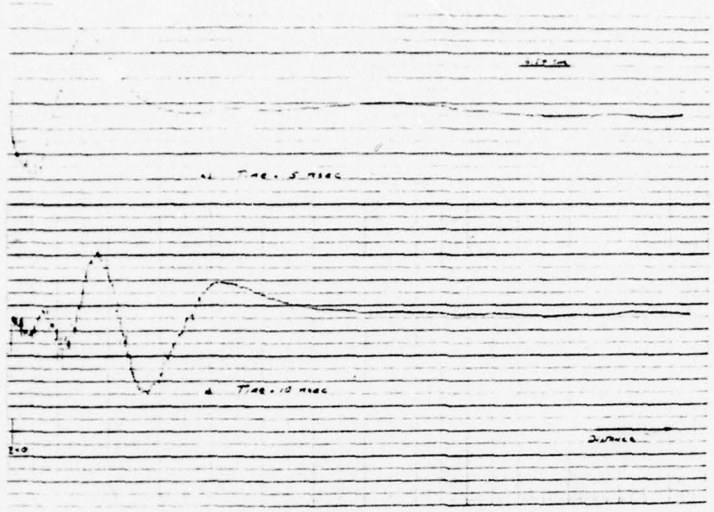

time = 5 nsec

time = 10 nsec

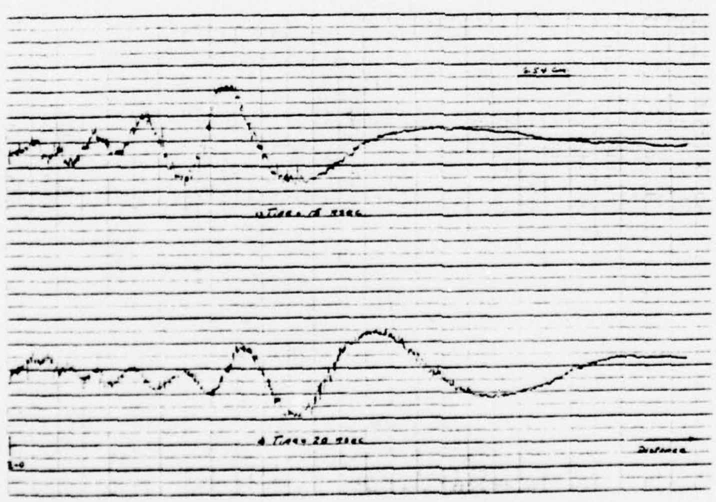

time = 15 nsec

time = 20 nsec

Fig. 4.3 Evolution in space of initial disturbance
b) "negative" pulse

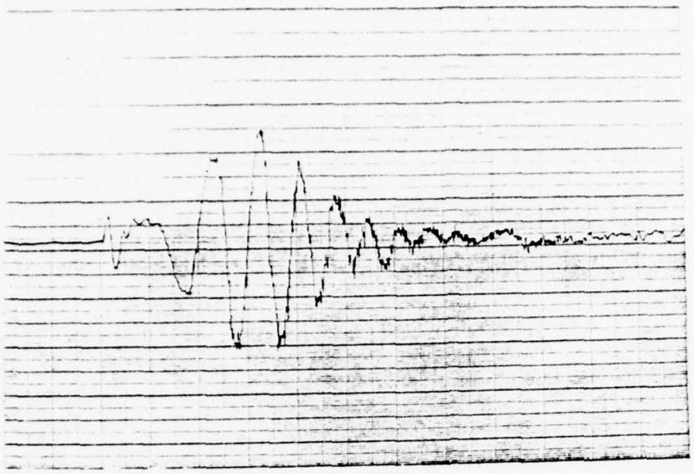

a) z = 27 cm

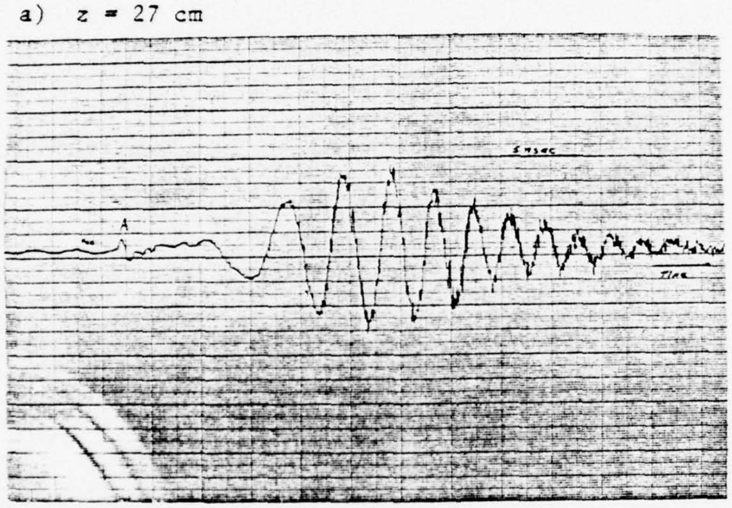

b) z = 56 cm

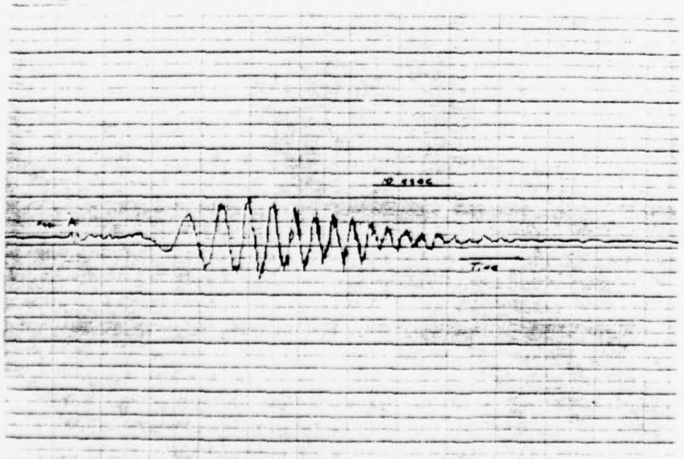

c) z = 90 cm

Fig. 4.4 Linear Oscillograms for different Receiver positions (positive pulse) f_p = 1.4 GHz

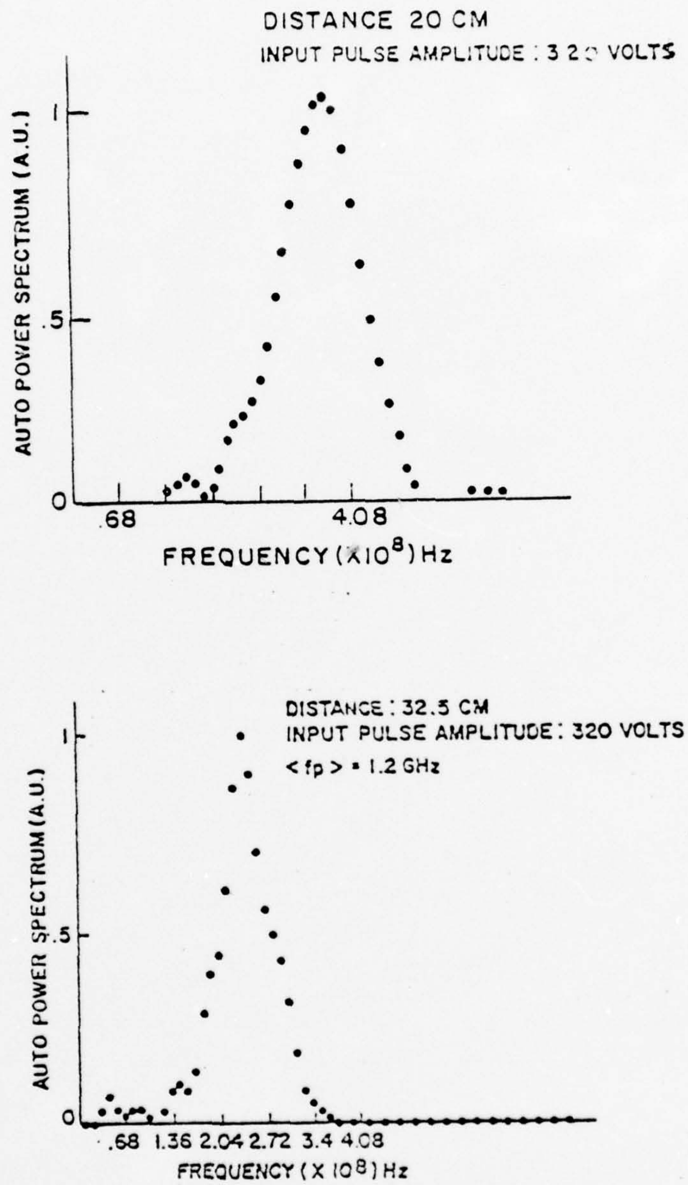

Fig. 4.5 Fourier transform of wavepacket for different positions

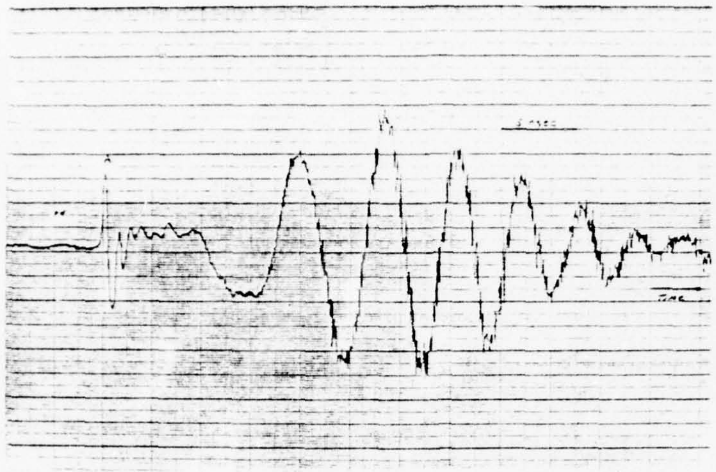

a) f_p = .76 GHz

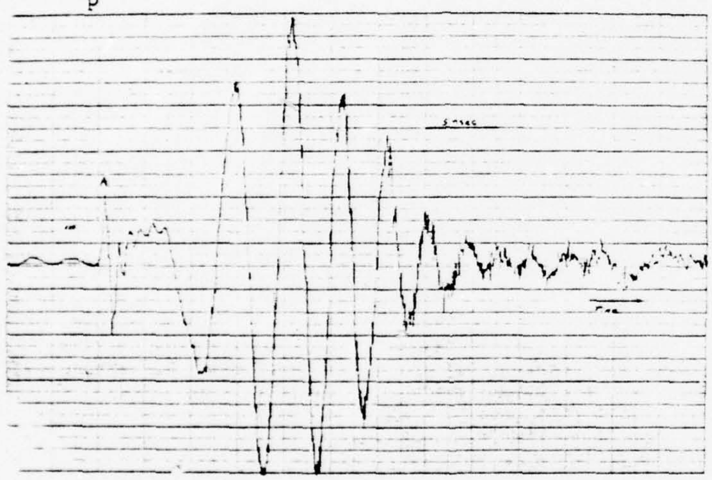

b) f_p = . 9 GHz

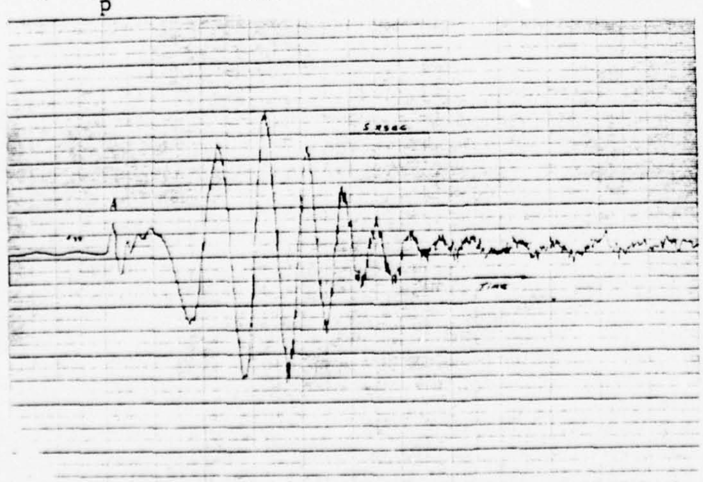

c) f_p = 1.4 GHz

Fig. 4.6 Linear Oscillograms for different plasma frequencies z = 27 cm.

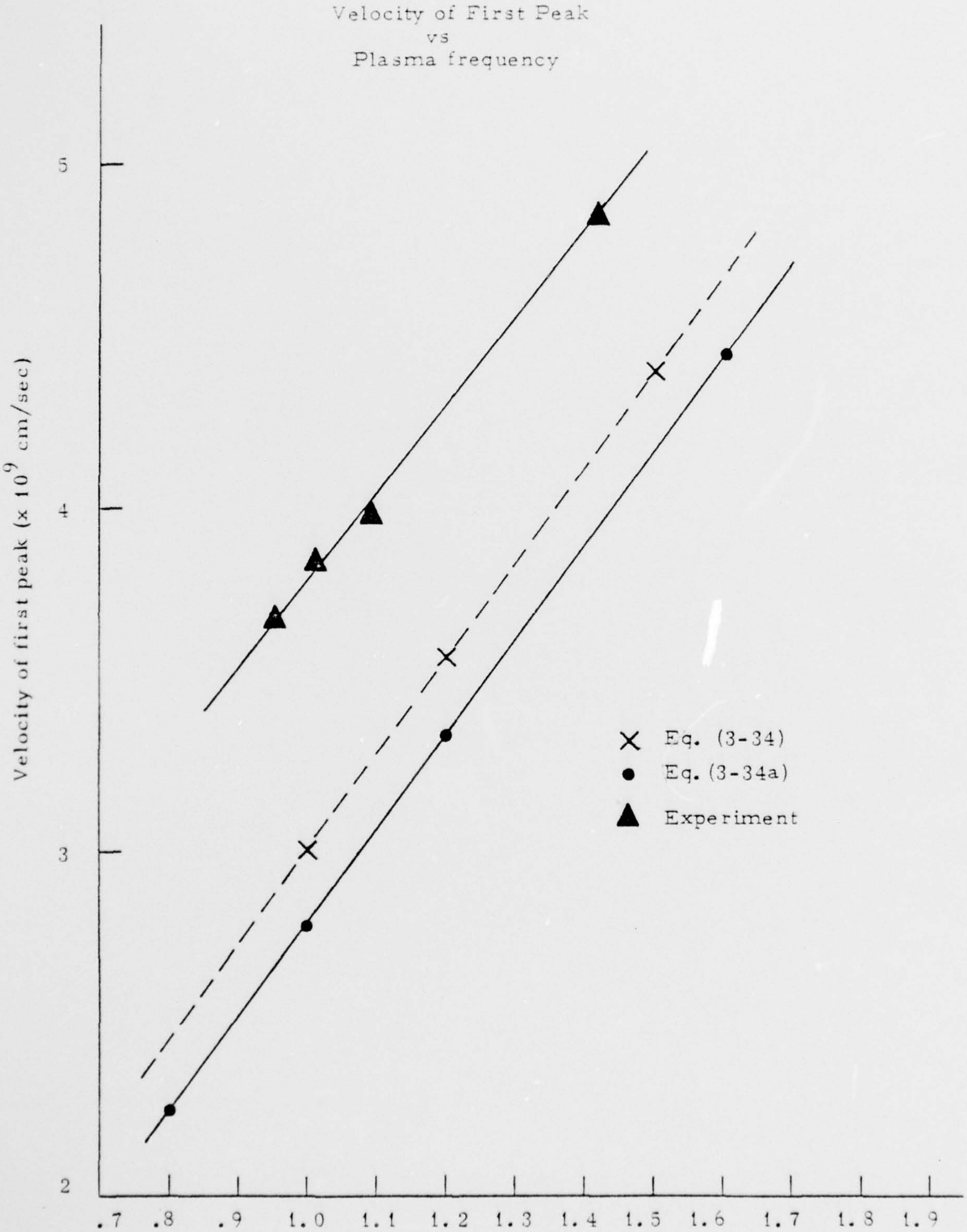
Velocity of First Peak
vs
Plasma frequency
Velocity of first peak (x 10^9 cm/sec)
5
4
3
2
.7
.8
.9
1.0
1.1
1.2
1.3
1.4
1.5
1.6
1.7
1.8
1.9
Eq. (3-34)
Eq. (3-34a)
Experiment

Figure 4.7

For receiver positions far away from the launcher, i.e., at large values of z, the far field solution, equation (3-54) is applicable. This implies that the observed oscillograms should behave as Airy functions of argument $\omega_p(t - z/v_o)/(3\alpha' z/b)^{1/3}$. Using the asymptotic approximation for the Airy function, the solution (3-54) takes the form:

$$E_z \sim \frac{1}{\sqrt{\pi}} \frac{1}{(3\alpha' z' t')^{1/4}} \sin\left[2/3\ t'^{3/2} + \pi/4\right] t > z/v_o$$

where $t' = \omega_p (t - z/v_o)/(3\alpha' z')^{1/3}$ $z' = z/b$

the zeros of the above equation occur at:

$$t' = (n - 1/4)^{2/3} \frac{3}{4} \pi^{2/3} (3\alpha' z')^{1/3} \tag{4-1}$$

These values can be directly compared to the properly normalized zeros of the observed oscillograms. In Table (4-1), we tabulate the zeros obtained from equation (4-1) and from two different oscillograms. These are also plotted in Figure (4-8). If instead of using the average plasma frequency as measured using the Cavity method, a plasma frequency is chosen as to fit the nth experimental crossing to the nth theoretical crossing; we observe that all other (n-1) crossings fall to within 6% of the theoretically predicted values. Larger deviations are obtained for the n = 0 and n = 1 crossings where the asymptotic expansion does not provide an accurate representation. The value of ω_p obtained in this fashion is 20% off from the value measured by the Cavity method. The discrepancy lies in the fact that, the Cavity method measures the average plasma frequency of a non uniform plasma column, whereas the ω_p obtained by matching the nth zero is obtained from a theory that assumes an uniform column. The plasma frequency thus derived corresponds to a value near the edge of the non uniform column. Thus, we have developed a method for measuring the plasma frequency, near the edge of the column, from the zero crossings of the observed time oscillograms. It has a higher resolution than the Cavity method as seen from Figs.

Table 4.1

Parameters:

Receiver distance (z) = 54.375 cm

Column Radius (b) = .66 cm

Normalized distance (z′) = 82.386

a' = 1.48887

v_o (experimental) = 3.895×10^9 cm/sec.

f_p (from cavity) = .9 GHz

Zero crossing (n)	t′	Experimental t′ (ω_p measured using cavity)	Experimental t′ (ω_p chosen so as to fit nth zero crossing)	
			(a)	(b)
0	9.14898	12.16	9.623	9.8
1	19.02	28.16	22.28	22.7
2	33.43	43.34	34.33	34.99
3	45.19	57.11	*45.19	46.0
4	55.56	69.33	54.85	55.9
5	65.020	80.	63.30	64.528
6	74.01	90.65	71.71	73.10
7	82.3131	102.07	80.75	*82.3131
8	90.2908	111.23	88.	89.7
9	97.899	121.1	95.82	97.68
10	105.1395	130.293	103.08	105.06
11	112.28	139.4490	110.32	112.45
	119.158	148.55	117.52	119.79
	125.821	156.187	123.56	125.9

*nth zero matched

f_p corresponding to column $\begin{cases} \text{(a)} = .712\text{ GHz} \\ \text{(b)} = .725\text{ GHz} \end{cases}$

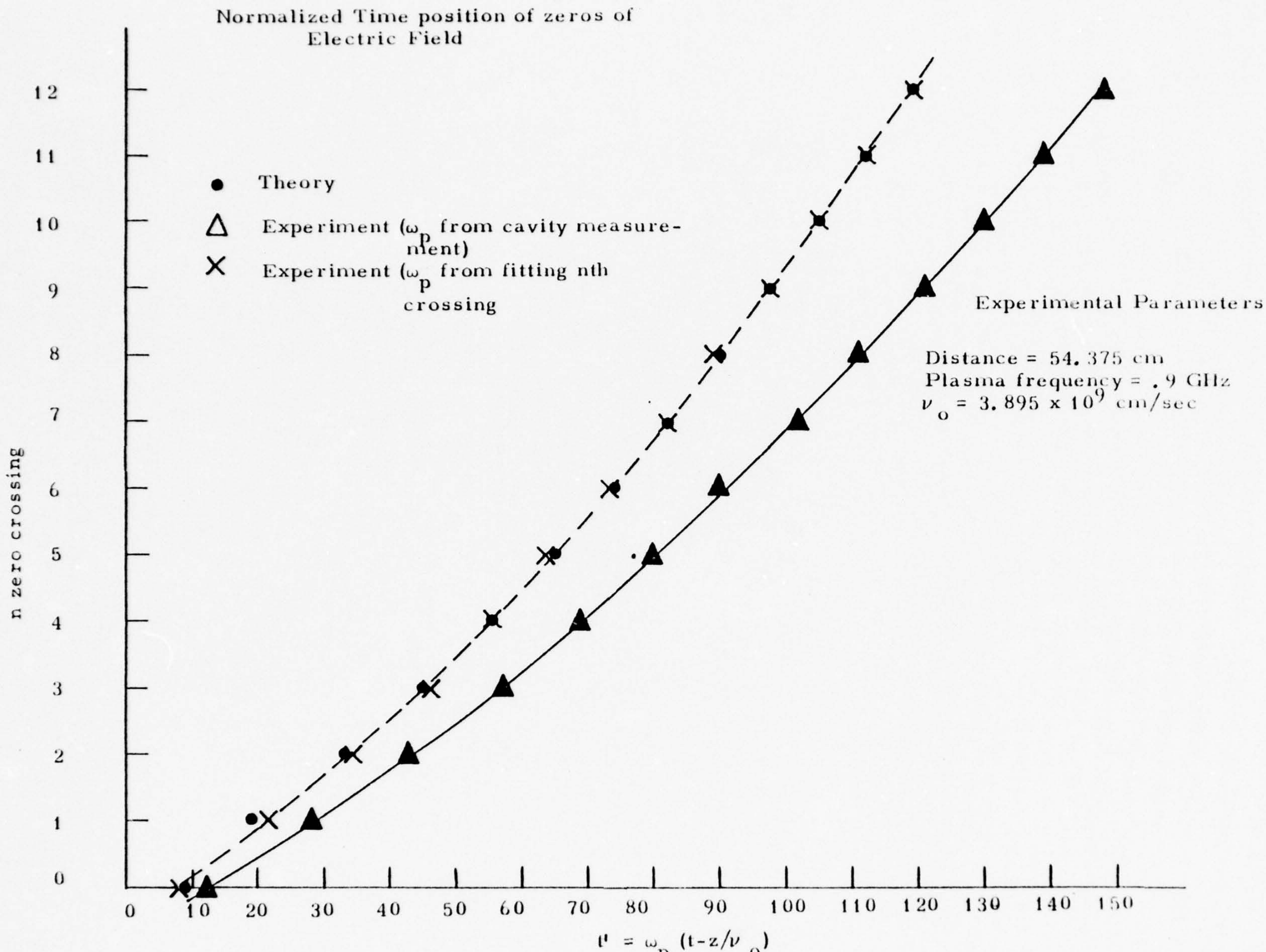
Normalized Time position of zeros of Electric Field
Theory
Experiment (ω_p from cavity measurement)
Experiment (ω_p from fitting nth crossing
Experimental Parameters
Distance = 54.375 cm
Plasma frequency = .9 GHz
ν_o = 3.895 x 10^9 cm/sec
n zero crossing
0
1
2
3
4
5
6
7
8
9
10
11
12
0
10
20
30
40
50
60
70
80
90
100
110
120
130
140
150
$t' = \omega_p (t-z/\nu_o)$

Figure 4.8

(4.8). The average plasma frequency as measured by the Cavity was .9 GHz for both oscillograms, whereas due to small background pressure change, the number density had drifted slightly causing a change in the propagation characteristics of the wavepacket. The drift corresponded to a 5% change which was not detected by the Cavity.

Qualitatively, the behavior of the envelope of the observed oscillograms is as predicted by equation (3-54). However, quantitatively, the rates of decay of the envelopes do not agree. In Figure (4-9), we display the envelope amplitude as a function of time. Two rates of decay are observed. For rates just to the right of the maximum amplitude, the decay goes as $t^{-3/4}$, whereas for large times the rate goes as t^{-1}. The asymptotic result of equation (3-54) predicts an uniform decay rate of $t^{-1/4}$. To account for the difference, two fundamental assumptions made in the derivation of the theory must be modified if a quantitative description of the amplitude is desired. First, in the desivation of the collision term, the dependence of $(\psi_\alpha, \nu\,\psi_\alpha)$ on frequency was neglected in order to get at analytical results. Secondly, sheath effects which introduce strong landau dampling of the slow waves at high frequency must be included in the theory. The high attenuation ($\sim t^{-1}$) observed for the high frequencies is an indications that this mechanism may be present.

The last parameter considered was tube radius. Figures 4-10a and 4-10b display recordings in time and space obtained using a tube of radius .325 cm. The behavior of the packet is as predicted by the theory of chapter III with the proper value of radius b. A large discrepancy is noted (see Fig. 4-11) between the zero crossings of the observed oscillations normalized to the Cavity measured plasma frequency and those computed from equation 4-1. Also shown in Fig. 4-11 are the crossings computed by normalizing the experimental nth crossing to the corresponding theoretical value. The large difference for this tube between the Cavity measured ω_p and the nth crossing computed ω_p is consistent with the previous explanation given for this difference. It lies in the fact that the small column has a stronger transverse inhomogeneity in the number density than the larger tube.

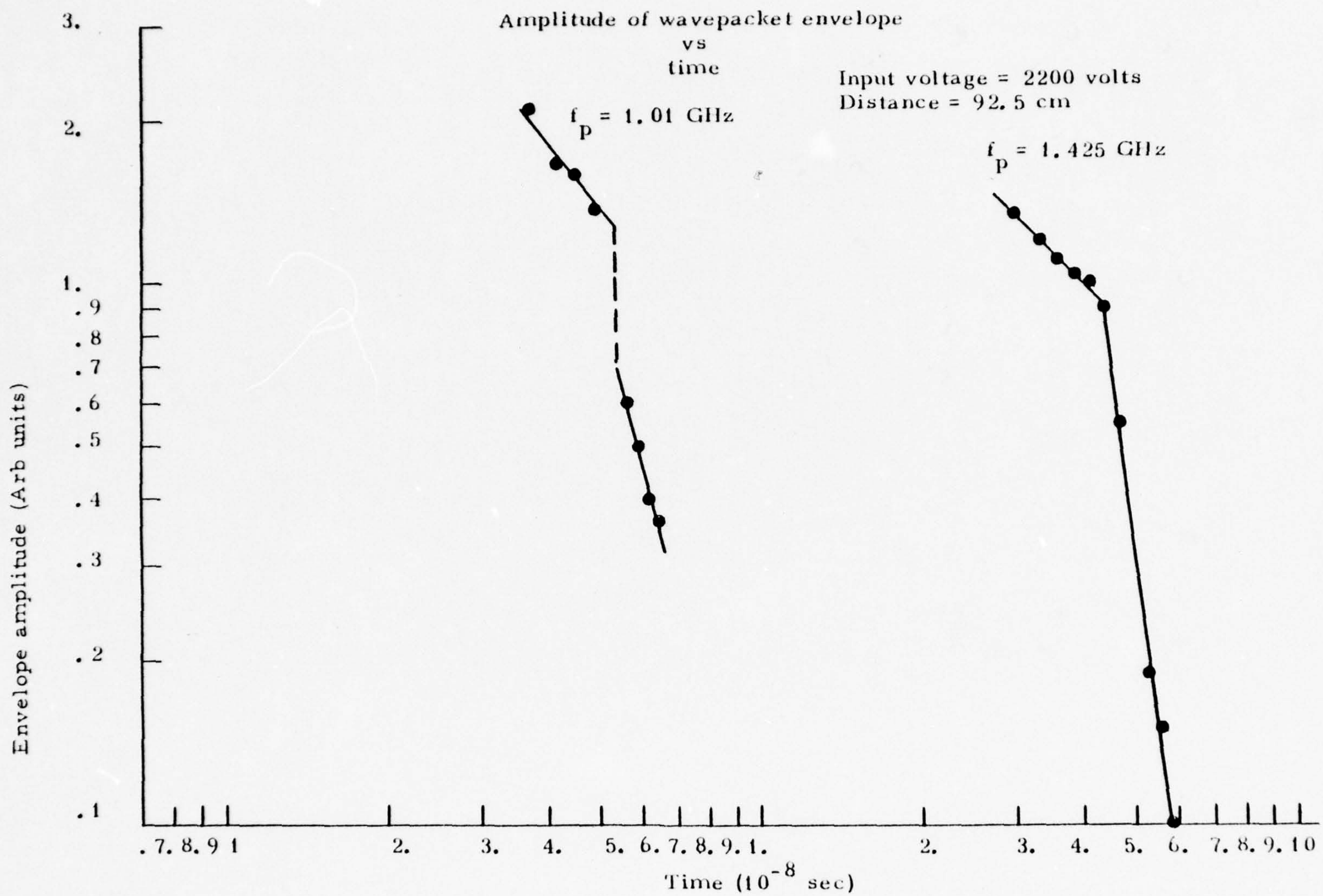

Amplitude of wavepacket envelope
vs
time
Input voltage = 2200 volts
Distance = 92.5 cm
f_p = 1.01 GHz
f_p = 1.425 GHz
Envelope amplitude (Arb units)
3.
2.
1.
.9
.8
.7
.6
.5
.4
.3
.2
.1
.7. 8. 9 1
2.
3.
4.
5. 6. 7. 8. 9. 1.
2.
3.
4.
5.
6.
7. 8. 9. 10
Time (10^{-8} sec)

Figure 4.9

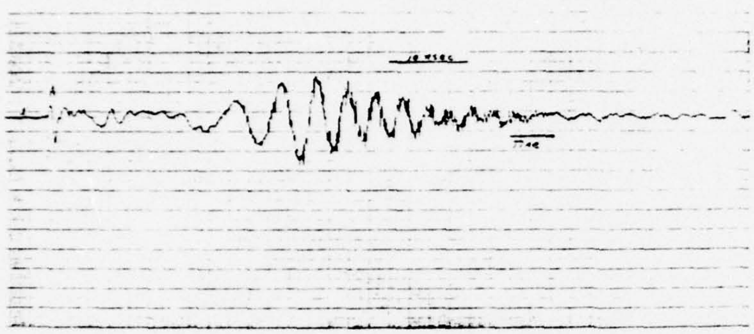

a) f_p = .79 GHz   z = 56 cm

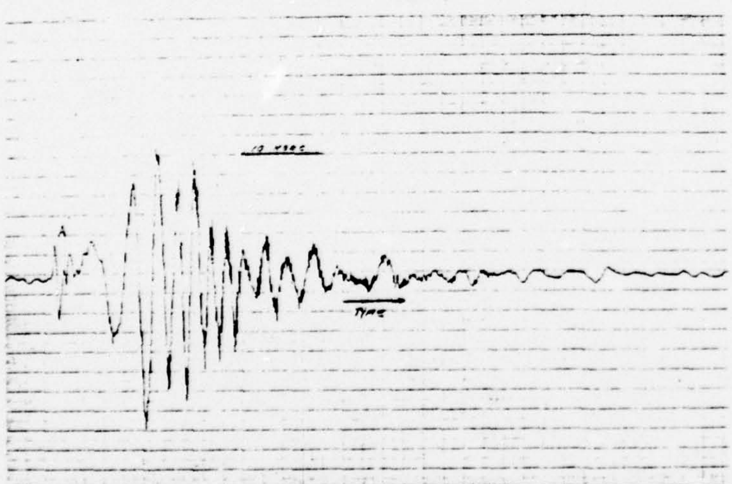

b) f_p = .79 GHz   z = 27 cm.

Fig. 4.10 Oscillograms for differen plasma frequencies. Tube radius = .3 cm .

Figure 4.11 Zero Crossing for Small Tube

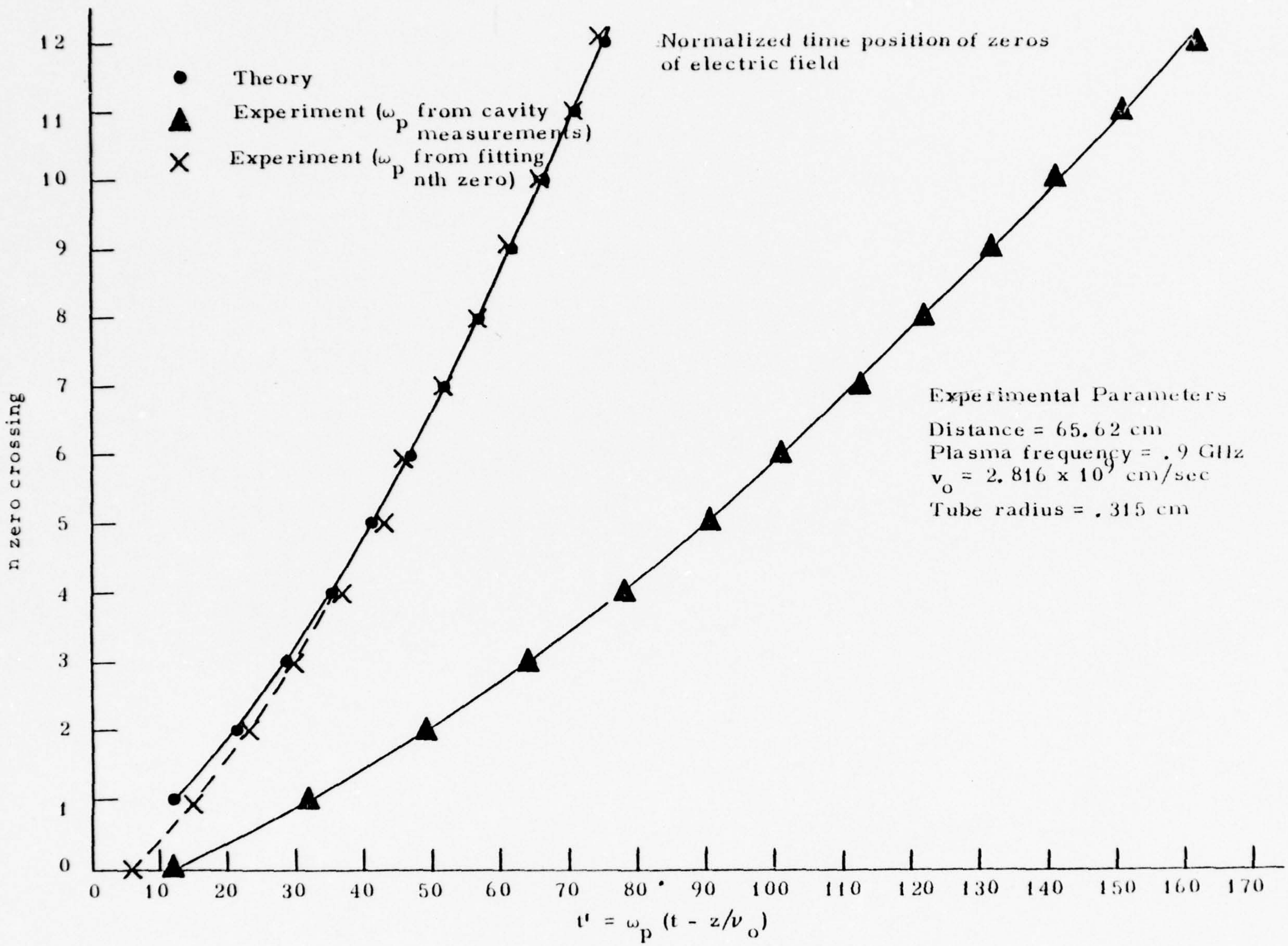

4.1.2 Nonlinear Regimes

As the amplitude of the initial pulse increases, nonlinear effects start to play a role. Experiments in this regime were carried out using peak field strengths greater than 600 volts/cm, at the launching plates. It is important to note that for all experiments (both zero and finite magnetic fields), the signals observed in the oscilloscope are normalized so that if the response were linear, the observed oscillogram as a function of input pulse strength will coincide. This is accomplished by keeping the total attenuation, in the path the signal travel, constant. Thus to go from the linear to the nonlinear regime, the attenuation is transferred from the input of the launching plates to the input of the oscilloscope. In this fashion, effects that are clearly amplitude dependent are identified.

In Figure 4-12, the profile in time of the wavepacket is shown as a function of input pulse amplitude. The positive pulse was used as the source. Qualitatively, these diagrams are similar, although quantitatively they differ in the law governing the decrease of the amplitude in time and in space. Moreover, the characteristics of the first two oscillations have changed.' Note that the maximum normalized amplitude of the nonlinear response is less than for the linear case, implying that the surface wavepacket has reached saturation. In Figures 4-13 and 4-14, the behavior of the amplitude as a function of space and time for the linear and nonlinear cases are displayed. The slower decay rate observed for the non linear case is explained from the dynamics of the propagation as described by the model developed in section 3.3. For positive pulse, $E_z(0,t) \sim -|E_p(0,t)|$, where E_p is the pulse field strength. Thus for any value of σ, the solution of the K de V equation is always oscillatory and the character of the solution is very similar to the linear result. [42] A physical understanding of the processes taking part in the propagation of the high amplitude pulse may be gained from the fourier transform of the observed oscillograms as a function of plasma frequency and receiver location. In Figure 4-15, we display side by side the nonlinear response, and the corresponding power spectrum as a function of plasma frequency. In Figure 4-16, the plasma frequency is kept constant and the recordings are shown for 3 different positions.

These diagrams show the channeling of energy from the lower fre-

RESPONSE AS A FUNCTION OF INPUT PULSE STRENGTH

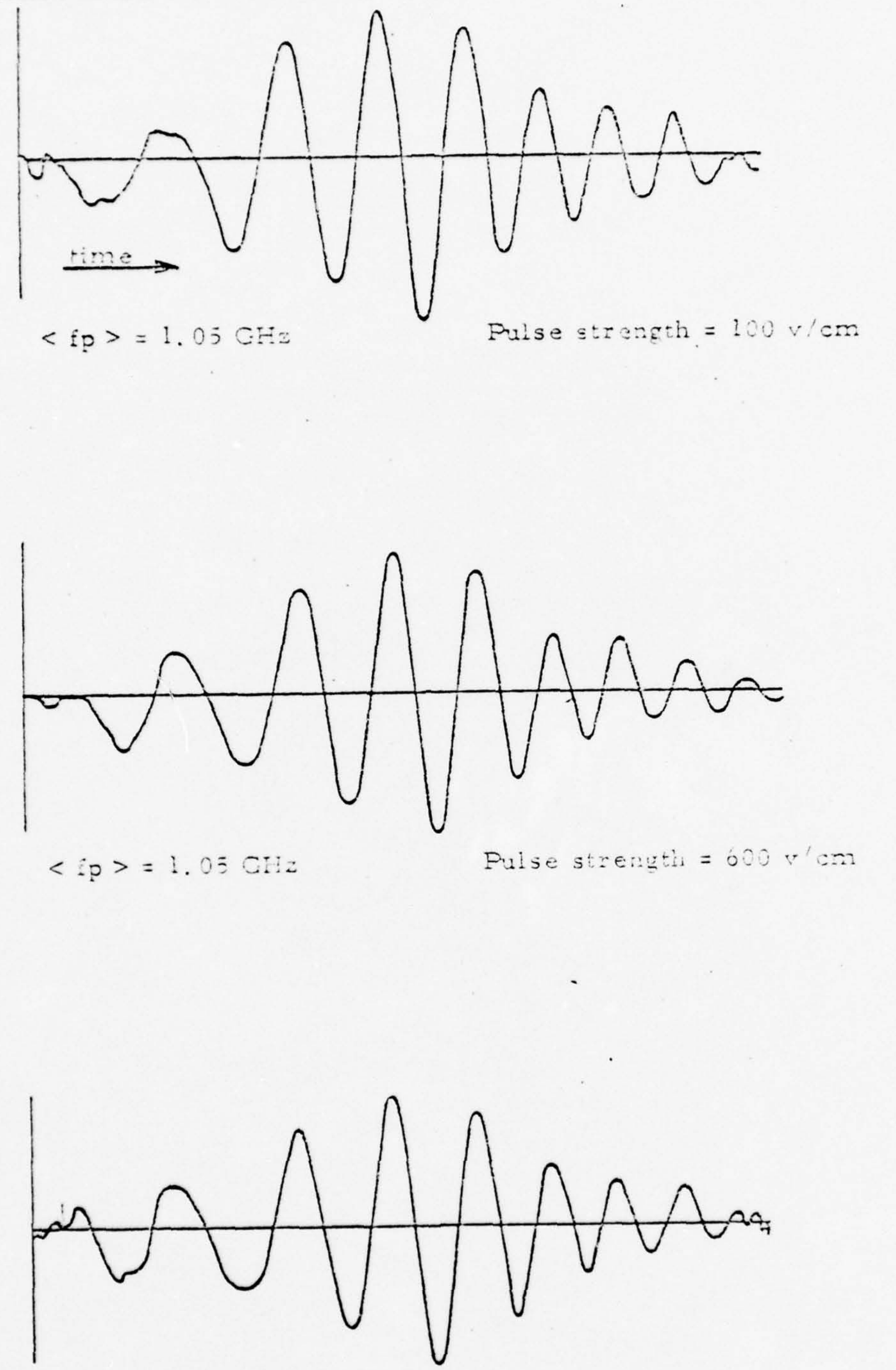

Figure 4.12

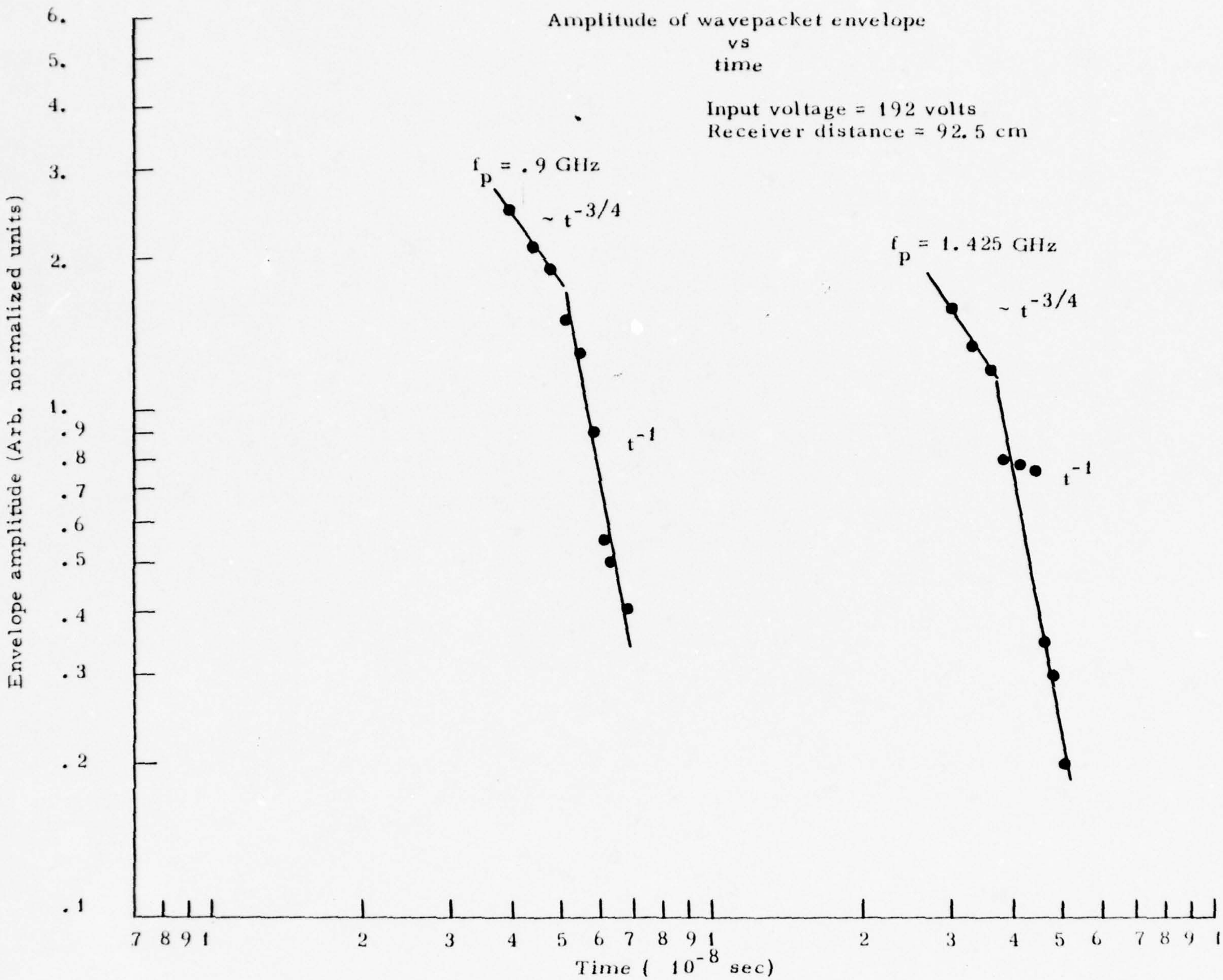
Amplitude of wavepacket envelope
vs
time
Input voltage = 192 volts
Receiver distance = 92.5 cm
f_p = .9 GHz
~ $t^{-3/4}$
t^{-1}
f_p = 1.425 GHz
~ $t^{-3/4}$
t^{-1}
Envelope amplitude (Arb. normalized units)
6.
5.
4.
3.
2.
1.
.9
.8
.7
.6
.5
.4
.3
.2
.1
7 8 9 1 2 3 4 5 6 7 8 9 1 2 3 4 5 6 7 8 9 1
Time (10^{-8} sec)

Fig. 4.13

Figure 4.14
Amplitude of wavepacket
vs
distance

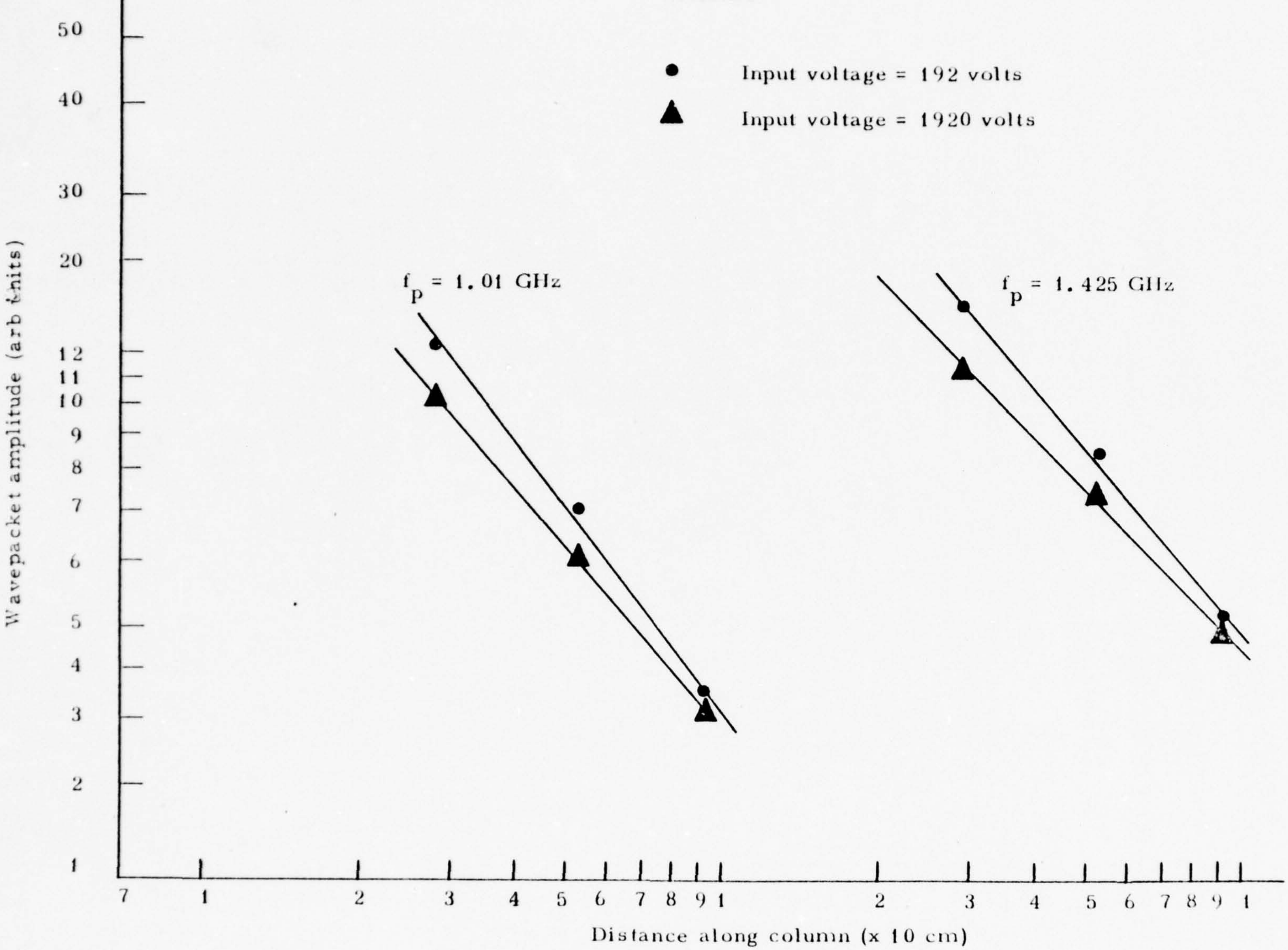

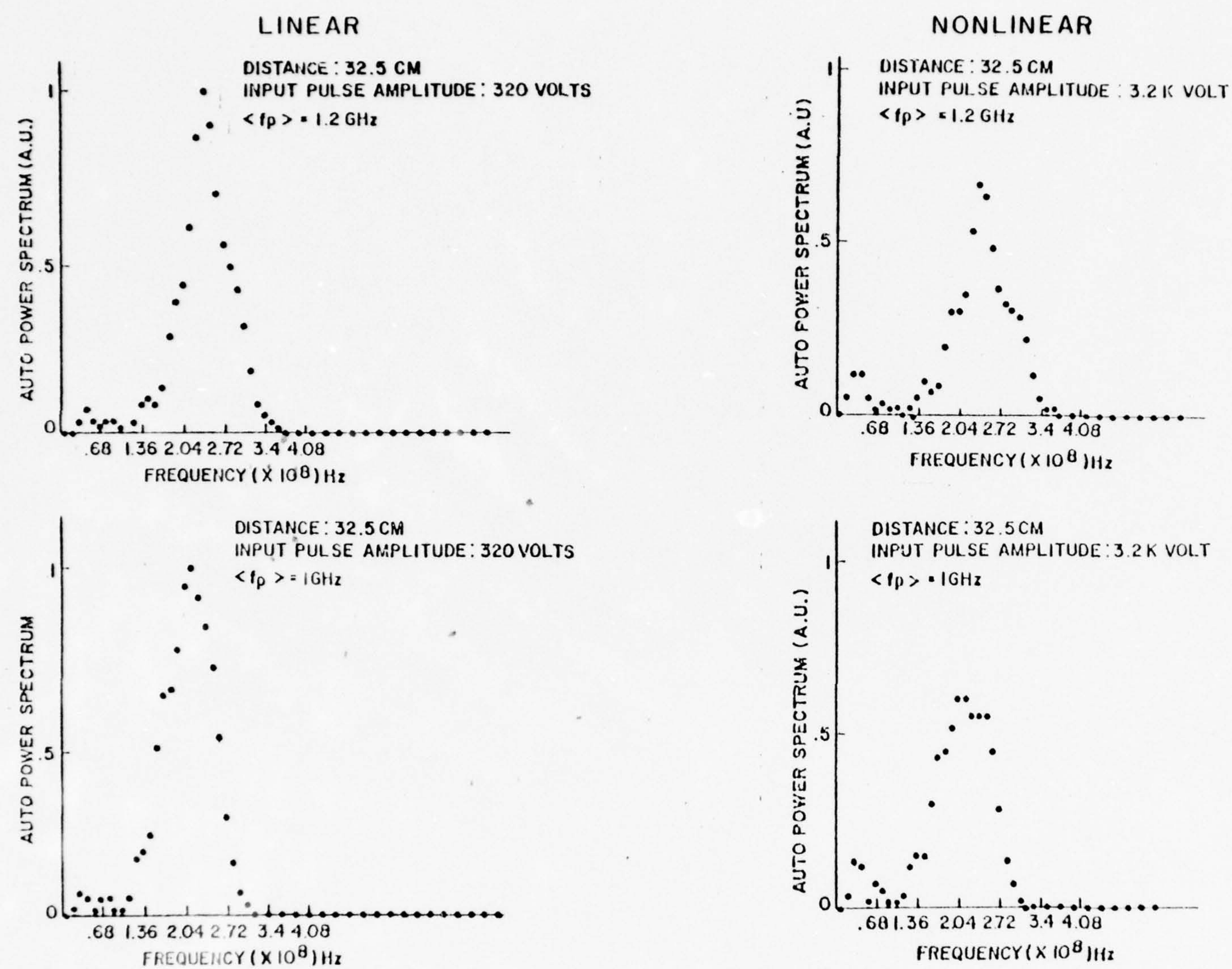

Fig. 4.15 Linear and Nonlinear Spectrum for different plasma frequencies.

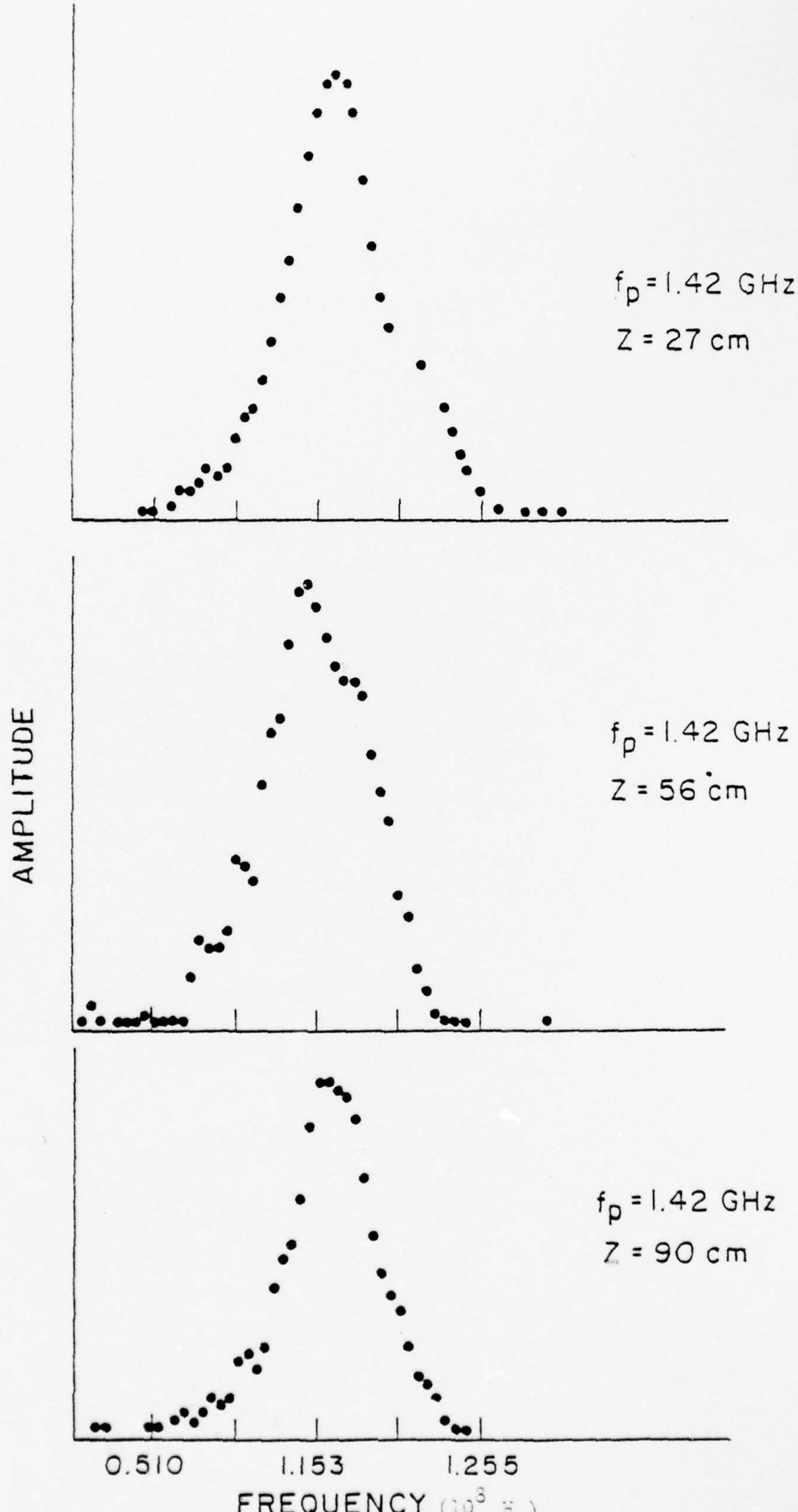

Fig. 4.16 Nonlinear spectrum for different receiver locations.

quencies to the higher frequencies which in turn are strongly attenuated as explained in section 3-3. This accounts for the saturation phenomena observed. Note that the region of interaction (inflection point retion in negative slope side of the power spectrun) is a function of the time of interaction between the different frequency components of the packet. For a fixed receiver position as the plasma frequency is decreased, the packet velocity decreases thus increasing the interaction time. Similarly, for a fixed plasma frequency, the further away from the launcher the more time the components had to interact. This phenomena causes the inflection point in the power spectrum to move toward lower frequencies.

The effects described above were not observed when the negative pulse was used as the exciter. Even though for this polarity Equation 3-48 predicts quantitatively different results, the maximum amplitude available at the plates and the width of the pulse were such that σ is always much, much less than σ_c. Figure 4-17 shows the plasma response for the maximum pulse strength available with the negative generator. Also shown is the power spectrum of the response. As can be seen from the diagrams, nonlinear effects were not observed using this excitation as expected from the values of the nonlinear parameter for this pulse.

4.2 Finite Axial Magnetic Field

4.2.1 Linear Regime

Since all experimental "idiosyncrasis" have already been discussed. In this and the following subsection we need only present the results. Pulse amplitudes corresponding to field strengths of 61 Volts/cm were used to excite the linear Bulk Waves. The pertinent parameters for this series of experiments were the plasma frequencies and axial field strength. In figure 4.18, we display time oscillograms, recorded 48 cm away from the launcher, as a function of plasma frequency with $\underset{\sim}{B}o$ fixed and in Fig. 4.19 as a function of axial field strength (with plasma frequency fixed). Again, the region marked with an A in these oscillograms, correspond to electromagnetic radiation that will still be observed if the plasma were not present. From these diagrams, we compute characteristic parameters that describe the propagating wave packet and compare them with the theoretical values obtained from equation (3.54).

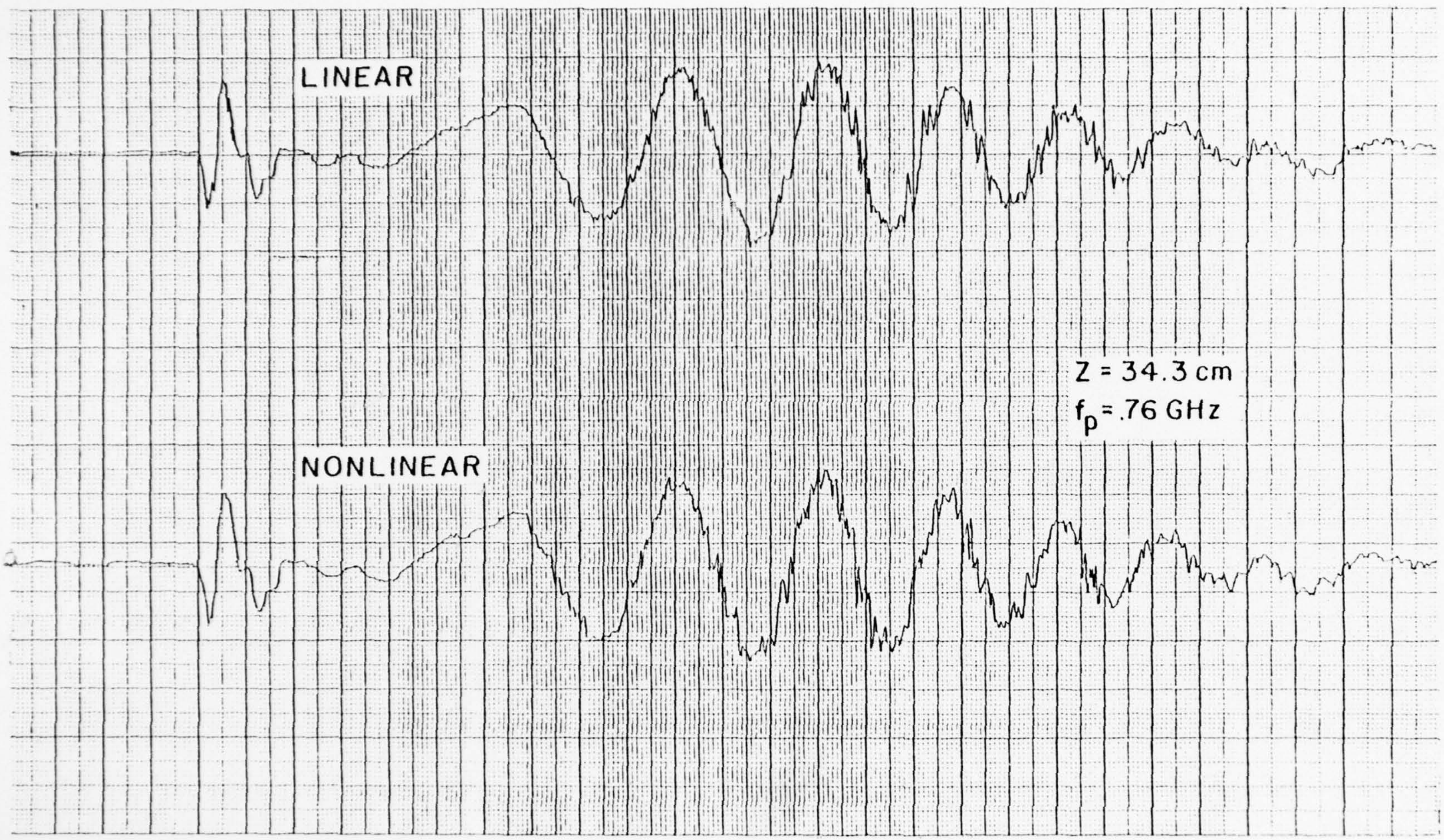

Fig. 4 - 17 Response to high negative pulse.

a) f_p = 1.4 GHz

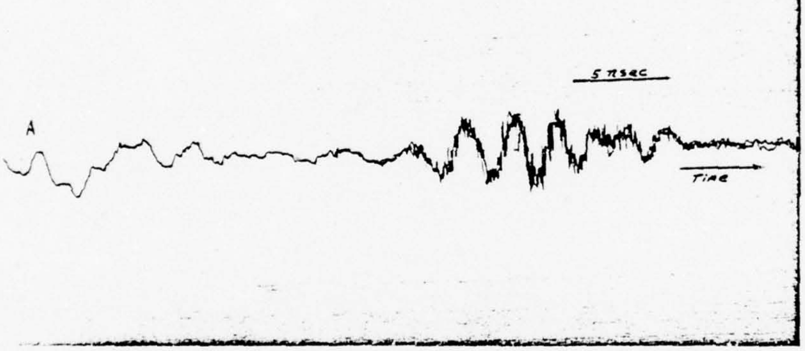

b) f_p = 1.6 GHz

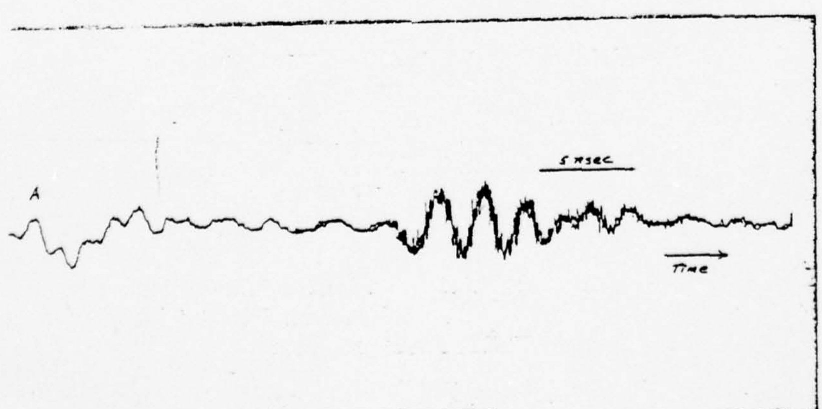

c) f_p = 1.7 GHz

Fig. 4.18 Linear Oscillograms for different plasma frequencies
Cyclotron frequency = .6 GHz

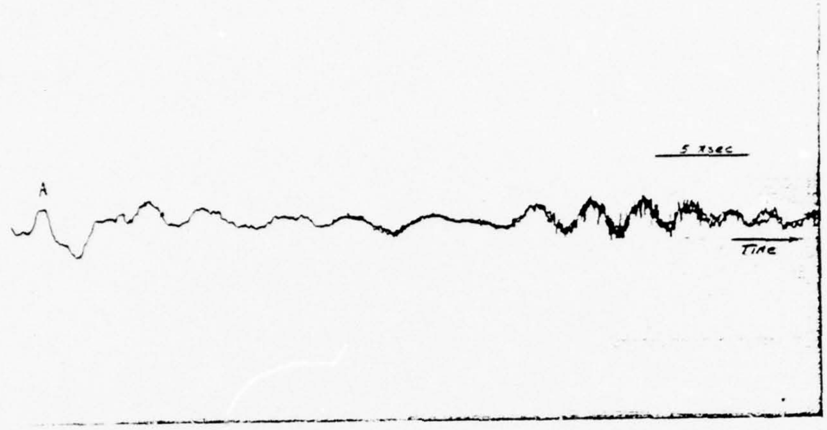

a) f_c = . 6

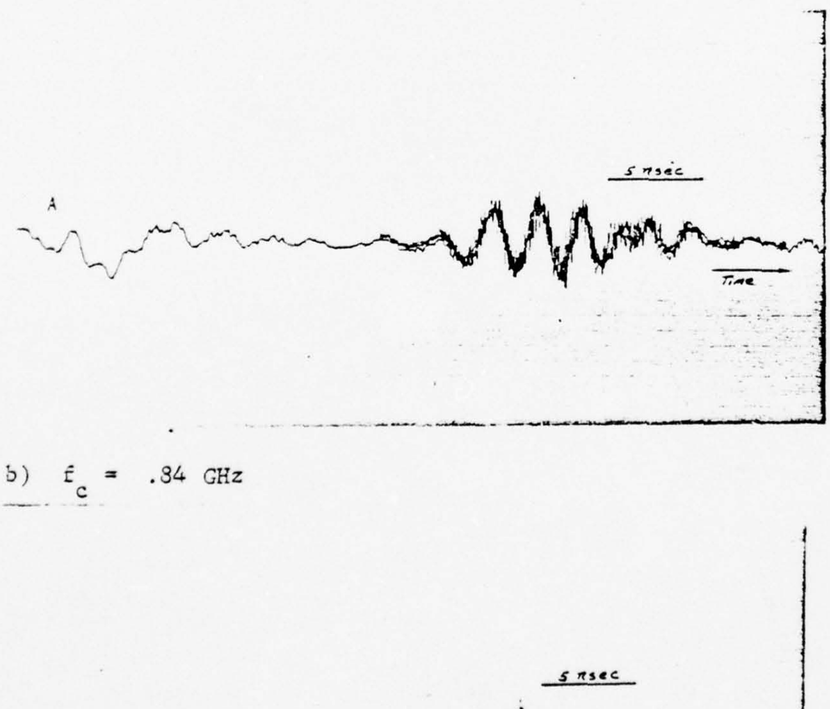

b) f_c = .84 GHz

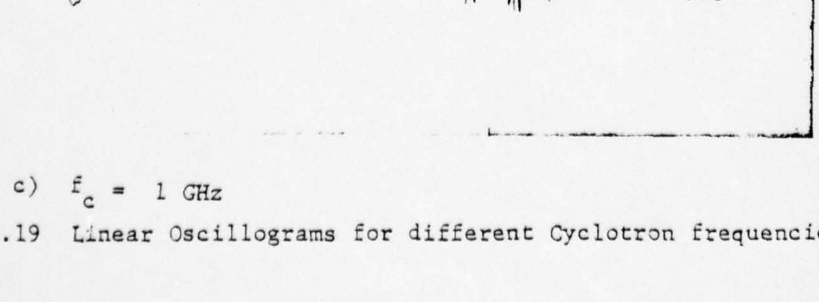

c) f_c = 1 GHz

Fig. 4.19 Linear Oscillograms for different Cyclotron frequencies.

When the DC axial magnetic field is applied, the wavepackets are observed to be noisier than for the zero field case (compare the oscillograms in figure 4-18 to figure 4-2 for example). Therefore care must be exercised in processing the data. To calculate zero crossings and to digitalize, the waveforms are retraced so as to smooth out the jitters. In fig. 4-20, the zero crossings of the experimental wavepacket are compared to those of equation 3-54. For this case, choosing the values of ω_p and ω_c so that one theoretical zero-crossing is matched with the corresponding experimental value, all other crossings are matched to within 10% of each other. The chosen value of up is within 20% of that measured by the cavity and ω_c is within 8% of that measured using a Gauss meter. Another characteristic of the wavepacket is the velocity of the first peak. Fig. 4-21 shows the behavior of this velocity as a function of plasma and cyclotron frequencies. The behavior is as predicted by the theoretical model (see Fig. 3.3). The quantitative dependance of amplitude vs. time was not determined qualitatively however, the waveforms behave as expected from eq. 3-54.

For this regime, the experiments compared quite favorably to the linear theory.

4.2.2 Nonlinear Regime

As the input electric field is increased from 61 volts/cm, gross nonlinear phenomena begin to occur. From figure 4-22, one observes that signals arrive sooner than the linear waves and considerable modification of the original wavepacket begins to take place. Close examination of the lower trace, for which the exciting pulse is largest, show what appear to be superposition of two wavepackets. Note the discontinuity in phase between oscillations. That this indeed is so can be seen from the Fourier transform of the oscillogram. The spectral amplitude and phase for each waveform in figure 4-22 is shown in figures 4-23 to 4-26. At linear levels (figure 4-23), only one peak (C) is shown corresponding to the wavepacket of figure 4-22a. The slope of the phase represents a time delay from some reference point (the point of arrival of EM signal for example). It can be used to calculate the group velocity of the packet since the distance the signal has travelled is also known.

Figure 4. 20

NORMALIZED TIME POSITION OF ZEROS OF ELECTRIC FIELD

$B_0 \neq 0$

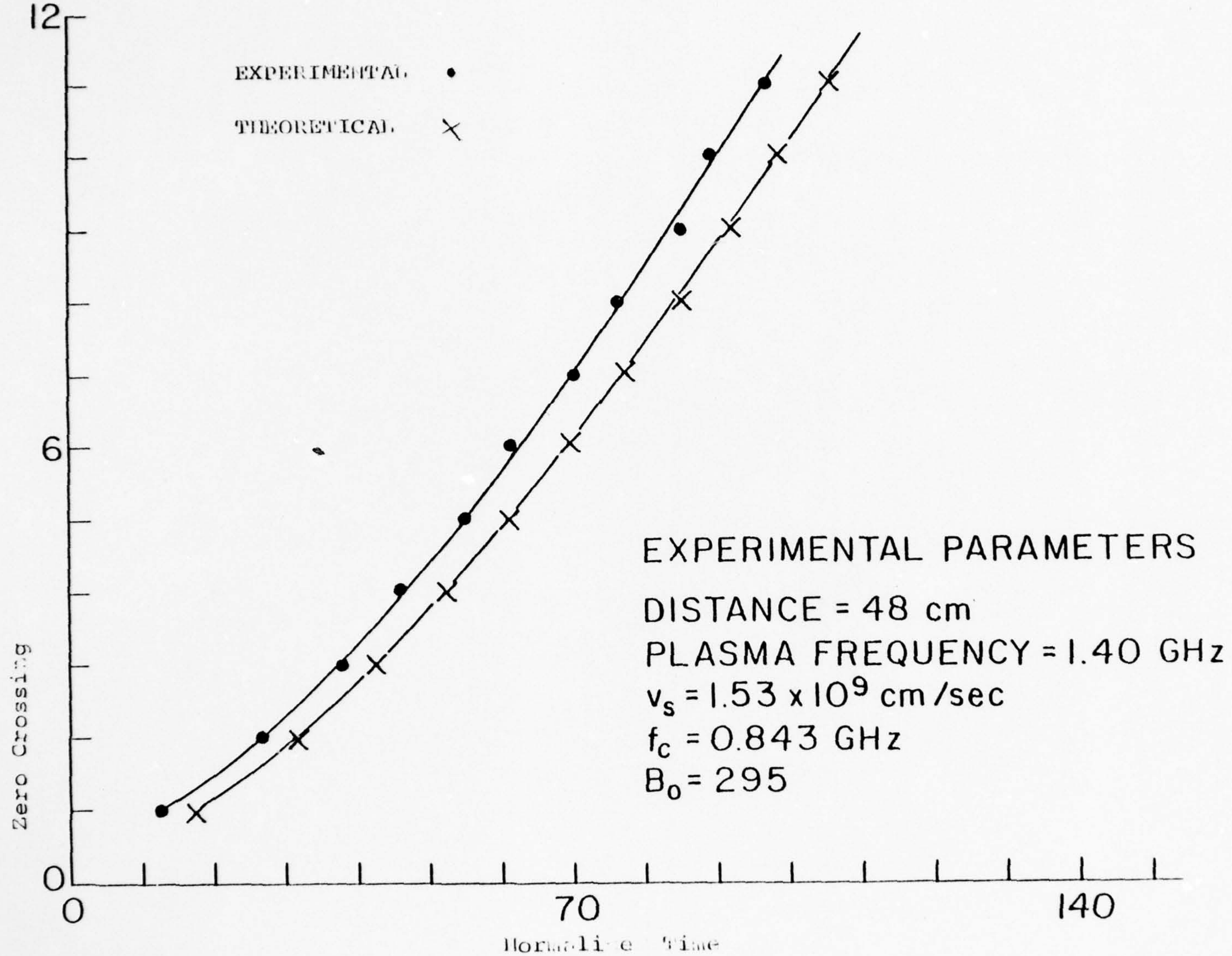

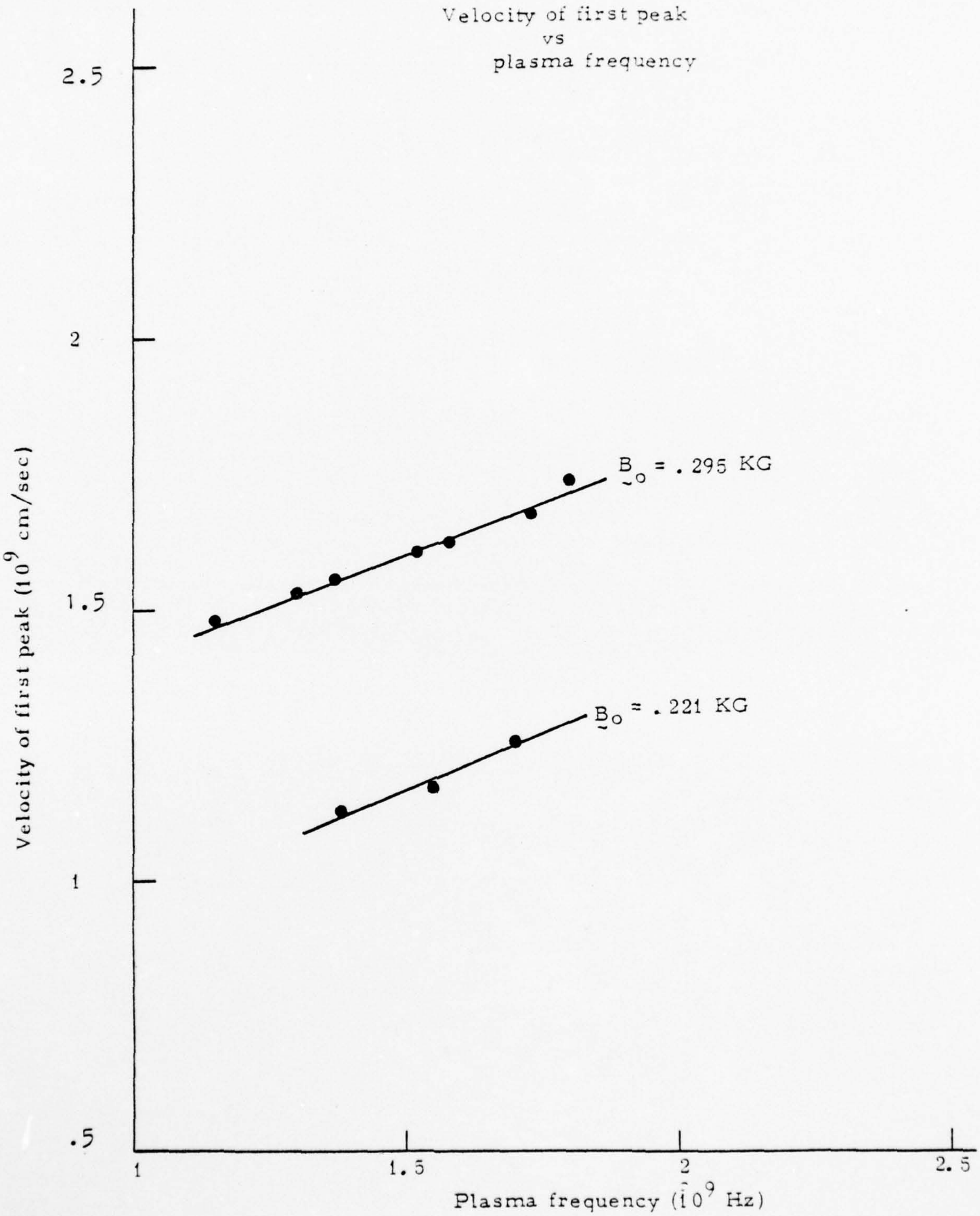
Velocity of first peak
vs
plasma frequency
2.5
2
1.5
1
.5
Velocity of first peak (10^9 cm/sec)
B_o = .295 KG
B_o = .221 KG
1
1.5
2
2.5
Plasma frequency (10^9 Hz)

Figure 4.21

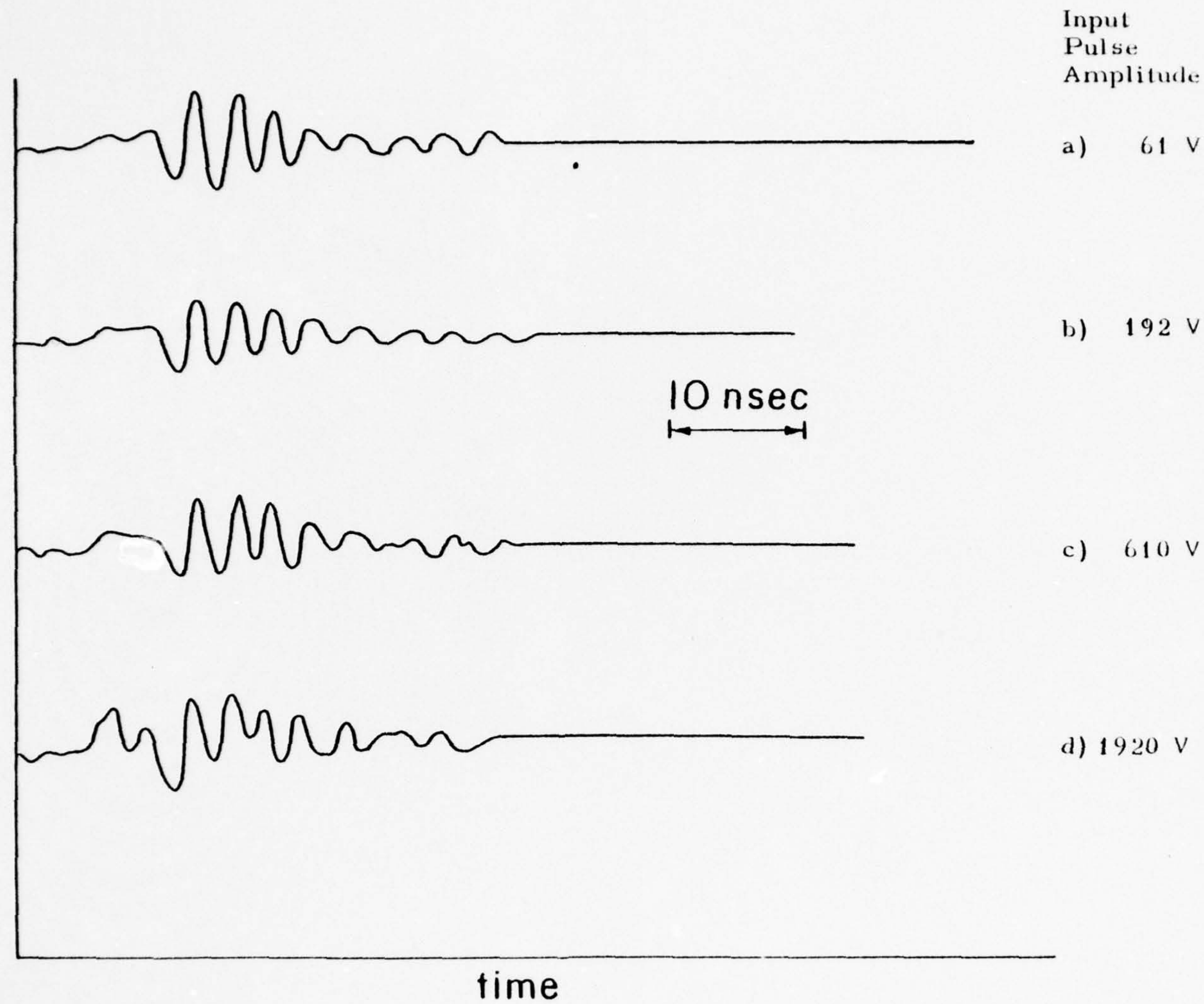

Fig. 4.22 Oscillogram taken at z = 56 cm
Cyclotron frequency = .6 GHz

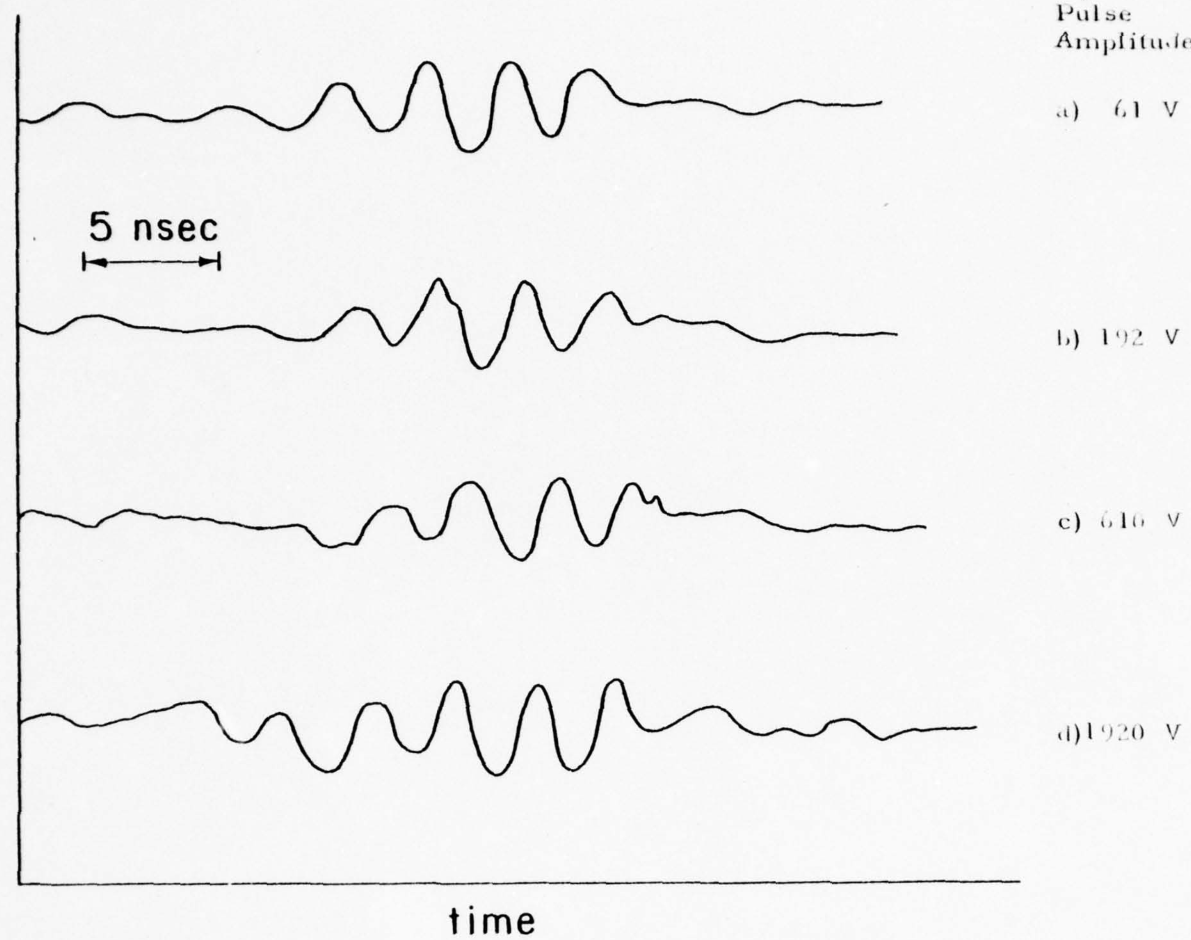

Fig. 4.22a Oscillogram taken at z = 34 cm
Cyclotron frequency = .6 GHz

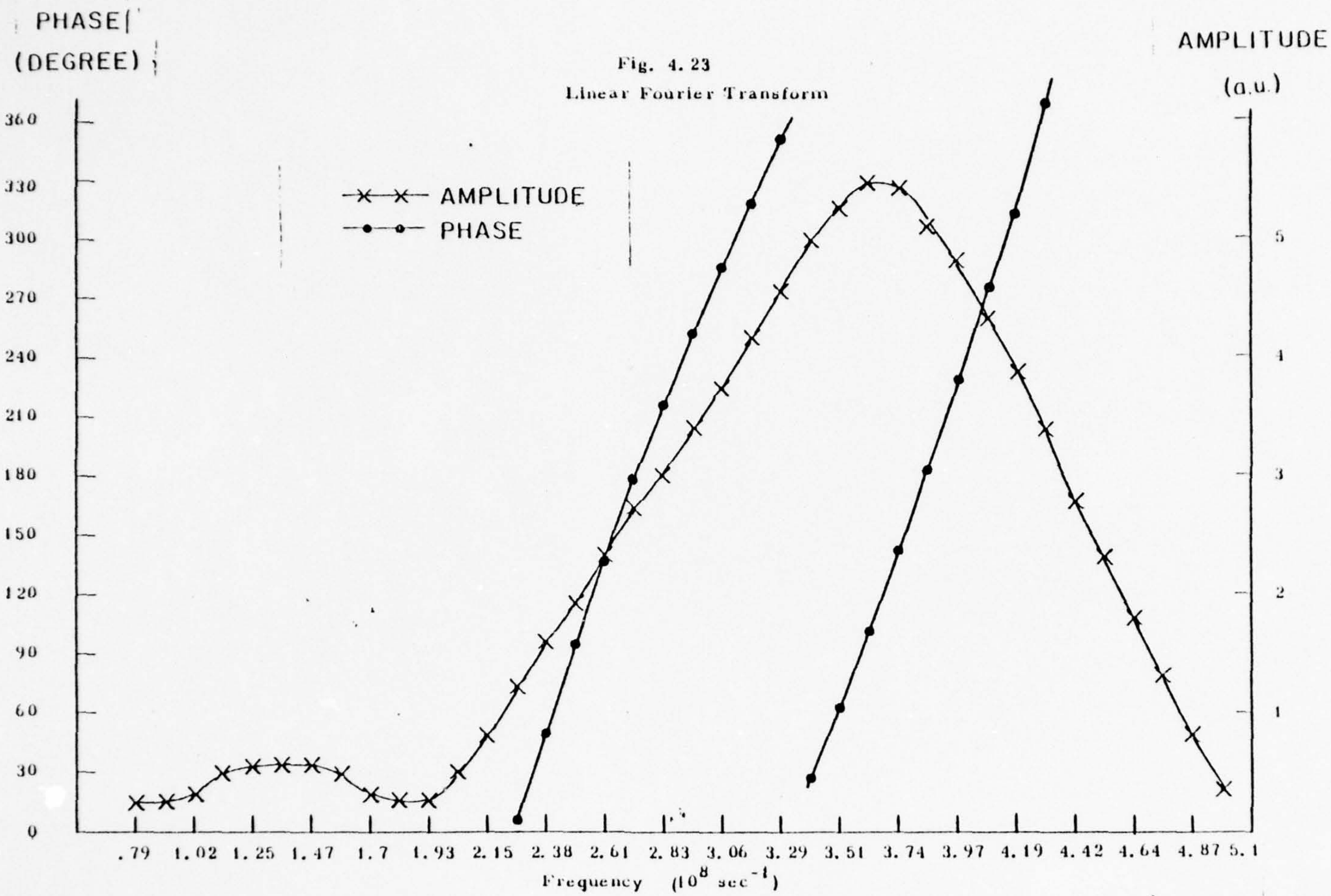

Fig. 4.23
Linear Fourier Transform

Fig. 4. 24 Fourier Transform of Figure 4. 22b

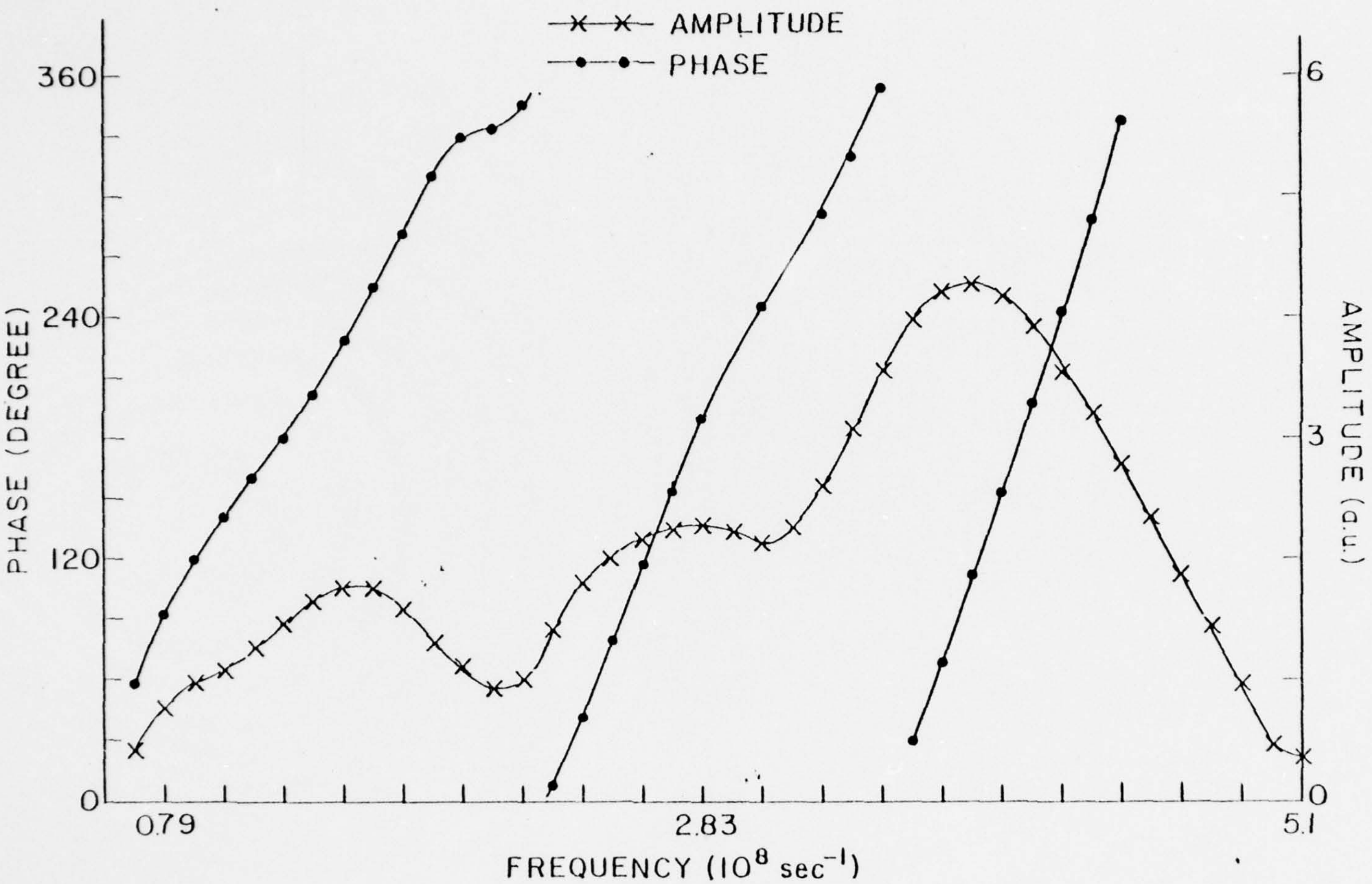

Fig. 4. 25 Fourier Transform of Fig. 4. 22c

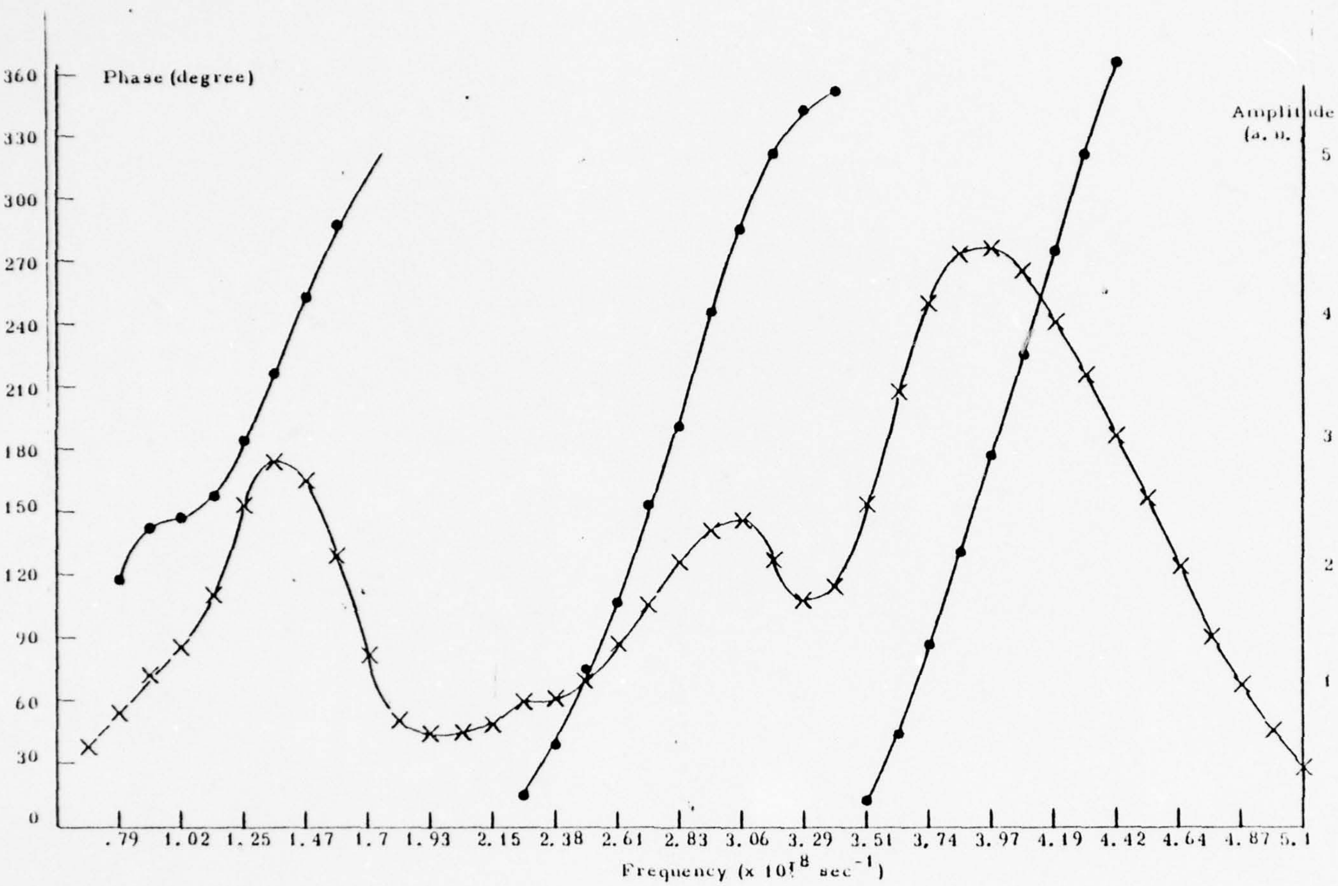

Fig. 4.26 Fourier Transform of Figure 4.22 d

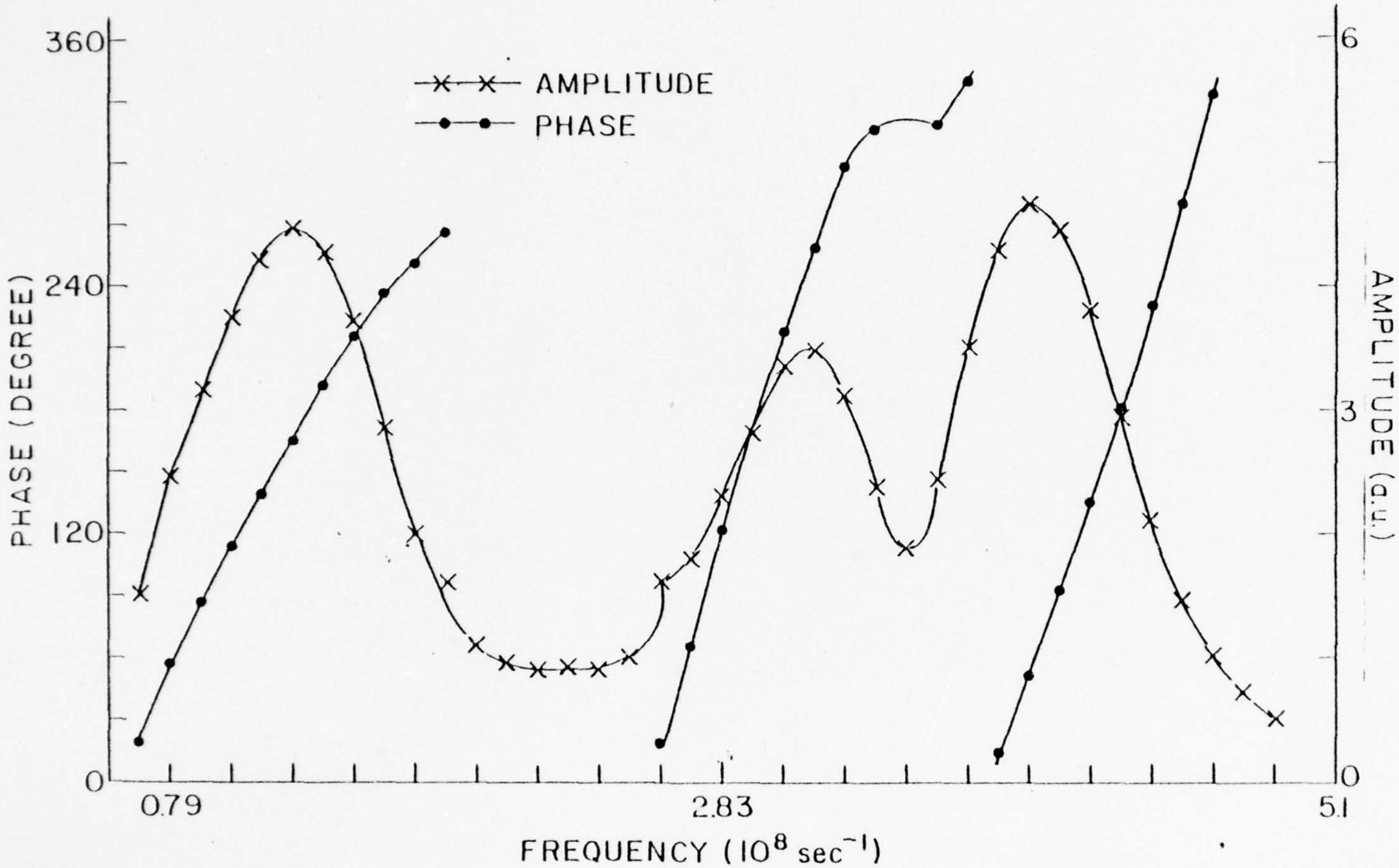

At higher amplitude two distinct phenomena occurred (figures 4-24 to 4-26). First is the appearance of a low frequency peak at f = .14 GHz (A), and second is the splitting of the original peak (C) into two ((B) and (C)). Recalling the technique used in obtaining these oscillograms (loop gain constant) it is evident that these changes are due to nonlinear phenomena. Moreover, the possibility of these peak being higher order modes was ruled out by the fact that the group delay for these modes is much greater than for the lowest order mode (see equation 3-37).

From this figure , the amplitude of peak A is observed to increase very rapidly as the input level is increased. The frequency shift is negligible. No further analysis has been made of this packet but it is suspected that it belongs to the class of solitary waves.

The main concern is with the splitting of the packet (C). As the input level is increased, there is a shift to higher frequencies of the original peak. A gradual appearance of another peak B at the low frequency side indicates another wavepacket. From the slopes of the phase at these two peaks the difference in group velocity has been calculated. The higher frequency packet (C) was found to have a longer delay and hence a lower velocity. According to the modulation theory, the difference between the time of arrival is proportional to the amplitude (see section 3.3). This is clearly shown in figure 4-27; moreover the observation that the higher frequency wavepacket travels at a lower velocity is also in agreement with the modulation theory results.

Since there is no absolute measure of the field strengths in the plasma, a quantitative comparison of this velocity difference between theory and experiment is not possible. But from the measured time difference and the group velocity of the wave, we can calculate the required field amplitude. From equation 3-63 , to achieve the largest observed separation of 3.4 ns over a distance of 56 cm, the wave amplitude of the wavepacket required is about 50 v/cm. This field represents a total energy of about 1.3×10^{-9} joules in the wavepacket. The energy contained in the exciting electric field impulse is about 3×10^{-5} joules. Since most of the energy of the impulse goes into the dummy load and radiated to outside the parallel plate structure,

AD-A037 663 POLYTECHNIC INST OF NEW YORK BROOKLYN DEPT OF ELECTR--ETC F/G 20/9
AN EXPERIMENTAL AND THEORETICAL STUDY OF THE PROPAGATION OF HIG--ETC(U)
JUN 76 E E KUNHARDT, B R CHEO AF-AFOSR-2668-74
UNCLASSIFIED POLY-EE/EP-76-011 AFOSR-TR-77-0158 NL

2 OF 2
AD
A037663

END
DATE
FILMED
4-77

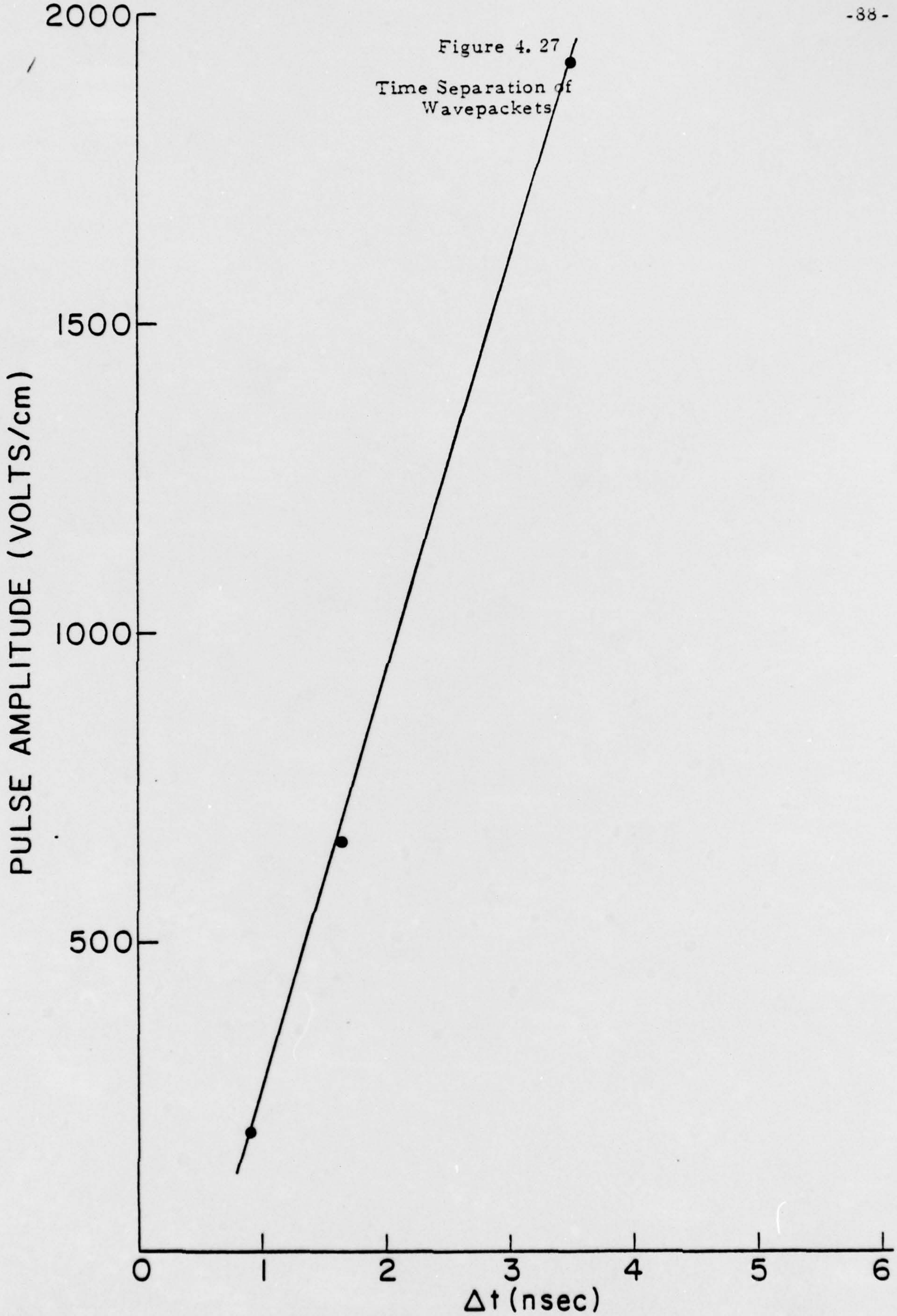

Figure 4. 27

Time Separation of Wavepackets

it is of interest to estimate the coupling efficiency, i.e. how much energy can be coupled into the plasma. As a rough upper bound estimate, assume that when the impulse field arrives at the plasma tube, the 2kV/cm field is applied to all electrons in the region between the plates during the pulse duration ($\Delta t \approx 0.4$ ns), and each electron would gain a momentum of $eE\Delta t$. The total kinnetic energy gained by all electrons in the region in this way is of the order of 9×10^{-7} joules. Comparing the orders of magnitude of the three energy levels, the 50 v/cm field required to produce the measured separation of the wavepackets is certainly reasonable for the experimental setup used. The modulational splitting of the wavepacket has been observed.

V. Concluding Remarks

In the foregoing, we have described an experimental and theoretical investigation of the propagation of finite amplitude slow waves excited by high amplitude baseband pulses. The subject of symmetric slow mode propagation has been incorporated into the framework of nonlinear dispersive waves. Theoretically, it has been shown that for typical experimental conditions (i.e., $\omega_c = 0$, $\omega_c < \omega_p$, $\omega_c >> \omega_p$), the propagation of the symmetric slow mode is described by the Kortewig de Vries equation, with the magnitude and sign of the various coefficients of the KdeV equation being different in the various regimes considered. This implies that given equal initial conditions, different effects in the propagation mode will be observed. The close interplay between theory and experiment leads to a good understanding of the experimental results. Although linear experiments on the propagation of this mode have previously been done,[31] far better resolution has been obtained here. To our knowledge, neither the experimental nor theoretical results of the nonlinear problem have been previously reported.

There are two areas which need further investigation. The results of that investigation will further substantiate the theory developed here and will aid in the experimental verification of the general theoretical results obtained for non-stationary waves propagating in accordance with the K de V equation.[42]

First, as mentioned in Section 4.3.3, the nature of the initial peak in the frequency spectrum has not been determined and second, nonlinear experiments where the polarity of the exciting pulse is negative must still be performed. We will not consider the first area further and instead comment only on the second problem. The first implication of reversing the polarity is that, theoretically, the phenomena observed for the weak field case should now occur for the zero magnetic field case and vice versa. This is a consequence of the sign of the nonlinear term in equations (3-47) and (3-48).

In conclusion, it must be noted that in order to experimentally obtain a wider range of parameters, the experiment as described should be modified in two ways: the duration of the pulse should be increased, and the cathode arrangement changed. Increasing the pulse duration enhances the nonlinear effects (see equations(3-57) and (3-58)), whereas

changing the cathode, to a flat cathode for instance, will eliminate the rotational instability of the column, observed at high magnetic fields.

VI. Appendices

6.1 Formal derivation of operators

Equation (3-10) may be written approximately up to second order in the field variables as:

$$\underset{\sim}{u} = \underset{\sim}{u}^{(1)} + \underset{\sim}{u}^{(2)} \tag{6-1}$$

where,

$$m d_t \underset{\sim}{u}^{(1)} + m\nu_c \underset{\sim}{u}^{(2)} = - e n_o \underset{\sim}{E} - e\mu_o \underset{\sim}{u}^{(1)} \times \underset{\sim}{H}_o \tag{6-2}$$

and

$$m d_t \underset{\sim}{u}^{(2)} + m\nu_c \underset{\sim}{u}^{(2)} = - \frac{m}{n_o} \nabla . \underset{\sim}{u}^{(1)} \underset{\sim}{u}^{(1)} - e\tilde{n} \underset{\sim}{E} - e\mu_o \underset{\sim}{u}^{(2)} \times \underset{\sim}{H}_o \tag{6-3}$$

Formally solving (6-2) and (6-3),

$$\underset{\sim}{u}^{(1)} = - (m d_t \underset{\approx}{1} - e\mu_o \underset{\sim}{H}_o \times \underset{\approx}{1} + m\nu_c \underset{\approx}{1})^{-1} e n_o \underset{\sim}{E} \tag{6-4}$$

$$u^{(2)} = - (m d_t \underset{\approx}{1} - e\mu_o \underset{\sim}{H}_o \times \underset{\approx}{1} + m\nu_c \underset{\approx}{1})^{-1} [\frac{m}{n_o} \nabla . \underset{\sim}{u}^{(1)} \underset{\sim}{u}^{(1)} + e\tilde{n} \underset{\sim}{E}] \tag{6-5}$$

Defining the inverse operator:

$$\Pi (d_t, \underset{\sim}{H}_o, \nu_c) = (m d_t \underset{\approx}{1} - e\mu_o \underset{\sim}{H}_o \times \underset{\approx}{1} + m\nu_c \underset{\approx}{1})^{-1} e n_o \tag{6-6}$$

the total current from (6-1)= (6-4)-(6-6) and (3-13) is given by:

$$\underset{\sim}{u} = - \Pi \{ \underset{\sim}{E} + \frac{m}{n_o^2 e} \nabla . \underset{\approx}{\pi} \underset{\sim}{E} \underset{\approx}{\pi} \underset{\sim}{E} - \frac{\epsilon_o}{e n_o} \underset{\sim}{E} \nabla . \underset{\sim}{E} \} \tag{6-7}$$

which is used to arrive at equations (3-15).

Defining the time Fourier transform of a field variable as:

$$f(\underset{\sim}{r}, t) = \int_{-\infty}^{\infty} f(\underset{\sim}{r}, \omega) e^{-i\omega t} \frac{d\omega}{2\pi}$$

Applying the above to equations (6-6) and (6-7), we obtain:

$$\underset{\approx}{\Pi}(\omega, \underset{\sim}{H}_o, \nu_c) \rightarrow \begin{pmatrix} \Pi_1 & -\Pi_2 & 0 \\ \\ \Pi_2 & \Pi_1 & 0 \\ 0 & 0 & \dfrac{n_o e}{im^*\omega} \end{pmatrix} \qquad \begin{aligned} \Pi_1 &= \frac{n_o e}{im^*\omega\left[1 - \dfrac{(e\mu_o H_o/m^*)^2}{\omega^2}\right]} \\ \Pi_2 &= \frac{n_o e(e\mu_o H_o/m^*)}{m^*\omega^2\left[1 - \dfrac{(e\mu_o H_o/m^*)^2}{\omega^2}\right]} \end{aligned} \tag{6-8}$$

$$\underset{\sim}{u}(\underset{\sim}{\Omega}, \omega) = -\underset{\approx}{\Pi}(\omega_1 \underset{\sim}{H}_o, \nu_c)\{\underset{\sim}{E}(\underset{\sim}{\Omega}, \omega) + \frac{m}{n_o^2 e}\int \nabla . \underset{\approx}{\Pi}(\omega_1, \underset{\sim}{H}_o, \nu_c)\underset{\sim}{E}\omega_1 \underset{\approx}{\Pi}(\omega_2, \underset{\sim}{H}_o, \nu_c)\underset{\sim}{E}\omega_2 d\lambda$$

$$- \frac{\epsilon_o}{en_o}\int \underset{\sim}{E}\omega_1 \nabla . \underset{\sim}{E}\omega_2 d\lambda\,\} \tag{6-9}$$

where $m^* = m(1 + i\nu_c/\omega)$

and for any two vectors $\underset{\sim}{F}(\underset{\sim}{\Omega}, t)$ and $\underset{\sim}{G}(\underset{\sim}{\Omega}, t)$,

$$\int \underset{\sim}{F}\omega_1 \underset{\sim}{G}\omega_2 d\lambda = \int \underset{\sim}{F}(\underset{\sim}{r}, \omega_1)\, \underset{\sim}{G}(\underset{\sim}{r}, \omega_2)\delta(\omega - \omega_1 - \omega_2)d\omega_1 d\omega_2$$

Using (6-8) and (6-9), the transform of L in equation (3-16) is given by

$$L(-i\omega, \nabla_t \rightarrow i \begin{pmatrix} i\omega\epsilon_o[\underset{\approx}{1} + \dfrac{e}{\epsilon_o\omega}\underset{\approx}{\Pi}(\omega, H_o, \nu_c)] & \nabla_t x \underset{\approx}{1} \\ \\ -\nabla_t x \underset{\approx}{1} & i\omega\mu_o \underset{\approx}{1} \end{pmatrix}$$

6.2 <u>Evaluation of the eigenvectors</u>

The eigenvalue equation (3-19) may be expressed solely in terms of the transverse components of ψ_α as:[40]

$$\omega(\underset{\approx}{\epsilon}_t \epsilon_o - \frac{1}{\omega^2 \mu_o}\underset{\sim}{z}_o x \nabla_t \nabla_t x \underset{\sim}{z}_o) \,.\, \underset{\sim}{E}_{\alpha_t} = \kappa_\alpha \underset{\sim}{H}_{\alpha_t} x \underset{\sim}{z}_o$$

$$\omega(\mu_o \underset{\approx}{1}_t - \frac{1}{\omega^2 \epsilon_o}\underset{\sim}{z}_o x \nabla_t \frac{1}{\epsilon_3}\nabla_t x \underset{\sim}{z}_o) \,.\, \underset{\sim}{H}_{\alpha_t} = \kappa_\alpha \underset{\sim}{z}_o x \underset{\sim}{E}_{\alpha_t} \tag{6-10}$$

where

$$\underset{\approx}{\epsilon} = \underset{\approx}{\epsilon}_t + \underset{\sim}{z}_o \underset{\sim}{z}_o \epsilon_3 = \begin{cases} \underset{\approx}{1} + \dfrac{e}{\epsilon_o \omega} \underset{\approx}{\Pi}(\omega, H_o, \nu_c) & \rho < b \\ \\ \underset{\approx}{1} & \rho > b \end{cases} \tag{6-11}$$

and the longitudinal field components may be obtained from the transverse components via:

$$\begin{pmatrix} E_{\alpha_z} \\ \\ H_{\alpha_z} \end{pmatrix} = \begin{pmatrix} 0 & (i\omega\epsilon_3\epsilon_o)^{-1} \; \nabla_t \times \underset{\sim}{z}_o \\ \\ -(i\omega\mu_o)^{-1} \; \nabla_t \times \underset{\sim}{z}_o & 0 \end{pmatrix} \begin{pmatrix} \underset{\sim}{E}_{\alpha_t} \\ \\ \underset{\sim}{H}_{\alpha_t} \end{pmatrix} \tag{6-12}$$

Note that since the operator L_o takes different forms in the range $0 < \rho < \infty$, likewise $\underset{\sim}{\psi}_\alpha$'s will have different representations.

In general, the total field corresponding to $\underset{\sim}{E}_{\alpha_t}$ and $\underset{\sim}{H}_{\alpha_t}$ will have both E_{α_z} and H_{α_z} components.[40] This implies that no TE or TM mode representation is possible; therefore a complete set of modes must be composed of TE and TM modes. In the following analysis, we will restrict to the cases: a) zero static magnetic field, b) infinitely large magnetic field and c) weak magnetic fields, i. e. $\omega_{te} < \omega_{pe}$, and the column is surrounded by a perfect condition. The first two cases result in substantial simplification in the form of the eigenvectors and eigenvalues. For these cases, Eqs. (2-3) can be satisfied with either E_{α_z} or H_{α_z} equal to zero. This implies that two independent solutions are possible. Since neither the nonlinearity nor the boundary couple the two solutions and since initially only E modes are generated by the electric current source, only these will be considered in the field representation. For the low magnetic field case, we make the assumption that the waves are slow and, therefore, are primarily TM type, i. e., the actual field eigenvectors are approximated by quasistatic eigenvectors.

An implicit assumption, when representing the total fields as a superposition of modal fields, is that the modal set (or eigenvectors)

is complete, i.e., they form a basis in terms of which any arbitrary vector may be represented. A statement of completeness may be expressed as follows:[40]

$$\sum_{\alpha} \psi_{\alpha_t^*}(\Omega') \; \psi_{\alpha_t}(\underset{\sim}{\Omega}) = \underset{\approx}{1}\, \delta(\underset{\sim}{\Omega} - \underset{\sim}{\Omega}') \tag{6-13}$$

The sumation in (6-13) is to be interpreted as an integral for the case of continuous spectrum and as a sum for the discrete spectrum. A direct procedure for determining the spectrum utilizes the characteristic Green's function for E modes.[40] The properties of the Green's function in the complex κ_α plane are investigated; and from pole and branch singularities, which contribute to the integral of Green's function along a suitable contour in the complex κ_α plane, the eigenvectors are obtained. In this case, the question of completeness is assured although normalization as in (3-19a) is not. This procedure will be used subsequently for the determination of the mode vectors of the zero axial magnetic field case.

For the other two cases, we proceed directly to obtain that part of the spectrum associated with guided waves.

6.2.1 <u>Eigenvectors for zero magnetic field</u>

When $\underset{\sim}{H}_o$ is zero, then tensor $\underset{\approx}{\epsilon}$ degenerates into a scalar quantity. In the plasma region, $\underset{\approx}{\epsilon} \rightarrow \underset{\approx}{1}\left(1 - \frac{\omega p^2}{\omega^2}\right)$. Since for an E mode $\nabla_t \cdot \underset{\sim}{z}_o \times E_{\alpha_t} = 0$, we have (from equation (6-10) for the scalar Green's function:[40]

$$\nabla_t \cdot \frac{\epsilon}{\kappa_\perp^2} \cdot \nabla_t g + \epsilon g = -\,\delta(\rho - \rho') \tag{6-14}$$

where

$$\kappa_{\perp i}^2 = \begin{cases} \kappa_{\perp i}^2 = \omega^2 \mu_o \epsilon_o - \epsilon \kappa_\alpha^2 & \rho < b \\ \kappa_{\perp 2}^2 = \omega^2 \mu_o \epsilon_o - \kappa_\alpha^2 & \rho < b \end{cases}$$

Boundary conditions for g may be obtained from (6-14), since it is valid for all ρ. By integrating across $\rho = b$ and $\rho = \rho'$, we have the conditions:

1) g is continuous at $\rho = b$ and $\rho = \rho'$

$$2)\ \frac{\epsilon}{\kappa_{\perp i}^2} \nabla_t g \Big/_{\rho'_-}^{\rho'_+} = -1 \qquad (6\text{-}15)$$

$$3)\ \frac{\epsilon}{\kappa_{\perp i}^2} \nabla_t g \Big/_{b_-}^{b^+} = 0$$

for a symmetric source of electric current located at $\rho = b^+$, the solution to (6-14) satisfying (6-15) is:

$$g = \begin{cases} \dfrac{-J_o(\kappa_{\perp 1} b)\, J_o(\kappa_{\perp 1} \rho)}{\Delta} & \rho < b \\[2ex] \dfrac{-J_o^2(\kappa_{\perp 1} b)}{H_o^2(\kappa_{\perp 2} b)} \quad \dfrac{H_o(\kappa_{\perp 2} b)\, H_o(\kappa_{\perp 2} \rho)}{\Delta} & \rho > b \end{cases} \qquad (6\text{-}16)$$

$$\text{where } \Delta = \frac{\epsilon\, J_1(\kappa_{\perp 1} b)\, H_o(\kappa_{\perp 2} b)}{\kappa_{\perp 1}} - \frac{J_o(\kappa_{\perp 1} b)\, H_1(\kappa_{\perp 2} b)}{\kappa_{\perp 2}} \qquad (6\text{-}17)$$

and J_1, J_o, H_o, H_1 are Bessel functions of the first and second kind, respectively.

The spectral representation in (6-13) may now be obtained by integrating the scalar Greens function along a contour that encloses all singularities of g. The desired relationship is given by[40]:

$$\sum_{\alpha} \phi_{\alpha}(\kappa_{\perp i}\rho)\,\phi_{\alpha}^{*}(\kappa_{\perp i}\rho) = \frac{1}{2\pi i}\oint_{c} g(\rho,\rho';\kappa_{\alpha})\,d\kappa_{\alpha}$$

$$= \begin{cases} -\dfrac{1}{2\pi i}\displaystyle\oint_{c} \dfrac{J_{o}(\kappa_{\perp 1} b)\,J_{o}(\kappa_{\perp 1}\rho)\,d\kappa_{\alpha}}{\Delta} \\ -\dfrac{1}{2\pi i}\displaystyle\oint_{c} \dfrac{J_{o}^{2}(\kappa_{\perp 1} b)}{H_{o}^{2}(\kappa_{\perp 2} b)}\;\dfrac{H_{o}(\kappa_{\perp 2} b)\,H_{o}(\kappa_{\perp 2}\rho)\,d\kappa_{\alpha}}{\Delta} \end{cases} \qquad (6\text{-}18)$$

the transverse component of $\underset{\sim}{E}_{\alpha}$ is obtained from ϕ_{α} using,

$$\underset{\sim}{E}_{\alpha_t} = -\frac{\kappa_{\alpha}}{\kappa_{\perp i}^{2}\,\omega\epsilon_{o}}\,\nabla_{t}\, g \qquad i = \begin{cases} 1 & \rho < b \\ 2 & \rho > b \end{cases} \qquad (6\text{-}19)$$

The integrand in (6-18) is analytic everywhere except for a finite number of poles and branch points. For real κ_{α}, only a single pole exists at $\Delta = 0$; the branch point corresponds to $\kappa_{\perp 2} = 0$ for which $\kappa_{\alpha} = \pm\,\omega\sqrt{\mu_{o}\epsilon_{o}}$. The pole contribution gives rise to a guided surface mode, while the branch cut contribution gives rise to a radiation field.[46] For the excitation problem both contributions must be included, specially at the source. In the far field we only consider the guided wave, but as observed in Chapter III; we do not know the absolute field strength of the guided mode since we neglect to include the amount of energy extracted from the source by the other mode types. For guided modes, $\kappa_{\perp 1} = i|\kappa_{\perp 1}|$, $\kappa_{\perp 2} = i|\kappa_{\perp 2}|$ and from (6-18), we have for the guided modes:

$$\phi_{\alpha} = \begin{cases} \dfrac{I_{o}(\kappa_{\perp 1}\rho)}{\sqrt{\partial_{\kappa_{\alpha}}\Delta}} & \rho < b \\[2ex] \dfrac{I_{o}(\kappa_{\perp 1} b)}{K_{o}(\kappa_{\perp 2} b)}\;\dfrac{K_{o}(\kappa_{\perp 2}\rho)}{\sqrt{\partial_{\kappa_{\alpha}}\Delta}} & \rho > b \end{cases}$$

with κ_α given by:

$$\frac{\epsilon\, I_1(\kappa_{\perp 1} b)\, K_o(\kappa_{\perp 2} b)}{\kappa_{\perp 1}} + \frac{I_o(\kappa_{\perp 1} b)\, K(\kappa_{\perp 2} b)}{\kappa_{\perp 2}} = 0 \tag{6-20}$$

From (6-19) the transverse field components are given by:

$$\underset{\sim}{E}_{\alpha_t} = \begin{cases} \dfrac{\kappa_\alpha\, I_o'(\kappa_{\perp 1}\rho)}{\omega\epsilon_o \kappa_{\perp 1}\sqrt{\partial_{\kappa_\alpha}\Delta}}\ \underset{\sim}{\rho} & \rho < b \\[2ex] -\dfrac{I_o(\kappa_{\perp 1} b)}{K_o(\kappa_{\perp 2} b)}\ \dfrac{\kappa_\alpha\, K_o'(\kappa_{\perp 2}\rho)}{\kappa_{\perp 2}\,\omega\epsilon_o\sqrt{\partial_{\kappa_\alpha}\Delta}}\ \underset{\sim}{\rho} & \rho > b \end{cases} \tag{6-21}$$

$$\underset{\sim}{H}_{\alpha_t} = \begin{cases} \dfrac{\epsilon}{\kappa_{\perp 1}}\ \dfrac{I_1(\kappa_{\perp 1}\rho)}{\sqrt{\partial_{\kappa_\alpha}\Delta}}\ \underset{\sim}{\theta} & \rho < b \\[2ex] -\dfrac{I_o(\kappa_{\perp 1} b)}{K_o(\kappa_{\perp 2} b)}\ \dfrac{K_1(\kappa_{\perp 2}\rho)}{\kappa_{\perp 2}\sqrt{\partial_{\kappa_\alpha}\Delta}}\ \underset{\sim}{\theta} & \rho > b \end{cases} \tag{6-22}$$

Even though the potential functions are orthonormal; the transverse components of the eigenvector do not satisfy condition (3-19a). Proper normalization is introduced by defining a normalization factor as follows:

$$N_\alpha = 2\int_o^b \frac{I_1^2(\kappa_{\perp 1}\rho)\,\epsilon\,\kappa_\alpha}{\kappa_{\perp 1}^2\sqrt{\partial_{\kappa_\alpha}\Delta}\ \omega\epsilon_o}\,\rho\, d\rho + 2\,\frac{I_o^2(\kappa_{\perp 1} b)}{K_o^2(\kappa_{\perp 2} b)}\int_b^\infty \frac{K_1^2(\kappa_{\perp 2}\rho)}{\kappa_{\perp 2}^2\,\omega t_o\sqrt{\partial_{\kappa_\alpha}\Delta}}\,\rho\, d\rho$$

the above can be rewritten as:

$$N_\alpha = \frac{2\,\beta\,\kappa_\alpha}{\omega\epsilon_o\,\partial_{\kappa_2}\Delta} \tag{6-23}$$

where

$$\beta = \int_0^b \frac{I_1^2(\kappa_{\perp 1}\rho)\,\epsilon}{\kappa_{\perp 1}^2}\rho\,d\rho + \frac{I_o^2(\kappa_{\perp 1}b)}{K_o^2(\kappa_{\perp 2}b)}\int_b^\infty \frac{K_1^2(\kappa_{\perp 2}\rho)}{\kappa_{\perp 2}^2}\rho\,d\rho \qquad (6\text{-}24)$$

(6-24) is evaluated explicitly by using the formulae[47]:

$$\int_0^b I^2(\kappa_{\perp 1}\rho)\rho\,d\rho = -\tfrac{1}{2}b^2\{I_1'^2(\kappa_{\perp 1}b) - (1 + \frac{1}{\kappa_{\perp 1}^2 b^2})I_1^2(\kappa_{\perp 1}b)\}$$

$$\int_0^\infty K_1^2(\kappa_{\perp 2}\rho)\rho\,d\rho = \tfrac{1}{2}b^2\{K_1'^2(\kappa_{\perp 2}b) - (1 + \frac{1}{\kappa_{\perp 2}^2 b^2})K_1^2(\kappa_{\perp 2}b)\} \quad ,$$

the characteristic equation (6-20), and the approximate dispersion equation (3-15). In the region $\kappa_{\perp 1} b < 1$, we can expand the Bessel functions in the small argument regime and obtain:

$$\beta = \frac{b^2}{2} I_o(\kappa_{\perp 1} b)\,\frac{\omega_p^2 v_d^2}{\omega^4} \qquad (6\text{-}25)$$

where

$$\frac{1}{v_d^2} = \frac{1}{\omega_p^2 v_o^2} - \frac{1}{C^2} \qquad \text{with } v_o \text{ given by (3-34)}$$

and $C \equiv$ speed of light.

The longitudinal component of the eigenvector as defined in (3-22) is obtained from (6-23), (6-21) and (6-12).

6.2.2 Eigenvectors for large Magnetic fields

In the limit of large magnetization, i.e., $\omega_c/\omega >> 1$ $\omega_c >> \omega_p$; transverse electron motion is effectively inhibited and the plasma becomes non-gyrotropic. The tensor $\underline{\underline{\epsilon}}$ in equation (6-10) for $\rho < b$ reduced to:

$$\underline{\underline{\epsilon}} \longrightarrow \begin{pmatrix} 1 & 0 & 0 \\ 0 & 1 & 0 \\ 0 & 0 & 1 - \frac{\omega_p^2}{\omega^2} \end{pmatrix}$$

The guided eigenvector components may be obtained from a potential ϕ as:

$$\underset{\sim}{E}_{\alpha_t} = - \frac{\kappa_\alpha}{\kappa^2_{\perp 2}} \nabla_t \, \phi \tag{6-26a}$$

and

$$\underset{\sim}{H}_{\alpha_t} = \frac{\omega\epsilon_o}{\kappa_\alpha} \underset{\sim}{z}_o \times \underset{\sim}{E}_{\alpha_t} \tag{6-26b}$$

where ϕ obeys the equation:

$$\nabla^2_t \, \phi + \kappa^2_{\perp i} \, \phi = 0 \tag{6-27}$$

with

$$\kappa^2_{\perp i} = \begin{cases} \kappa^2_{\perp 1} = \left(1 - \dfrac{\omega_p^2}{\omega^2}\right) \kappa^2_{\perp 2} & \rho < b \qquad (6\text{-}28) \\[2ex] \kappa^2_{\perp 2} = (\omega^2 \mu_o \epsilon_o - \kappa^2_\alpha) & \rho > b \qquad (6\text{-}29) \end{cases}$$

equation (6-27) is solved subject to two different boundary conditions: 1) column surrounded by a perfect conductor and 2) column in free space.

1) for a perfect conducting boundary the solution with proper behavior at $\rho = 0$ and $\rho = b$ is:

$$\phi = A \, J_o(\kappa_{\perp 1} \rho) \tag{6-30}$$

with $\kappa_{\perp 1} b = p_n$, where p_n is the n^{th} zero of the Bessel function J_o. Using (6-26) and (6-12), the eigenvector components are given by:

$$\psi_\alpha \longrightarrow A' \begin{pmatrix} \dfrac{\kappa_\alpha}{\kappa_{\perp 1}} \left(1 - \dfrac{\omega_p^2}{\omega^2}\right) J_1(\kappa_{\perp 1} \rho) \, \underset{\sim}{\rho} + i \, J_o(\kappa_{\perp 1} \rho) \underset{\sim}{z} \\[3ex] \dfrac{\omega\epsilon_o}{\kappa_{\perp 1}} \left(1 - \dfrac{\omega_p^2}{\omega^2}\right) J_1(\kappa_{\perp 1} \rho) \, \underset{\sim}{\theta} \end{pmatrix} \tag{6-31}$$

the normalization constant is determined from the orthonormality condition (3-19a):

$$1 = A' \int_0^b \{(i\kappa_\alpha)^* \frac{i\omega\epsilon_o}{\kappa_{\perp 1}^2} (1 - \frac{\omega_p^2}{\omega^2})^2 \, J_1^2(\kappa_{\perp 1}\rho) + i\kappa_\alpha (\frac{i\omega\epsilon_o}{\kappa_{\perp 1}^2}[1 - \frac{\omega_p^2}{\omega^2}]^2 \, J_1^2(\kappa_{\perp 1}\rho))^* \} \rho \, d\rho$$

for κ_α real, we have

$$A' = \frac{\kappa_{\perp 1}}{\sqrt{\omega\kappa_\alpha\epsilon_o} \; (1 - \frac{\omega_p^2}{\omega^2}) \, b \, J_1(\kappa_{\perp 1} b)}$$

If the α index is separated into two indecis: $m \equiv$ mode type, $n \equiv$ mode in mode type; we have:

$\psi_\alpha \to \psi_{mn} \to \psi_n$ since only E modes are considered.

2) Column in free space

The solution (6-30) of (6-28) is still valid in the region $\rho < b$, the plasma region. For $\rho > b$, the solution that satisfies boundary conditions at $\rho = b$ and appropriate to the discrete spectrum is:

$$\phi = A' \frac{J_o(\kappa_{\perp 1} b)}{K_o(\kappa_{\perp 2} b)} \quad K_o(\kappa_{\perp 2}\rho) \qquad (6\text{-}31)$$

where $\kappa_{\perp 2}$ and $\kappa_{\perp 1}$ are real and given by (see 6-29):

$$\kappa_{\perp 2}^2 = \kappa_\alpha^2 - \omega^2 \mu_o \epsilon_o$$

and the boundary characteristic equation

$$\frac{\kappa_{\perp 1} J_1(\kappa_{\perp 1} b)}{J_o(\kappa_{\perp 1} b)} = \frac{\kappa_{\perp 2} K_1(\kappa_{\perp 2} b)}{K_o(\kappa_{\perp 1} b)} \qquad (6\text{-}32)$$

from (6-30), (6-31) and (6-26); the field components of the eigenvector are:

$$\underline{\underline{\nu}} = L - L_o = i \begin{pmatrix} \dfrac{-i\omega\epsilon_o\omega_p^2\nu_c^2}{(\omega^2+\nu_c^2)\omega^2} + \dfrac{\epsilon_o\nu_c\omega_p^2}{(\omega^2+\nu_c^2)} & 0 \\ 0 & 0 \end{pmatrix}$$

in the regime $\nu_c/\omega \ll 1$,

$$\underline{\underline{\nu}} \simeq i \begin{pmatrix} \dfrac{\omega_p^2\nu_c\epsilon_o}{\omega^2+\nu_c^2} & 0 \\ 0 & 0 \end{pmatrix}$$

using above, we can expand the collision coefficient as in (3-21)

$$\gamma(\omega) = (\psi_\alpha, \underline{\underline{\nu}}\,\psi_\alpha) = i\int_0^b \underset{\sim}{E}_\alpha \cdot \underset{\sim}{E}_\alpha^* \,\frac{\omega_p^2\nu_c\epsilon_o}{\omega^2+\nu_c^2}\,\rho\,d\rho$$

$$= \frac{i\,\omega_p^2\nu_c}{\omega^2+\nu_c^2}\,\frac{\kappa_\alpha}{\omega 2\beta}\left\{\int_0^b \frac{I_1(\kappa_{\perp 1}\rho)}{\kappa_{\perp 1}^2}\,\rho\,d\rho + \int_0^b \frac{I_o^2(\kappa_{\perp 1}\rho)}{\kappa_\alpha^2}\,\rho\,d\rho\right\}$$

The integrals in the bracket are evaluated using the formulae in section 6.2. After approximating in $\kappa_{\perp 1} b < 1$ region:

$$\gamma(\omega) = \frac{i\omega_p^2\nu_c}{(\omega^2+\nu_c^2)}\,\frac{\kappa_\alpha}{2\omega\beta}\,\frac{b^2 I_o^2(\kappa_{\perp 1} b)}{\kappa_\alpha^2}$$

using the expression for β from 6.2 and the linear approximation for κ_α i.e.$_\perp$ $\kappa_\alpha \sim \omega/v_o$

$$\gamma(\omega) = \frac{i\;\omega^2}{(\omega^2+\nu_c^2)v_o}$$

for $\nu_c/\omega < 1$,

$$\gamma(\omega) \sim \frac{i\,\nu_c}{v_o} \quad \text{independent of frequency.} \qquad (6\text{-}35)$$

for $\rho < b$,

$$E_{\alpha_z} = iA' \frac{J_o(\kappa_{\perp 1} b)}{K_o(\kappa_{\perp 2} b)} K_o(\kappa_{\perp 2}\rho) \qquad (6\text{-}33a)$$

$$E_{\alpha_\rho} = -A' \frac{J_o(\kappa_{\perp 1} b)}{K_o(\kappa_{\perp 2} b)} \frac{\kappa_\alpha}{\kappa_{\perp 2}} K_1(\kappa_{\perp 2}\rho) \qquad (6\text{-}33b)$$

$$H_{\alpha_\theta} = -A' \frac{J_o(\kappa_{\perp 1} b)}{K_o(\kappa_{\perp 2} b)} \frac{\omega\epsilon_o}{\kappa_{\perp 2}} K_1(\kappa_{\perp 2}\rho) \qquad (6\text{-}33c)$$

for $\rho > b$, solution (6-31) holds. The normalization constant A' is obtained via (3-19a) as follows:

$$1 = 2A'^2 \frac{\kappa_\alpha \omega\epsilon_o}{\kappa_{\perp 2}} \left\{ \int_o^b \frac{\kappa_{\perp 1}^2}{\kappa_{\perp 2}^2} J_1^2(\kappa_{\perp 1}\rho)\rho\, d\rho + \frac{J_o^2(\kappa_{\perp 1} b)}{K_o^2(\kappa_{\perp 2} b)} \int_b^\infty K_1^2(\kappa_{\perp 2}\rho)\rho\, d\rho \right\}$$

evaluating the integral as in (6-24); the approximate value for the normalization constant is:

$$A' = \frac{\kappa_{\perp 2}}{\omega_p b\, J_o(\kappa_{\perp 1} b)} \sqrt{\frac{\omega}{\kappa_\alpha \epsilon_o}} \qquad (6\text{-}34)$$

the desired eigenvector is given by (6-31), (6-33) and (6-34).

6.3 Explicit evaluation of nonlinear and collision operators

Using the eigenvectors derived in the previous section and the approximate dispersion relations presented in section 3.2, we can explicitly evaluate the collision and nonlinear operators in equation (3-28).

6.3.1 Zero Magnetic field

When $\underset{\sim}{H}_o = 0$, the operator $\underset{=}{\nu}$ in equation (3-21) takes the form:

$$\underset{=}{\nu} = L - L_o = i \begin{pmatrix} \dfrac{-i\omega\epsilon_o\omega_p^2\nu_c^2}{(\omega^2+\nu_c^2)\omega^2} + \dfrac{\epsilon_o\nu_c\omega_p^2}{(\omega^2+\nu_c^2)} & 0 \\ 0 & 0 \end{pmatrix}$$

in the regime $\nu_c/\omega << 1$,

$$\underset{=}{\nu} = i \begin{pmatrix} \dfrac{\omega_p^2\nu_c\epsilon_o}{\omega^2+\nu_c^2} & 0 \\ 0 & 0 \end{pmatrix}$$

using above, we can expand the collision coefficient as in (3-21)

$$\gamma(\omega) = (\psi_\alpha, \underset{=}{\nu}\,\psi_\alpha) = i\int_o^b \underset{\sim}{E}_\alpha \cdot \underset{\sim}{E}_\alpha^* \frac{\omega_p^2\nu_c\epsilon_o}{\omega^2+\nu_c^2}\,\rho\, d\rho$$

$$= \frac{i\,\omega_p^2\nu_c}{\omega^2+\nu_c^2}\,\frac{\kappa_\alpha}{\omega 2\beta}\left\{\int_o^b \frac{I_1(\kappa_{\perp 1}\rho)}{\kappa_{\perp 1}^2}\,\rho\, d\rho + \int_o^b \frac{I_o^2(\kappa_{\perp 1}\rho)}{\kappa_\alpha^2}\,\rho\, d\rho\right\}$$

The integrals in the bracket are evaluated using the formulae in section 6.2. After approximating in $\kappa_{\perp 1} b < 1$ region:

$$\gamma(\omega) = \frac{i\omega_p^2\nu_c}{(\omega^2+\nu_c^2)}\,\frac{\kappa_\alpha}{2\omega\beta}\,\frac{b^2 I_o^2(\kappa_{\perp 1} b)}{\kappa_\alpha^2}$$

using the expression for β from 6.2 and the linear approximation for κ_α i.e. $\kappa_\alpha \sim \omega/v_o$

$$\gamma(\omega) = \frac{i\ \omega^2}{(\omega^2+\nu_c^2)v_o}$$

for $\nu_c/\omega < 1$,

$$\gamma(\omega) \sim \frac{i\,\nu_c}{v_o} \quad \text{independent of frequency.} \qquad (6\text{-}35)$$

the above equation is the same equation obtained by Trivelpiece et al[8] since $\frac{\partial \kappa_\alpha}{\partial \omega} \sim v'_o$ for $\omega << \omega_p$.

Neglecting the effects of collisions, the nonlinear term in equation (2-21) is expanded as:

$$i\,[\underset{\sim}{E}_\alpha(\omega), N'(\mathcal{A}_\alpha \underset{\sim}{E}_\alpha(\omega))]$$

$$= \frac{1}{\omega}\int\{((\frac{e\epsilon_o}{m}\frac{\omega_p^2}{\omega_1\omega_2} + \frac{e\epsilon_o}{m})\,[\mathcal{A}_\alpha(z,\omega_1)\mathcal{A}_\alpha(z,\omega_2)\nabla_T\cdot \underset{\sim}{E}_\alpha^{\omega_2}(\underset{\sim}{E}_\alpha^{\omega_1}, \underset{\sim}{E}_\beta^{*\omega})$$

$$+\mathcal{A}_\alpha(z,\omega_1)\partial_z\mathcal{A}_\alpha(z,\omega_2)\underset{\sim}{E}_\alpha^{\omega_2}(\underset{\sim}{E}_\alpha^{\omega_1}, \underset{\sim}{E}_\beta^{*\omega})]$$

$$+\frac{e\omega_p^2\epsilon_o}{\omega_1\omega_2 m}\mathcal{A}_\alpha(z,\omega_2)\,[\underset{\sim}{E}_\alpha^{\omega_2}\cdot(\underset{\sim}{z}_o\partial_z\mathcal{A}_\alpha(z,\omega_1)\underset{\sim}{E}_\alpha^{\omega_1})$$

$$+\mathcal{A}_\alpha(z,\omega_1)\,\underset{\sim}{E}_\alpha^{\omega_2}\cdot\nabla_T\underset{\sim}{E}_\alpha^{\omega_1}]\,,\,\underset{\sim}{E}_\alpha^{*\omega}\}\,\delta(\omega-\omega_1-\omega_2)d\omega_1 d\omega_2$$

where $\underset{\sim}{E}_\alpha^{\omega_i}$ is the eigenvector associated with the amplitude $\mathcal{A}_\alpha(z,\omega_i)$. In order to simplify the above equation, we expand $\mathcal{A}_\alpha(z,\omega_1)\partial_z\mathcal{A}_\alpha(z,\omega_2)$ up to second order as:

$$\mathcal{A}_\alpha(z,\omega_1)\partial_z\mathcal{A}_\alpha(z,\omega_2) = \mathcal{A}_\alpha(z,\omega_1)\,i\kappa_\alpha(\omega_2)\mathcal{A}_\alpha(z,\omega_2) \qquad (6\text{-}36)$$

Using this expansion, the first square bracket term becomes zero while the second is expanded to:

$$= \frac{e\epsilon_o\omega_p^2}{m\omega}\int\frac{\mathcal{A}_\alpha(z,\omega_1)\mathcal{A}_\alpha(z,\omega_2)}{\omega_1\ \omega_2}\{\int_o^b[E_{\alpha\rho}^{\omega_2}\partial_\rho E_{\alpha\rho}^{\omega_1}E_{\alpha\rho}^{\omega *} + E_{\alpha\rho}^{\omega_2}\partial_\rho E_{\alpha\rho}^{\omega_1}E_{\alpha z}^{\omega *}$$

$$+i\,\kappa_\alpha(\omega_1)E_{\alpha z}^{\omega_2}E_{\alpha\rho}^{\omega_1}E_{\alpha\rho}^{\omega *} + i\,\kappa_\alpha(\omega_1)E_{\alpha z}^{\omega_2}E_{\alpha z}^{\omega_1}E_{\alpha z}^{\omega *}]\,\rho\,d\rho\}\delta(\omega-\omega_1-\omega_2)d\omega_1 d\omega_2$$

$$(6\text{-}37)$$

putting in for the eigenvector components from section 6-2 we obtain

equation (3-29).

Putting in for β from section 6.2 and letting $I_1(\kappa_{\perp 1}\rho) \sim \frac{1}{2}\kappa_{\perp 1}\rho$, $I_1^{(2)'} \sim \kappa_{\perp 1}^{(2)}/2\, I_o(\kappa_{\perp 1}\rho)$ i.e. $\kappa_{\perp 1} b < 1$ regime, the nonlinear term corresponding to P is evaluated as:

$$= \frac{e}{m}\int \frac{\omega_1\omega_2\omega\, b^4}{2^6(\omega_p^2 v_d v_o^3 b^6 \epsilon_o)^{\frac{1}{2}}}\, \mathcal{A}_a(z,\omega_1)\, \mathcal{A}_a(z,\omega_2)\,\delta(\omega-\omega_1-\omega_2)\,d\omega_1 d\omega_2 \qquad (6\text{-}38)$$

where

$$v_d^2 = \frac{v_o^2}{(1-v_o^2/c^2)}$$

and for $\kappa_a(\omega)$ the linear contribution has been used. Similarly the contribution due to ω is evaluated

$$= -\frac{e}{m}\int\Big\{ \frac{\omega_1^2\,\omega}{(\epsilon_o b^6\omega_p^6 v_o v_d^6)^{\frac{1}{2}}}\;\frac{1}{I_o^{(1)} I_o^{(2)} I_o^{(o)}}\int_o^b \frac{I_o^{(2)} I_1^{(o)} I_1^{(1)}}{\kappa_{\perp 1}^{(1)}\,\kappa_{\perp 1}^{(o)}}\,\rho\, d\rho$$

$$-\frac{v_o\omega_2}{(v_o b^6 v_d^6\epsilon_o)^{\frac{1}{2}}}\;\frac{1}{I_o^{(1)} I_o^{(2)} I_o^{(o)}}\int_o^b \Big[I_o^{(1)} I_o^{(2)} I_o^{(o)} - \kappa_{\perp 1}^{(1)}\frac{I_1^{(1)} I_1^{(2)} I_o^{(o)}}{\kappa_{\perp 1}^{(2)}}\Big]\rho\, d\rho\Big\}$$

$$\mathcal{A}_a(z,\omega_1)\mathcal{A}_a(z,\omega_2)\,\delta(\omega-\omega_1-\omega_2)\,d\omega_1 d\omega_2 \qquad (6\text{-}39)$$

letting $I_1 \sim \frac{\kappa_{\perp 1}}{2} I_o$ and expanding I_o to first order (for $\kappa_{\perp 1} b < 1$), the integrals in (6-39) can be readily evaluated. Combining the result with equation (6-38), we arrive at equation (3-39).

6.3.2 Infinite Magnetic field.

When the magnetic field is large, the nonlinear term in equation (3-21) reduces to:

$$i[N(\mathcal{Q}_\alpha \underset{\sim}{E}_\alpha \cdot \underset{\sim}{E}_\alpha)] = \frac{\epsilon_o e}{m\omega} \int \{ (\frac{2\omega_p}{\omega_1 \omega_2} + 1) \mathcal{Q}_\alpha(z,\omega_2) \partial_z \mathcal{Q}_\alpha(z,\omega_1) \int_0^b E_{\alpha_z}^{\omega_2} E_{\alpha_z}^{\omega_1} E_{\alpha_z}^{\omega} \rho \, d\rho$$

$$+ \mathcal{Q}_\alpha(z,\omega_1)\, \mathcal{Q}_\alpha(z,\omega_2) \int_0^b E_{\alpha_z}^{\omega_2} \nabla_T \cdot \underset{\sim}{E}_{\alpha_T}^{\omega_1} E_{\alpha_z}^{\omega *} \rho \, d\rho \} \, \delta(\omega - \omega_1 \omega_2) d\omega_1 d\omega_2 \quad (6\text{-}40)$$

from equation (3-13) and (3-10), we have to first order:

$$\nabla_T \cdot \underset{\sim}{E}_{\alpha_T} = -i \kappa_\alpha (1 - \frac{\omega_p^2}{\omega^2}) E_{\alpha_z}$$

Using above equation and the expansion of (6-36) in (6-39), we obtain for nonlinear term:

$$= \frac{\epsilon_o e}{m\omega} \int \{ (\frac{2\omega_p}{\omega_1 \omega_2} + \frac{\omega_p^2}{\omega_1^2}) \, i \, \kappa_\alpha(\omega_1) \mathcal{Q}_\alpha(z,\omega_1) \mathcal{Q}_\alpha(z,\omega_2) \int_0^b E_{\alpha_z}^{\omega_1} E_{\alpha_z}^{\omega_2} E_{\alpha_z}^{\omega *} \rho \, d\rho \}$$

$$\delta(\omega - \omega_1 - \omega_2) d\omega_1 d\omega_2$$

Putting in for E_{α_z} from section 6.2,

$$= -\frac{\epsilon_o e}{m\omega} \int \{ (\frac{2\omega_p}{\omega_1 \omega_2} + \frac{\omega_p^2}{\omega_1^2}) \; \kappa_\alpha(\omega_1) \mathcal{Q}_\alpha(z,\omega_1) \mathcal{Q}_\alpha(z,\omega_2) A'(\omega) A'(\omega_2) A'(\omega_3)$$

$$\int_0^b J_o^3 \, (\kappa_{\perp 1} \rho) \rho \, d\rho \} \; \delta\,(\omega - \omega_1 - \omega_2) d\omega_1 d\omega_2 \quad (6\text{-}41)$$

the form of (6-41) is the same for both cases: column in free space and column surrounded by perfect conductor. The difference lies in the explicit form the normalization coefficient $A'(\omega)$ takes. When the column is surrounded by a perfect conductor the normalization is (from section 6. 2):

$$A'(\omega) = \frac{\kappa_{\perp 1}}{b} \; \frac{1}{(\omega \kappa_\alpha \epsilon_o)^{\frac{1}{2}} (1 - \frac{\omega_p^2}{\omega^2}) \; b \, J_1(\kappa_{\perp 1} b)} \quad (6\text{-}42)$$

where $\kappa_{\perp 1} b = p_n$. p_n is the n^{th} zero of J_o. Assuming that only the

lowest order mode is present (higher order modes are slower and consequently attenuated at a faster rate)[34],

$$\kappa_{\perp 1} b = 2.405$$

and equation (6-41) becomes:

$$= + \frac{e}{m}\int\left\{ \frac{(2\omega_1 + \omega_2)}{\omega_p^4}\left(\frac{\upsilon_\infty}{\epsilon_o}\right)^{\frac{1}{2}} \frac{(2.405)^3}{b^6} \frac{\int_o^b J_o^3(\kappa_{\perp 1}\rho)\rho\, d\rho}{J_1^3(\kappa_{\perp 1} b)}\right\} \mathcal{a}_a(z,\omega_1)$$

$$\mathcal{a}_a(z,\omega_2)\,\delta(\omega-\omega_1-\omega_2)d\omega_1 d\omega_2 \qquad (6\text{-}43)$$

In the above derivation, it is assumed that $\omega < \omega_p$, so that the linear portion of the dispersion equation gives the maximum contribution to the nonlinear term. For the column in free space,

$$A'(\omega) = \frac{\kappa_{\perp 2}}{\omega_p b J_o(\kappa_{\perp 1} b)}\sqrt{\frac{\omega}{\kappa_a \epsilon_o}} \qquad (6\text{-}44)$$

and (6-41) becomes

$$= \frac{e}{m}\int\left\{ \frac{(2\omega_1 + \omega_2)}{\omega_p \upsilon_\infty^3 b^3}\sqrt{\frac{\upsilon_\infty}{\epsilon_o}} \frac{\int_o^b J_o^3(\kappa_{\perp 1}\rho)\rho\, d\rho}{J_o^3(\kappa_{\perp 1} b)}\right\} \mathcal{a}_a(z,\omega_1)\mathcal{a}_a(z,\omega_2)\delta(\omega-\omega_1-\omega_2)d\omega_1 d\omega_2$$

$$(6\text{-}45)$$

where the same assumptions leading to (6-43) have been used. (6-43) and (6-45) lead to (3-42).

The collision operator for large magnetic fields is given by:

$$\underline{\underline{\nu}} = L - L_o = i \begin{pmatrix} -i\omega\epsilon_o \underline{\underline{\epsilon}}' & 0 \\ 0 & 0 \end{pmatrix}$$

where

$$\epsilon' = \begin{pmatrix} 0 & 0 & 0 \\ 0 & 0 & 0 \\ 0 & 0 & \frac{\nu_c^2 \omega_p^2}{\omega^3(\omega^2+\nu_c^2)} + i\,\frac{\nu_c \omega_p^2}{\omega^2(\omega^2+\nu_c^2)} \end{pmatrix}$$

The collision term takes the form (for $\nu/\omega < 1$),

$$(\psi_\alpha, \underset{=}{\nu}\, \psi_\alpha) = i \int_0^b E_{\alpha_z} E_{\alpha_z}^* \left(\frac{\omega_p^2 \nu_c \epsilon_o}{\omega^2 + \nu_c^2} \right) \rho\, d\rho$$

putting in for the longitudinal component of the eigenvector,

$$= i \cdot \left[\int_0^b A'^2(\omega)\, J_o^2(\kappa_{\perp 1} \rho) \rho\, d\rho \right] \frac{\omega_p^2 \nu_c \epsilon_o}{\omega^2 + \nu_c^2} \tag{6-46}$$

Again, the above form applies for both column in free space and column surrounded by conductor. Using (6-42), the collision coefficient when the column is surrounded by a perfect conductor is,

$$\gamma(\omega) = \frac{\kappa_{\perp 1}^2 \propto}{\omega_p^2 b^2} \quad \frac{\int_0^b J_o^2(\kappa_{\perp 1} \rho) \rho\, d\rho}{J_1^2(\kappa_{\perp 1} b)} \qquad \text{for } \nu_c/\omega < 1$$

and again we have assumed that $\omega < \omega_p$, so that the major contribution to κ_α arises from the linear term.

Similarly, for the column in free space:

$$\gamma(\omega) = \frac{\nu_c}{\nu_\infty b^2 J_o^2(\kappa_{\perp 1} b)} \int_0^b J_o^2(\kappa_{\perp 1} \rho) \rho\, d\rho$$

6.3.3 Weak Magnetic field.

To obtain the Kernel given in (3-30); the nonlinear term in equation (2-21) is expanded in component form, and consistent with the slow mode assumption, we only retain the term arising from the coupling of the longitudinal electric field. For $\omega < \omega_c < \omega_p$, this term is given by:

$$= i \int \left[\frac{n_o e^3}{m^2} \left(2 - \frac{\omega_p^2}{\omega_p^2 + \omega_c^2}\right) \frac{1}{\omega_1 \omega_2 \omega} + \frac{\epsilon_o e}{m} \frac{1}{\omega} \frac{\omega_p^2 \omega_c^2}{\omega_1^2 (\omega_p^2 + \omega_c^2)} \right] \kappa_\alpha(\omega_1) a_\alpha(z, \omega_1) a_\alpha(z, \omega_2)$$

$$(E_z^{(1)} E_z^{(2)}, E_z^*)\ \delta(\omega - \omega_1 - \omega_2)\, d\omega_1 d\omega_2$$

Using the expression for the z component of the eigenvector (from 6. 2. 3) to explicitly write the inner product:

$$= \frac{-e\epsilon_o}{m} \int\left[\left(2-\frac{\omega_p^2}{\omega_p^2+\omega_c^2}\right)\frac{\omega_p^2}{\omega_1\omega_2\omega} + \frac{\omega_p^2\omega_c^2}{\omega\omega_1^2(\omega_p^2+\omega_c^2)}\right] \kappa_\alpha(\omega_1)\mathcal{A}_\alpha(z,\omega_1)\mathcal{A}_\alpha(z,\omega_2)$$

$$A(\omega_1)\,A(\omega_2)\,A(\omega) \int_0^b J_o^3(\kappa_{\perp 1}\rho)\rho\, d\rho \quad \delta(\omega-\omega_1-\omega_2)d\omega_1 d\omega_2$$

Putting in for the normalization coefficient $A(\omega)$ and proceeding as in 6. 3. 2, we arrive at the final form (3-44).

REFERENCES

1. W. B. Kunkel, "Plasma Physics in Theory and Applications," McGraw Hill (1966).

2. V. L. Ginzburg, "Propagation of Electromagnetic Waves in Plasma" Gordon and Breach (1960).

3. T. H. Stix, "The Theory of Plasma Waves," McGraw - Hill (1962).

4. V. N. Tsytovich, "Nonlinear Effects in Plasma," Plenum Press (1970).

5. R. C. Davidson "Methods in Nonlinear Plasma Theory," Academic (1972).

6. F. Einaudi, R. N. Sudan, "A Review of the Nonlinear Theory of Plasma Oscillations," Plasma Phys. 11, pp. 359-389 (1969).

7. Y. Akao and Y. Ida, "Electron Density Measurements of a Plasma Column by Surface Wave Resonances" J. Applied Physics, Vol. 35 pp. 2565-2570, (1964).

8. A. Trivelpiece and R. W. Gould, "Space Charge Waves in Cylindrical Plasma Columns," J. Applied Phys, Vol 30 pp. 1784-1793, (1959).

9. M. A. Heald and C. B. Wharton, "Plasma Diagnostics with Micro-Waves," John Wiley & Sons (1965).

10. V. M. Ristic, S. A. Self and F. W. Crawford J. Applied Phys. 40 pp. 52-44, (1969).

11. R. J. Briggs, "Electron-Stream Interaction with Plasmas," MIT Press (1964).

12. A. V. Longinov, "Excitation of Electromagnetic Waves in a Plasma by Longitudinal Electric Fields" Soviet Physics - Technical Physics Vol. 17, pp. 1273-1282, (1973).

13. P. J. Barrett, H. G. Jones and R. N. Franklin, "Dispersion of Electron Plasma Waves" Plasma Physics Vol. 10, pp. 911-918, (1968).

14. B. B. O'Brien Jr., "Slow Wave: Transmission Modes of an Isotropic Inhomogeneous Cylindrical Hot Plasma." Plasma Physics Vol. 9, pp. 369-400, (1967).

15. C. N. Lashmore - Davies, "Theory of High Frequency Electrostatic Waves in a Non-Uniform Plasma in the presence of Magnetic Field," Plasma Physics, Vol. 11 pp. 271-284, (1969).

16. W. P. Allis, S. J. Buchsbaum and A. Berss "Waves in Anisotropic Plasma" MIT Press., (1963).

17. P. A. Sturrock, "Nonlinear Effects in Electron Plasma." Proc. Roy. Soc., A242:277 (1957).

18. L. A. Turlock, C. R. James, "Nonlinear Interation of Electromagnetic Waves in Bounded Plasma," IEEE Trans. AP-16:737 (1968).

19. A. N. Kondratenko, V. I. Liolunovich and P. N. Rybin, "Nonlinear Theory of Electromagnetic Waves in a Bounded Plasma," Izvestiya Vuz. Radiofizika p. 176 April (1966).

20. R. F. Whitmer, E. B. Barrett, "Nonlinear Interaction of an Electromagnetic Wave with a Plasma Layer in the Presence of a Static Magnetic Field, I. Theory of Harmonic Generation," Phys. Rev. 121: 661 (1961).

R. F.. Whitmer, E. B. Barrett, "II. Higher Harmonics and a Nonlinear Propagation Theory," Phys. Rev. 125, 1478 (1962).

E. B. Barrett, R. F. Whitmer and S. J. Tetenbaum, "III. Theory of Mixing," Phys. Rev. 135A:369 (1964).

S. J. Tetenbaum, R. F. Whitmer and E. B. Barrett, "IV Experimental Results," Phys. Rev. 135A:374 (1964).

21. C. N. Lashmore - Davis "The Coupled Mode Approach to Nonlinear Wave Interactions and Parametric Instabilities," Plasma Phys. Vol. 17, pp. 281-303, (1975).

22. G. Laval., R. Pellat and M. Perulli, Plasma Phys. 11, 579 (1969).

23. J. Larsen "Nonlinear Wave Interaction in a Plasma Column" Stanford University. Institute for Plasma Research SU-IPR-R-493, Oct. 1972.

24. L. Kunh "An Experimental and Theoretical Study of Wave Mixing in a Bounded Magnetoplasmas" Columbia University Sci., Report #6 August, 1968.

25. P. Heymann and K. Saver "Surface Wave Echo on a Plasma Column" Physics Letters. Volume 35A., p. 51, (1971).

26. Ajmera, R. and K. Lonngren, "Nonlinear Excitation of Propagating Surface Waves on a Plasma Column," Journal of Applied Physics Vol. 19 #5, pp. 2265-2268, April 1968.

27. H. J. Schmith, "Plasma Diagnostics with short Electromagnetic Pulses." IEEE Transactions on Nuclear Science. pp. 125-136, (1964).

28. J. R. Proni Jr., W. O. Doggett and W. H. Bennett "Signal Propagation Studies in a Low Density Plasma." Plasma Physics Vol. 13, pp. 191-198,(1971).

29. J. P. Treguier and D. Henry - "Propagation D'une Impulsion Hyperfrequence Sur le Mode Electrostatigue Longitudinal Dans un Plasma de Laboratorie. Plasma Physics, Vol. 14, pp. 667-675,(1972).

30. B. Anicin, and V. Babovic, "Excitation of Nanosecond Waves on Positive Columns," Journal Plasma Physics, Vol. 7, pp. 403-416, (1972).

31. O. Demokan, H. C. Hsuan, K. Lonngren and B. Anicin, "A Time of Flight Study of Waves Guided By a Plasma Column," Plasma Phys., Vol. 13, pp. 29-32,(1971).

32. D. L. Landt, H. C. S. Hsuan and K. E. Lonngren "Properties of Waves Guided by a Plasma Column as determined by Time-Of-Flight Measurements" Plasma Physics Vol. 16., pp. 407-412,(1974).

33. A. Sindoris, "Linear & Nonlinear Impulse Stimulated Emission from a Plasma Column," Ph.D. Thesis, NYN School of Eng. & Sci., October 1971.

34. H. Ikezi, P. J. Barrett, R. B. White and A. Y. Wong, "Electron Plasma Waves and Free Streeming Electron Bursts" Phys. Fluids Vol. 14, pp. 1997-2005 (1971).

35. Huddlestone and Leonard "Plasma Diagnostic Technique."

36. S. Sen, and S. Mukhopadhyays, "Microwave Measurement of Electron Collision Frequency in Mercury Vapor D. C. Glow Discharge Plasma Column," Institute of Radio Physics & Electronics, Calcutta University.

37. N. Marcuvitz, Lecture Notes on Plasma Dynamics, NYU School of Eng. & Sci.

38. P. C. Clemmow, J. P. Dougherty, "Electrodynamics of Plasmas," Addison-Wesley (1969).

39. G. Georges, Nonlinearities in Plasmas & Theoretical Investigation of Harmonic Generation in Stratified Geometry, Ph.D. Thesis, NYU, May 1971.

40. L. B. Felsen, and N. Marcuvitz, "Radiation and Scattering of Waves," Prentic Hall, (1973).

41. H. Washimi and T. Tanuiti, "Propagation of Ion-Acoustic Solitary Waves of Small Amplitude" Phys. Rev. Lett. 17, pp. 996-998,(1966).

42. Y. A. Berezin and V. I. Karpman, "Theory of Nonstationary Finite-Amplitude Waves in a Low-Density Plasma," JETP 19, pp. 1265-1271 (1964). "Nonlinear Evolution of Disturbances in Plasmas and Other Dispersive Media," JETP 24, pp. 1049-1056 (1967).

43. B. Kadomtsev and V. Karpman, "Nonlinear Waves," Soviet Physics Uspekhi, Vol. 14, #1, p. 40, (1971).

44. A. Scott, F. Chu and D. McLaughlin, "The Solition: A New Concept in Science," Proc. IEEE, Vol. 61 #10, p. 1443, (1973).

45. G. B. Whitham "Linear and Nonlinear Waves" John Wiley & Sons, (1974).

46. R. E. Collin "Field Theory of Guided Waves" McGraw-Hill, NY, (1960).

47. G. N. Watson "Theory of Bessel Functions."

48. K. Saeki and H. Ikezi "Electron Plasma Wave Shocks in a Bounded Plasma" Physical Review Letters 29, pp. 253-255, (1972).

49. W. M. Manheimer "Nonlinear Development of an Electron Plasma Wave in a Cylindrical Waveguide" The Physics of Fluids 12, pp. 2426-2428, (1969).